Assessing Normalized Difference Vegetation Index (NDVI) data to estimate winter wheat yields and analyze winter wheat by homogeneous subregions at field scale in Kansas.

by

Rebecca Lima Albuquerque Maranhão

B.S., University of Brasilia, 2013
M.S., University of Brasilia, 2015

AN ABSTRACT OF A DISSERTATION

submitted in partial fulfillment of the requirements for the degree

DOCTOR OF PHILOSOPHY

Department of Geography
College of Arts and Sciences

KANSAS STATE UNIVERSITY
Manhattan, Kansas

2023

Abstract

Wheat (Triticum aestivum L.) is the 4th largest staple crop produced worldwide. While global demand has increased over the last 15 years, the rate of increase of global cereal production has slowed or stagnated. Accurate information about crop production is key for local-scale research, farmers, and decision-making evaluation due to the typically high spatial variability in agricultural production, especially in environmentally heterogeneous high-producing regions. The main goal of this dissertation was to investigate the potential of satellite imagery in predicting winter wheat yields and analyze winter wheat yields by homogeneous subregions at field scale in Kansas, the largest producer of winter wheat in the U.S. The first chapter examined the performance of different satellite sensors (from coarse to moderate resolution - MODIS, Landsat, and Sentinel) in predicting winter wheat yields. The following chapters analyze the winter wheat yield prediction using environmentally distinct subregions regarding weather and management practices and multisource data (NDVI, weather, and climate). Linear Regression and a robust machine learning model, (i.e., Random Forest) were applied to predict winter wheat yields. The results, using NDVI predictor variables, were not enough to explain field-scale winter wheat yield variability across much of Kansas, where Landsat USGS achieved the lowest prediction error among all sensors (RMSE = 0.95 Mg ha^{-1}). The results proved to be more accurate when using Landsat NDVI variables to predict winter wheat yields in more homogeneous subregions (NC, SC, and West), with the best prediction in NC (RMSE = 0.76 Mg ha^{-1}). NC, SC, and West Kansas achieved the best results when including weather and management variables along with NDVI (RMSE of 0.59 Mg ha^{-1} , 0.66 Mg ha^{-1}, and 0.69 Mg ha^{-1}in NC, SC, and West), and outperformed the prediction when using all fields-yields

across Kansas (RMSE=0.78 Mg ha^{-1}). The prediction model showed that it is possible to predict yield in early crop developmental stages; however, after adding weather and management variables, NDVI predictor variables in the late stages of the growing season were the most important for winter wheat yield prediction. NDVI was more significant in predicting winter wheat yields in NC and West than in SC Kansas. NC showed management of fertilizers (N, P, Cl) as good yield predictors and could be used along with NDVI to estimate yields. SC and West predictor variables relied more on variables related to environmental conditions or management practices related to environmental conditions, such as fungicide application, soil water storage, and sowing date. Overall, this research demonstrates that the applicability of empirical winter wheat yield modeling using NDVI predictor variables in Kansas is environmentally dependent. Lastly, winter wheat yield prediction using satellite imagery at the field scale could be benefited using this subregional scheme in Kansas.

Assessing Normalized Difference Vegetation Index (NDVI) data to estimate winter wheat yields and analyze winter wheat by homogeneous subregions at field scale in Kansas.

by

Rebecca Lima Albuquerque Maranhão

B.S., University of Brasilia, 2013
M.S., University of Brasilia, 2015

A DISSERTATION

submitted in partial fulfillment of the requirements for the degree

DOCTOR OF PHILOSOPHY

Department of Geography
College of Arts and Sciences

KANSAS STATE UNIVERSITY
Manhattan, Kansas

2023

Approved by:

Major Professor
Marcellus Marques Caldas

Abstract

Wheat (Triticum aestivum L.) is the 4th largest staple crop produced worldwide. While global demand has increased over the last 15 years, the rate of increase of global cereal production has slowed or stagnated. Accurate information about crop production is key for local-scale research, farmers, and decision-making evaluation due to the typically high spatial variability in agricultural production, especially in environmentally heterogeneous high-producing regions. The main goal of this dissertation was to investigate the potential of satellite imagery in predicting winter wheat yields and analyze winter wheat yields by homogeneous subregions at field scale in Kansas, the largest producer of winter wheat in the U.S. The first chapter examined the performance of different satellite sensors (from coarse to moderate resolution - MODIS, Landsat, and Sentinel) in predicting winter wheat yields. The following chapters analyze the winter wheat yield prediction using environmentally distinct subregions regarding weather and management practices and multisource data (NDVI, weather, and climate). Linear Regression and a robust machine learning model, (i.e., Random Forest) were applied to predict winter wheat yields. The results, using NDVI predictor variables, were not enough to explain field-scale winter wheat yield variability across much of Kansas, where Landsat USGS achieved the lowest prediction error among all sensors (RMSE = 0.95 Mg ha^{-1}). The results proved to be more accurate when using Landsat NDVI variables to predict winter wheat yields in more homogeneous subregions (NC, SC, and West), with the best prediction in NC (RMSE = 0.76 Mg ha^{-1}). NC, SC, and West Kansas achieved the best results when including weather and management variables along with NDVI (RMSE of 0.59 Mg ha^{-1} , 0.66 Mg ha^{-1}, and 0.69 Mg ha^{-1}in NC, SC, and West), and outperformed the prediction when using all fields-yields

across Kansas (RMSE=0.78 Mg ha^{-1}). The prediction model showed that it is possible to predict yield in early crop developmental stages; however, after adding weather and management variables, NDVI predictor variables in the late stages of the growing season were the most important for winter wheat yield prediction. NDVI was more significant in predicting winter wheat yields in NC and West than in SC Kansas. NC showed management of fertilizers (N, P, Cl) as good yield predictors and could be used along with NDVI to estimate yields. SC and West predictor variables relied more on variables related to environmental conditions or management practices related to environmental conditions, such as fungicide application, soil water storage, and sowing date. Overall, this research demonstrates that the applicability of empirical winter wheat yield modeling using NDVI predictor variables in Kansas is environmentally dependent. Lastly, winter wheat yield prediction using satellite imagery at the field scale could be benefited using this subregional scheme in Kansas.

Table of Contents

List of Figures

List of Tables

Acknowledgements

After five years, I can confirm that the day you plant the seed is not the day you eat the fruit. I feel the same about the Ph.D., which requires patience, perseverance, and curiosity. As a Brazilian musician, Caetano Veloso once said in a song, "It's a long way…". My achievement until now wouldn't be possible without the time, patience, and the people that helped me during this journey.

First, I would like to thank my parents, Silvia Santos Lima and Luiz Carlos Maranhao, for inspiring my sister and me to be creative and curious human beings and encouraging us to use our imagination and critical thinking since we were kids. Thank you for all the long hours in the car driving from our hometown (Brasilia) to Rio de Janeiro over so many summers and all the places we went to during these road trips. That was probably one of the many reasons I became a geographer and researcher. Thank you for boosting my confidence during the hard times and supporting me so much during these last years of my Ph.D.!

I want to thank my dog Sammy, my sweet boy, and my writing partner, who always stayed with me, lying under my desk for hours while I was studying. Thank you for our long walks to decompress, recharge, and develop new ideas. Thanks to all my friends I made in Kansas and the Department of Geography and Geospatial Sciences at Kansas State University, they made this place a very special place to live in. You all made Kansas feels like home to me. Kansas has changed me for good, and I am grateful for that. I will never forget it. I appreciate everything they've done for me.

I sincerely thank the College of Arts & Sciences and Graduate School at Kansas State University for the financial support of my doctorate studies as a Graduate Teaching Assistant. I

am also thankful to Chuck Martin, head of the Department of Geography, for assisting me in obtaining the financial support needed during these years as a Graduate Teaching Assistant. Thank you also, Wheat Alliance, for the financial support for my research and for funding me as a Graduate Research Assistant.

I'd like to thank Marcellus Caldas, my advisor, for the challenges you introduced to me and your mentoring during the Ph.D. program, who pushed me hard to keep learning and questioning, making me a better researcher. For showing me that responsibility and organization are fundamental keys to success. (I still need to work on that, though!). I sincerely thank my committee members, firstly, Jude Kastens and Romulo Lollato, for co-advising my research. I am grateful for having two experts, Jude in Mathematics and Remote Sensing and Romulo in Wheat Science. Without your mentoring, it would be hard to succeed! I am grateful to Dr. Kate Nelson, Dr. Douglas Goodin, and Dr. Jida Wang for being also my committee members, who helped me develop my skills using programming software and remote sensing during the Doctorate program. Thank you for sharing your tremendous knowledge that helped me develop this work.

Thank you to the University of Brasilia, the Department of Geography, and professors Renato Fontes Guimaraes, Osmar Abilio Diniz, and Potira Hermuche, who trained me in GIS and developed my research skills during my undergraduate and master's studies. Your exceptional work is the reason why I am here!

I would also like to thank Shawn Hutchinson for selecting me to participate as a research mentor in the capstone class Natural Resources and Environmental Sciences in the Fall of 2022. I had a fantastic experience mentoring students from different majors, doing fieldwork, and having weekly meetings to discuss our project. I am also grateful for all the incredible people and

scientists from various fields I've met during conferences in the U.S., especially at the American Association of Geographers and Graduate Climate Conference. It thrills me to meet so many fantastic minds and human beings.

Lastly, I would like to thank my sister Maria Cristina, my best friend. I am grateful for all your advice and emotional support during these last years.

Dedication

To my grandfather, Paulo Batista Lima,

for the notebooks over the summer when I was a kid so I could write my “novels.”

This dissertation is also dedicated to all immigrants and first-generation Latinos in Graduate School; you make this country more vibrant.

Chapter 1 - Introduction

1.1. Motivation

Although growing at a slower pace, the world population is expected to raise to ~ 9.7 billion by 2050 and ~ 10.9 billion by 2100 (Christensen et al., 2018). Increasing food production and improving food access while minimizing environmental impacts and maximizing social opportunities are main challenges in this century (Calicioglu et al., 2019). Currently, wheat (*Triticum aestivum* L.) contributes about 20% of energy and protein in human diets worldwide and is crucial for food security (Shiferaw et al., 2013). Due to its dietary importance and agronomic adaptability to a wide of climatic conditions in many geographic regions (Slafer et al., 2021), wheat is the most largely cultivated crop in the world, with China, India, Russia and the United States (U.S.) as the major producers (FAO,2023).

The U.S. produces 8% of the world's wheat, it ranks in the top three as a major wheat exporter. In the country, wheat ranks only behind corn (*Zea mays* L.) and soybeans (*Glycine max* L.) in terms of planted acreage, production, and gross farm receipts (U.S. Department of Agriculture, 2022). Approximately 9 million hectares are sown to winter wheat every year in the U.S. Southern Great Plains, which is the largest contiguous area of low-precipitation winter wheat cropland in the world (Fischer et al., 2014) . Located in the U.S Southern Great Plains, Kansas is the top producing state in the U.S., producing between 13 and 21% of the total winter wheat production (Obembe et al., 2021a). Most of the winter wheat is produced under rainfed conditions (Barkley et al., 2014; Schillerberg et al., 2019), and large geographic and temporal variability in environmental conditions impact winter wheat yields in this region (Couëdel et al., 2021; Lollato et al., 2017; Lollato, Bavia, et al., 2020).

Extreme meteorological events, such as heat waves, heavy storms, or droughts, are expected to increase yield variability and affect winter wheat growth and development (Olesen & Bindi, 2002). In the US southern Great Plains, compound hot-dry-windy events which limit winter wheat yield are also expected to increase (Zhao et al., 2022)Average temperatures in Kansas have significantly trended up during the last 121 years, a period in which the daily minimum temperature increased faster than the daily mean maximum temperature (Lin et al., 2017). The western half of Kansas, where the largest winter wheat production occurs, has experienced severe to extreme summertime drought for more than 25% of the 20th century (Cook et al., 1999). Thus, harsh environmental conditions in Kansas impact grain yield and interact with crop management outputs. For example, heat stress can impact wheat's response to nitrogen fertilization (Sadras et al., 2022). More broadly, environmental conditions characterizing the growing season for winter wheat largely determine optimal crop management practices (Jaenisch et al., 2021; Munaro et al., 2020) to improve grain yield in the different regions of the state.

Therefore, combined with the complexities of climate change, wheat productivity and food security will depend on the sustainable use and management of resources, including land, water and nutrients(Fischer et al., 2014; van Ittersum, 2016). A crucial component for food security is the accurate estimation of supply and demand of agricultural crops. The need for timely and efficient crop monitoring and yield estimation is key to update decision support systems and guarantee food supply(Komp & Haub, 2012). At a national and regional scale, this information can guide local governments to make decisions on food security or subsidies in case of extreme weather conditions, such as droughts, frost or heat events that can potentially damage crops (Franch et al., 2019; Zhong et al., 2019; Zhou et al., 2020). In the private sector, industry

and companies can promptly revise and define selling strategies (Everingham et al., 2002). At the field scale, reliable crop assessment can inform farmers to identify low yield productivity zones and improve their management practices (Lobell, 2013; Řezník et al., 2020) as well as insurance companies can use this data to update their insurance models (Bokusheva et al., 2016; Holman et al., 2023; Skakun et al., 2016).

1.2. Crop monitoring and yield assessment

When assessing crop yields, forecasts and estimations are performed in different ways. Forecasting is performed before the entire crop has been harvested, whereas estimates are made shortly after the crop has been harvested (Basso & Liu, 2019a). The estimation and forecast of crop yields can be undertaken by different approaches. The conventional method is mostly through farmer self-reports and field survey (Huddleston, 1978; Lobell et al., 2019). Farmer self-reports are made by interviews where farmers answer how much was harvested or what quantity they expect to harvest. Field survey or crop cut measure the grain weight harvested from a randomly selected portion of a farmer's plot. A large number of crop cuts conducted in a region can therefore give a reliable measure of average yields (Fermont and Benson, 2011).

The National Agricultural Statistics Service of the US Department of Agriculture uses both strategies, phone interviews and field surveys to forecast the yield of several commercial crops, including maize , soybean, and wheat (Basso & Liu, 2019b). At each forecast time during the growing season, the end of season predictions assume normal weather conditions for the remainder of the growing season(Morell et al., 2016). Similar yield forecasting based on field measurements and surveys are performed in national programs of other countries: Field Crop Reporting Series in Canada (https://www.statcan.gc.ca/en/dai/btd/fcrs), Brazilian Crop

Monitoring by National Supply Company (Conab) (https://www.conab.gov.br/info-agro/safras), Crop Estimates Committee (CEC) in South Africa (https://www.sagis.org.za/cec.html), and General Crop Estimation Survey (GCEP) in India https://agricoop.nic.in/#gsc.tab=0 . While these reports provide reasonably accurate approach and assist policymakers in formulating successful strategies to tackle national food security issues, the extension and aggregation demanded by regional and national surveys requires substantial resources in terms of logistics, labor, and time.

During the 1970s, with the greater availability of computing resources, empirical and mechanistic agricultural crop models developed rapidly (Passioura, 1996). Empirical models include statistical and machine learning (ML) approaches. The statistical modeling to forecast crops has been used for decades and establishes a function relation between yield predictors, commonly by agrometeorological data as inputs (e.g., precipitation and temperature) and the historical yield data (Johnson et al., 2021). This relationship is commonly used through linear regression models (Ansarifar et al., 2021; Landau et al., 2000), Bayesian implementations (Shirley et al., 2020) and partial least squares regression (Guo et al., 2021; Hu et al., 2018). The ML method builds an analysis system through data learning which does not give explicit expressions of the functional relationships between yield predictors and the resulting yield (Zhu et al., 2021). ML algorithms have been largely used recently to overcome some limitations found in regression models, regarding nonlinearity and collinearity from complex and large datasets. For instance, Artificial Neural Networks, Random Forest and Support Vector Machines are the most widely used algorithms in crop yield prediction studies (van Klompenburg et al., 2020).

Mechanistic models or process-based crop models assume that the system has a known structure, and that properties and processes of the components of the system can be described

mathematically (Palosuo et al., 2011; Vandendriessche & van Ittersum, 1995). These models can capture major genotype × environment × management (G × E × M) interactions that govern crop development, growth, and yield. In other words, mechanistic models use weather, soil, crop, and management information as input to simulate plant development and growth. Unlike statistical models, mechanistic models do not regress observed end-of-season grain yield with within season observations, instead they account with the effects of the interaction between GxExM on grain and biomass yield. For instance, APSIM (McCown et al., 1996), CROPSYST (Stöckle et al., 2003), CERES (Ritchie et al., 1989), SWAP (van Lier et al., 2015) and WOFOST (Diepen et al., 1989) are among the most used process-based crop yield models. Although these models can give accurate predictions of yield and exceptional information regarding impacts of different management and weather in crop yields, they require extensive parameter inputs that describe characteristics of the modeled situation (Chen et al., 2019) . Also, these models are many times used to simulate in-season yield potential (van Ittersum et al., 2013) with applications previously done for Kansas and the US southern Great Plains (e.g., Jaenisch et al., 2021; Lollato et al., 2017; 2019); which many times is well-above actual grain yields and thus not a realistic yield forecast. Thus, one of the potential limitations is the lack of proper spatial information and parameters at regional scale studies.

1.3. Satellite imagery for agricultural monitoring systems: A brief history

Since the launch of the first remote sensing weather satellite (TIROS-1) in 1960 and the first Earth resources satellite in 1972 (Landsat-1), several satellites with a variety of remote sensing sensors have been launched to study the Earth land cover, oceans, atmosphere or to monitor the weather (Tatem et al., 2008). Satellite remote sensing is capable to gather timely and

repetitive information about earth's surface, becoming a source of vegetation health information for crop condition monitoring and yield estimation at different scale levels (global, regional and local) (Lungu et al., 2020). In addition, remote sensing provides a spatial perspective (Day, 2017). It can help to identify areas where agricultural production is being affected by environmental conditions (precipitation, temperature, soil nutrients) (Kaur et al., 2020; Ryu et al., 2022; Wang et al., 2018), and to differentiate husbandry practices such as irrigation (Serrano et al., 2020; Wei et al., 2022),), tillage practices (Azzari et al., 2019), fertilizer application levels (Guan et al., 2019; Zhang et al., 2018), crop rotation (Waldhoff et al., 2017), and row spacing (Kimes and Kirchner, 1983).

During the 1970s new research programs were funded to create crop models that take advantage of the capabilities of remote sensing data to predict the yield of major crops. According to (Becker-Reshef et al., 2010), during this period, unexpected severe wheat shortages in Russia drew attention to the importance of timely and accurate prediction of world food supplies. In 1974, the Large Area Crop Inventory Experiment (LACIE) was created and funded by The National Aeronautics and Space Administration (NASA), US Department of Agriculture (USDA), and National Oceanic and Atmospheric Administration (NOAA) to develop a method for estimating wheat production worldwide by using Landsat data (Erickson, 1984).

The main objectives of LACIE were focused on: i) an economically important use of repetitive, multispectral, remote sensing from space; ii) test the capability of Landsat, together with climatological, meteorological, and conventional data sources, to estimate in advance the size of an important world food crop; and iii) to validate techniques that can provide timely estimates of crop production.

The successor to LACIE was a joint program for Agriculture and Resources Inventory Surveys Though Aerospace Remote Sensing (AgRISTARS) which began in 1978, and centered the research on major advancement in automation of large area crop classification and crop condition assessment (Wilson and Sebaugh, 1981). A series of field experiments were funded by AgRISTARTS to understand the spectral characteristics of major U.S crops that led to improved accuracies in classification and better understanding of the relationship between spectral changes in vegetation over the time and agronomics (Bauer, 1975; Gallo & Daughtry, 1987).The program focused also on the use of deterministic models to predict crop yields, where the performance relied on the availability of local climatic data with adequate spatial resolution (Doraiswamy et al., 2003). While substantial technological advances were brought to the crop modeling field, significant limitations were found as well, such as the limitation of remote sensing data availability to detect in detail the temporal changes in vegetation conditions and crop growth and cloud contamination that reduced the limited Landsat temporal coverage for the crop season.

After these important foundations and further advances in radiometric, spectral and spatial resolution as well greater frequency of remote sensing data, the integration of remotely sensed data in crop yield models has evolved significantly. Currently, one of the recent efforts that NASA and USDA have initiated is the Global Agricultural Monitoring (GLAM) Project (https://ipad.fas.usda.gov/glam.aspx). The GLAM project focus on enhancing the agricultural monitoring and crop-production estimation capabilities using the new generation of NASA satellite observations, building one of the most comprehensive data management systems for remotely sensed based global agricultural monitoring (Becker-Reshef et al., 2010). The system currently includes a customized web-based information-analysis and data-delivery system combining the capabilities of different satellite sensors: Advanced Very High-Resolution

Radiometer (AVHRR) (1981- present), SPOT Vegetation (1998- present), MODIS (2000-present) and MODIS Rapid Response (2001-deprecated).

Currently, several other crop monitoring projects at global and regional scale provide critical agricultural information: the USAID Famine Early Warning System (FEWS-NET) (Backer & Billing, 2021) and the JRC's Monitoring Agricultural ResourceS (MARS) action of the European Commission (Baruth et al., 2008) with two different topics: agricultural production estimates of EU countries (Agri4Cast) and food security in food insecure countries (FoodSec); the European Union Global Monitoring of Food Security (GMFS) program (Komp & Haub, 2012) and the Crop Watch Program at the Institute of Remote Sensing Applications of the Chinese Academy of Sciences (Wu et al., 2015).

1.4. Remote Sensing for crop yield modeling

Remote sensing used for agriculture in general can be based on sensor platform and type of sensor. Sensors are typically mounted in satellites, aerial and ground-based platforms (Khanal et al., 2020). Since 1970, satellite products have been extensively used for crop monitoring and yield prediction at large scale. Recently, aerial platforms, which include aircraft and unmanned aerial vehicles and ground-based platforms (hand-held, free stating in the field and mounted on tractor or farm machinery) have been used for crop modeling within-field at local scale (Sishodia et al., 2020). Ground-based sensors have better temporal, spectral and spatial resolution in comparison to airborne and satellite sensors, being useful for forecasting yields, nutritional requirements of plants, crop plant disease detection(Cruppe et al., 2017) water demands and weed control. Yet, its efficiency is limited to small areas compared with aircraft and satellite sensors that can evaluate much larger areas at a time (Wójtowicz et al., 2010).

Sensors will vary in spatial, temporal, and spectral resolution. Spatial resolution affects the area of the smallest pixel that can be identified, or the minimum ground area in pixels that can be identified by remote sensing. As spatial resolution improves, the area of the smallest pixel decreases, and the homogeneity of soil or crop characteristics within the pixel increases. A coarse resolution means that the heterogeneity in soil or plant characteristics within the pixel will increase (Mulla, 2013). Temporal resolution is described as a revisit time or frequency allocated to any sensor (Ali et al., 2022). For example, a sensor with high temporal resolution is able to track changes in vegetation with more detail over time than a sensor with lower temporal resolution.

Spectral resolution is associated to the sensors precision in characterizing the spectral response. The band wavelength of multispectral imaging equipment is generally between 400 and 900 nm, mainly including blue, green, red, red edge and near-infrared. Hyperspectral sensors present a higher spectral resolution collecting reflectance data over a wide spectral range at small spectral increments (Verger et al., 2014). Compared to multispectral instruments that collect reflectance data in broadbands (greater than 40nm), hyperspectral present narrow bands (typically 10nm) allowing a better characterization and discrimination of distinct spectral features of objects found on the ground (Mulla, 2013). Although hyperspectral sensors have outstanding performance with high precision characterization of spectral response, they are expensive and involve more complicated data processing (Bian et al., 2022).

Lastly, sensors can differ in passive or active sensors. Passive sensors are mostly multispectral or hyperspectral and rely on solar illumination to measure the radiation emitted from the surface. Active sensors generate their source of radar radiation, measuring the magnitude of transmitted energy scattered by the Earth back to the radar antenna (Hosseini et al.,

2015). For instance, active sensors such as Synthetic Aperture Radar (SAR) instruments have their sources of energy divided into different categories including the X band (2.5–3.75 cm), C band (3.75–7.5 cm), and L band (15–30 cm) (Teimouri et al., 2019). Several studies have examined the potential of X , C and L bands to estimate Leaf Area Index (LAI) , a potential indicator of crop productivity (Hosseini et al., 2015; McNairn et al., 2002).

Among the satellite sensors used for large scale analysis, coarse-resolution sensors with a spatial resolution between 250m and several kilometers, such as the Advanced Very High-Resolution Radiometer (NOAA-AVHRR), Spot-Vegetation (VGT) and the Moderate Resolution Imaging Spectroradiometer (MODIS), have provided daily coverage and availability of historical datasets back to 1980-1990, and these sensors have extensively been used for building empirical models for crops yield forecasting (Bégué et al., 2018). With a higher spatial resolution (1 to 30m), Sentinel-2, Landsat 8, RapidEye, WorldView-2 , SPOT-6 are utilized to assess and estimate agricultural production at regional and local scales (Jin et al., 2018). Table 1 shows the most used satellites and their popular applications in crop modeling.

Table 1-1- Spatiotemporal resolutions of the satellite sensors used for crop modeling applications.

Satellite sensor	Activity period	Spatial/Spectral Resolution	Temporal Resolution	Application in crop modeling
Landsat 1	1972-1978	MS 80 km	18 days	Yield estimation, crop monitoring and identification (Odenweller and Johnson, 1989)
AVHRR	1979-present	MS 1.1 km	1 day	Yield prediction (Huang et al., 2013)
Landsat 5 TM	1984–2013	MS 30m	16 days	Biomass and crop yield estimation (Thenkabail et al., 1994)
SPOT-1	1986–1990	MS 20 m	2–6 days	Spectral reflectance measurements (Gallo & Daughtry, 1987; Wiegand et al., 1992) and crop discrimination (Murakami et al., 2001)
SPOT-2	1990–2009	MS 20 m	2–6 days	Crop identification (Hubert-Moy, 2001)
LiDAR	1995	VIS 10 cm	N/A	Crop discrimination (Andújar et al., 2013), crop height measurement and nutrient status (Eitel et al., 2014)
RadarSAT	1995-2013	C-band SAR 30 m	1–6 days	Crop identification and monitoring (McNairn et al., 2002)
IKONOS	1999-2015	MS	3 days	Conventional and conservation tillage practices discrimination (Viña et al., 2003) .
Landsat 7	1999–present	MS 30m	16 days	Vegetation index time series for crop monitoring (Roy & Yan, 2020)
EO-1 Hyperion	2000–2017	HS 30m	16 days	Biophysical characterization and discrimination of crop types (Thenkabail et al., 2013)
MODIS Terra/Aqua	999–present, 2002–present	MS 250–1000 m	1-2 days	Monitoring, classification and yield estimation (Lopresti et al., 2015; H. T. T. Wardlow et al., 2007)

Table 1-1. Continued

SPOT-4	1998-2012	MS 20 m	5 days	Vegetation indices for biophysical variability(Locke et al., 2000)
VGT-1		1 km	10 days	Vegetation trends in various agricultural systems (Yin et al., 2012)
SPOT-5	2002–2015	MS (Visible and NIR–10 m, SWIR–20 m)	2–3 days	Crop identification and yield estimation (Duro et al., 2012; C. Yang et al., 2009)
VGT- 2		1 km	10 days	Crop discrimination (Kamthonkiat et al., 2005a)
RADARSAT-2	2007-present	C-band SAR 1–100 m	3 days	Leaf Area Index (LAI) estimation (Hosseini et al., 2015)
RapidEye	2008-present	MS 6.5 m	1–5.5 days	Nutrient estimation (Magney et al., 2017; Martins et al., 2019)
WorldView-2	2009–present	MS 1.4 m	1.1 days	Leaf Area Index (LAI) estimation (Guo et al., 2021) and plant disease detection (Dhau et al., 2018)
SPOT-6	2012–present	MS 6 m	1-day	Vegetation indices for measuring nitrogen status (Amirruddin & Muharam, 2019)
Landsat-8 OLI	2013–present	MS 30m	16 days	Biomass and Leaf Area Index (LAI) estimation (Dong et al., 2020) and crop yield estimation (Skakun et al., 2019).
SPOT-7	2014–present	MS 6 m	1-day	Vegetation indices for measuring nitrogen status (Yadegari et al., 2020)
Worldview-3	2014–present	MS 1.24 m	<1 day	Identification of tillage practices (Hively et al., 2018)
Sentinel-1	2014–present	C-band SAR 5–40 m	1–3 days	Soil moisture assessment (El Hajj et al., 2017)

Table 1-1. Continued

Sentinel-2	2015–present	MS (Visible and NIR: 10 m, Red edge and SWIR: 20 m)	10- 5 days	Crop identification, monitoring and yield estimation **(Hunt et al., 2019; Y. Zhao et al., 2020)**
SMAP	2015–present	L band SAR 1–3 km	2–3 days	Soil moisture assessment (Chan et al., 2018)
Planet/PlanetScope	2016 - present	MS 3.7-4.1 m pixel size (resampled to 3 m)	1 day	Within-field variability in crop growing conditions, precision agriculture and yield estimation (Houborg & McCabe, 2016; Pang et al., 2022)

Satellite sensors record information about the Earth's surface by measuring the transmission of energy from the surface in different portions of the electromagnetic spectrum. Biophysical features of plants can be retrieved across these different parts of the electromagnetic spectrum since plant type, water content and canopy characteristics affects the light reflected in each spectral band differently (Knipling, 1970). Measured reflected light in ultraviolet, visible (blue, green, red) and near and mid infrared portions of the spectrum has commonly been used to develop various vegetation indices that provide useful information of plant structure and conditions, from crop growth to crop responses to stress (e.g., pests, diseases, temperature, soil, water, etc.) (Sishodia et al., 2020) .

Healthy vegetation has a particular spectral behavior where there is a strong absorption of energy in the red band by chlorophyll and reflective energy in the near- infrared (NIR) by leaf cellular structures. Mathematical combinations using these reflectances are particularly useful for vegetation characterization (Tucker, 1979). The Normalized Difference Vegetation Index (NDVI) proposed by Rouse et al. (1974) measured by the difference in reflectance values in red and NIR regions, is one of the most popular indices used since the 70s. NDVI is related to structural properties of plants such as LAI and green biomass (Jiang et al., 2010), but also to properties of productivity, like absorbed photosynthetic active radiation and foliar nitrogen (Jiao et al., 2017; Parece & Campbell, 2017) . Consequently, NDVI provides useful information to analyze crop growth (Shammi & Meng, 2021; Shen & Evans, 2021; Wardlow et al., 2007) and to estimate crop yield (Gao et al., 2018; Luciano et al., 2021; Skakun et al., 2019).

Along with NDVI, many other vegetation indices have been developed so far (Bannari et al., 1995; Leprieur et al., 1994). For instance, the green NDVI (GNDVI), enhanced vegetation index (EVI), and soil adjusted vegetation index (SAVI) have been broadly applied to tackle

potential limitations that may occur in NDVI, such as soil reflectance and signal saturation in dense vegetation (Adeniyi et al., 2020; Saad El Imanni et al., 2022; Shammi & Meng, 2021; Skakun et al., 2021).

Remotely sensed data has been used for crop yield estimation and forecasting using mechanistic crop models or empirical models. Crop mechanistic models (process -based) are designed to simulate development in time of crop state variables, encompassing variables such as LAI, above ground biomass, soil moisture and nutrient fluxes at the crop, soil and atmosphere interfaces. . Because the simulation time profiles of these variables depend on the spatial distribution of soil properties, climate conditions, canopy state variables (.g., LAI and biomass), and on farming practices (e.g., sowing date, plant density, nitrogen availability, etc.), process-based models are often developed at field scale studies (Levitan & Gross, 2018; Moulin et al., 1998). Remote sensing data can improve crop models with spatial and temporal information of soil properties and canopy state variables at larger scales. Therefore, satellite imagery data and mechanistic crop models have been integrated using data assimilations methods to improve the prediction accuracy of canopy state variables and yield of different crops at local, regional and national levels (Jin et al., 2018; Kasampalis et al., 2018).

For instance, there are four common approaches described by Delécolle et al. (1992) when integrating remote sensing data in mechanistic models: (i) the direct use of a driving variable (also called forcing method); (ii) the update of a state variable of the model derived from remote sensing i.e., continuously updating crop model simulation, assuming that a simulation data at day *t* can potentially improve the succeeding days; (iii) the re-initialization of the model, i.e., is the adjustment of an initial condition to obtain a simulation in agreement with the

remotely sensed derived observations and (iv) the calibration of the model, i.e., tuning the model parameters to obtain a simulation in agreement with remote data observations.

State variables in mechanistic models such as LAI have been broadly retrieved from remote sensing data and used as input into crop models. Thorp et al. (2010), Tripathy et al. (2013) and Yao et al. (2015) have estimated LAI using different remote sensing data and the simulated results of crop models were directly replaced by the estimated LAI to improve the simulated LAI and yield crop models. de Wit et al. (2012) estimated regional winter wheat yield with WOFOST through the assimilation of green area index (GAI) retrieved from MODIS observations. In this study, through a calibration approach, model parameters were optimized by minimizing the difference between simulated and observed GAI.

Mechanistic crop models have improved simulation ability of different crop growth status and crop yield under different stress environmental conditions at regional scales using remote sensing data. The main drawback is that they require expensive calculation and computing time, due to the substantial number of datasets and parameters. In contrast, empirical crop yield models do not incorporate information about processes that originate a response. As a result, empirical models are less data and computational intensive than mechanistic models (Kasampalis et al., 2018). Due to their straightforward implementation, statistical regression-based methods have a long history of using remotely sensed data within-season and actual crop yield to estimate yields (Durgun et al., 2020; Gaso et al., 2019; Kern et al., 2018; Lobell, 2013).For example, Ji et al., (2021) built three groups of yield regression models using phenological metrics from remote sensing to predict the yield in 314 counties within the US Corn Belt. In Europe, Panek and Gozdowski, (2021) estimated grain yield at country level using linear regression and NDVI metrics from MODIS satellite data.

Recently ML approaches have also been increasingly used to deal with non-linearities and overfitting from large datasets (Johnson et al., 2016; Schwalbert et al., 2020). Pang et al., (2022) proved the feasibility of applying Random Forest modeling on high resolution satellite and yield "big data" to estimate regional and local scale wheat yields in Australia. In a multi-source study using satellite imagery, climate data, soil maps and historical yield records in the U.S, Wang et al., (2020) found that ML approaches outperformed linear regression models, with the best performance being achieved from a AdaBoost model.

1.5 Challenges and opportunities in crop monitoring and yield estimation using remote sensing data.

The suitable selection of appropriate spatial and spectral resolution, and the methods for image processing, are essential for reliable yield estimation based on remote sensing data (Luciano et al., 2021). For instance, the high temporal frequency combined with broad spatial coverage and low cost, has made low-resolution satellite sensors a preferred choice for national and regional scale applications (Rembold et al., 2013) . Since the beginning of studies using remote sensing for crop monitoring, many scientists have used coarse spatial resolution (MODIS, AVHRR and SPOT-VEGETATION) to retrieve canopy state variables over large areas (Ji et al., 2008; Kamthonkiat et al., 2005b; Wardlow et al., 2007). Government institutions have in many countries used these types of data for national and regional crop monitoring and yield forecasting. For example, the USAID-funded FEWSNET (Famine Early Warning Systems Network) regularly elaborate food security reports and outlooks for the most food insecure countries around the world using low-resolution satellite images and their integration with ground data (M. E. Brown, 2008).

For crop yield prediction, the main advantage of low-resolution over moderate to high resolution sensors is their longer historical time series, often crucial to relate present conditions with similar conditions in the past. Coarse resolution sensors are more efficient when analyzing large clusters of the same type of vegetation since the variability in spectral responses from different land use and land covers at large scale can be a potential limitation providing mixed signals (Bégué et al., 2018).

Finer spatial and spectral resolution can explain the within field-crop variability during the growing season better than coarse resolution sensors, improving crop yield estimation (Skakun et al., 2021). Moderate satellite sensors such as the Landsat series and Sentinel-2 (30m and 10m) offer inexpensive delivery of information and are well suited for phenological monitoring (Hunt et al., 2019; Shen & Evans, 2021). The combination of Sentinel-2 constellations A and B provide imagery every five days with a spatial resolution of 10 meters, which facilitates characterizing the entire crop life cycle at high temporal resolution. However, combined data from Sentinel -2 were only available in 2017 and globally after December 2018.

Overall, moderate resolution sensors are most affected by the irregularities in cloud-free observations. Atmospheric contamination, such as cloud cover, reduce satellite imagery observations availability, compromising the assessment of timely biophysical information over the growing season (Skakun et al., 2017). High resolution sensors are the most adequate for within-field monitoring since it provides substantially more information for perceiving and predicting within-field physiological variations being crucial for farmers making decisions about where and when management should be varied across a field (Peralta et al., 2016). Recently, the Planet (www.planet.com) constellation (with 3 meters of spatial resolution) offers daily surface imagery increasing the chances of acquiring cloud-free images for crop yield prediction at field

scale. However, the acquisition of high-resolution data is still financially expensive for small farmers, whereas it is usually affordable to large commercial farms and private companies (Zhang et al., 2021). In addition, in studies focusing on crop monitoring at field scale across large regions, the main limitation of finer resolution is associated with the high costs in obtaining and processing large satellite imagery datasets (Rembold et al., 2013).

Currently, increased free access to moderate and high-resolution satellite data has provided new opportunities in the development and improvement of crop monitoring and yield prediction. Cloud-platforms, such as Google Earth Engine (GEE), Amazon and Microsoft AI for Earth, have greatly improved the capabilities of satellite imagery data storage and processing (Khanal et al., 2020). With regards to missing data that greatly affects satellite sensors with sparse revisit frequencies such as the Landsat series (16 days revisit frequency), several methods to reconstruct the vegetation seasonal growth course have been applied. The approaches can be divided in two broad categories: (1) methods that enable precise capturing of short-term variation during the growing season, by employing different types of statistical filters (Jiang et al., 2010) and (2) methods that fit mathematical functions (sinusoidal, logistic, Gaussian etc.) to part of a season, full season or sequence of seasons . The most recently and widely used are Savitzy-Golay filtering (Cao et al., 2018; X. Yang et al., 2022), least squares fits to asymmetric Gaussian functions(Ghaderpour & Vujadinovic, 2020; Jonsson & Eklundh, 2002), double logistic functions (Durgun et al., 2020), and variations of spline smoothing (Atzberger & Eilers, 2011; Hermance et al., 2007).

The application of remote sensing data in agriculture is continuously in development and improvement. With the increasing availability of satellite imagery data, cloud platforms, data processing approaches, and different crop modeling advances, there are many opportunities for

the analysis of crop monitoring and yield estimation at different scales. However, there are only a few studies dedicated to estimating yield at field scale (i.e. within the field) across large areas using methods based on remote sensing (Gaso et al., 2019; Schwalbert et al., 2020; Silvestro et al., 2017). This dissertation aims to fill the gap in the literature by investigating the potential of satellite imagery in predicting winter wheat yields and analyzing winter wheat yields by homogeneous subregions at field scale in Kansas. More specifically, this dissertation has three objectives:

Objective 1: Predicting and evaluating winter wheat yields at field scale using different satellite imagery sensors.

Objective 2: Evaluate the performance of winter wheat yields prediction using satellite imagery at field scale by subregions in Kansas.

Objective 3: Predicting and evaluating winter wheat yields at field level integrating multi source data, including satellite imagery, climate, and management practices, by subregions in Kansas.

Chapter 2 - Estimating winter wheat yields at field scale using Normalized Difference Vegetation Index metrics from multiple sources of satellite data in Kansas, USA

2.1. Introduction

Wheat (*Triticum aestivum L.*) is the 4th largest staple crop produced worldwide, reaching a record of 780 million tonnes in 2022 (Food and Agriculture Organization of the United Nations., 2023). While global demand has increase over the last 15 years with a growth of 25%, the rate of increase of global cereal production has slowed or stagnated. Although major improvements in wheat genetics resulted in higher grain yields, over the last 30 years, yield gains decreased, and yield stagnation has been reported in several major wheat producing regions in the world, such as U.S Southern Great Plains (Patrignani et al., 2014), Australia (Y. Zhao et al., 2020), the North China Plain (Geng et al., 2019) and Germany (Bönecke et al., 2020). Thus, concerns about global and national food security along with sustainable production has increased recently, emphasizing the need for more precise and timely crop yield information.

Total size of cropping area and crop yields information are key for the entire food supply chain at national, regional, and local level (Becker-Reshef et al., 2019). At a national and regional scale, winter wheat growth and yield knowledge are essential for international trading prices, decision-making policies (storage, transport, emergency responses), marketing, and insurance risk models. At a local level, the information is extremely helpful in guiding farmers to better crop management and financial decisions (Bokusheva et al., 2016; Luciano et al., 2021; Y. Zhao et al., 2020).

Crop yield statistical data by the U.S government is based on statistical data collected through interviews, questionnaires, and field surveys (USDA-NASS, 2023b). However, the resulted harvested yields from these surveys does not allow early coping strategies to be implemented by policymakers and producers.

Over the last four decades, satellite imagery data has increasingly been used for crop monitoring (Becker-Reshef, Justice, et al., 2010; M. Nguyen et al., 2020), crop mapping (Hunt et al., 2019; Mashonganyika et al., 2021; Skakun et al., 2017) and yield estimation (Johnson et al., 2021; Luciano et al., 2021; Yao et al., 2015), at local, regional, national and global scales, providing low-cost and timely biophysical information during the crop growth period (Skakun et al., 2019). The annual crop yield statistical data is limited to large scales (county to national level) and are often costly and time consuming, thus the additional use of satellite imagery data in crop yield monitoring is not only convenient but economical (Lungu et al., 2020).

Coarse satellite sensors such as the Advanced Very High-Resolution Radiometer (AVHRR) and the Moderate Resolution Imaging Spectroradiometer (MODIS) has provided consistent historical information about earth surface and has been widely used for national and regional scale crop yield forecasting (Becker-Reshef, Vermote, et al., 2010; Huang et al., 2013; Lopresti et al., 2015). An advantage from coarse resolution sensors is that is possible to have cloud-free images because of the higher revisit frequency (1-2 days). Compared to coarse satellite sensors, moderate spatial resolution (<30m) Landsat and Sentinel satellites has the potential to detect within-field variability and it has been used for crop yield estimation in smaller areas (Luciano et al., 2021; Saad El Imanni et al., 2022; Shen & Evans, 2021).

Remotely sensed data from satellite sensors can gather important spectral information from vegetation status. Vegetation indices (VIs) calculated from these spectral responses can

serve as a proxy for plant biomass, being widely used to derive crop yield estimates (García-Martínez et al., 2020; Z. Ji et al., 2021; Nolasco et al., 2021; Watson-Hernández et al., 2022). The Normalized Difference Vegetation Index (NDVI) developed based on the pioneering work by Rouse et al.(1974) and Tucker (1974) using the bands NIR and red domain, still one of the most popular indices for crop yield assessment (Moriondo et al., 2007).

Crop yield can be estimated with VIs using mechanistic or empirical approaches. Mechanistic crop yield models are more data intensive compared to empirical crop yield models as they use growth parameters such as crop physiological parameters, soil characteristics, and management information to run and calibrate plant growth models from which crop yield is derived (Huang et al., 2019; Kasampalis et al., 2018). When using an empirical approach, such as statistical models or machine learning, a VI is modeled as a function of crop yield, although other independent variables can be added to the model as well (Ji et al., 2021; Zhao et al., 2020).

Despite the promise of satellite imagery data as an applicable source of information for operational use of high-resolution sensors for crop yield forecasts at local scale across large areas, agricultural monitoring systems and national statistical offices publish pre-harvest forecasts on state and country-levels. Nevertheless, accurate subnational level information about crop production is a prerequisite for local-scale research or policy evaluation due to the typically high spatial variability in agricultural production (Yli-Heikkila et al., 2022).

Few studies have examined field-level yield across large areas prediction using remote sensing or crop modeling (Gaso et al., 2019; Schwalbert et al., 2018; Silvestro et al., 2017). Kansas is the largest producer of winter wheat in the U.S and could potentially benefit from timely and accurate yield prediction at field level, since the state is vulnerable to significant

volatility in yield due to climatic variability during the growing season (Lollato et al., 2017; Lollato, Bavia, et al., 2020; Tack et al., 2014, 2015)

This chapter investigates the potential of satellite imagery of differing resolutions (10 m to 250 m, or moderate to coarse) to predict field-level winter wheat yields in Kansas. This study aims to answer the following questions:

(i) Could remote sensing be used to predict winter wheat at the field level in Kansas?

(ii) Which satellite sensor has the best performance for winter wheat yield prediction?

2.2. Material and Methods

2.2.1. Study Area

The state of Kansas was selected as the study site for developing winter wheat yield prediction models, as it is the main winter wheat producing state in the U.S. In 2021, Kansas accounted for 10.4% of the state's total agricultural receipts and 22.1% of the nation's production, with an estimated direct impact of $1.3 billion in output and 3,231 jobs, playing an important role in the state's economy (Kansas Department of Agriculture, 2021).

The fields analyzed are located in Central and Western Kansas, where the majority of winter wheat is grown. There are steep gradients in precipitation, elevation, and temperature across Kansas, with precipitation ranging from ~450 mm in the west and ~1100 mm in the east (Lollato et al., 2020) resulting in winter wheat growing season precipitation ranging from ~200 to 650mm (Lollato et al., 2017). The average growing season temperature ranges from 7 to 12℃ from west to east due to elevation, which ranges from ~200 to 1200 m (Lollato et al., 2017).

2.2.2 Datasets

2.2.2.1. Field- specific geo-coordinates and yield data

Field-specific geo-coordinates were collected from a survey conducted by Jaenisch et al., (2021) during three consecutive seasons (i.e. harvest years of 2016, 2017, and 2018), in central and western Kansas, which represent ~92% of the state's wheat area. P. Producers completed the survey by telephone, e-mail, email or face-to-face.

The 656 field-yields geolocations were employed to create 656 polygons representing the boundaries of each field. The annual USDA Cropland Data Layer (CDL) datasets (USDA National Agricultural Statistics Service Cropland Data Layer, 2023) was used to evaluate the winter wheat geolocations. After removing records that did not correspond with winter wheat in the CDL, 499 samples remained (205 in 2016, 179 in 2017, and 115 in 2018). After applying additional data screening (see section: 2.2.4.2. NDVI time series), the final dataset comprised 160 samples (field-yield pairs), with a total area of 6490. 9 ha (Figure 2-1).

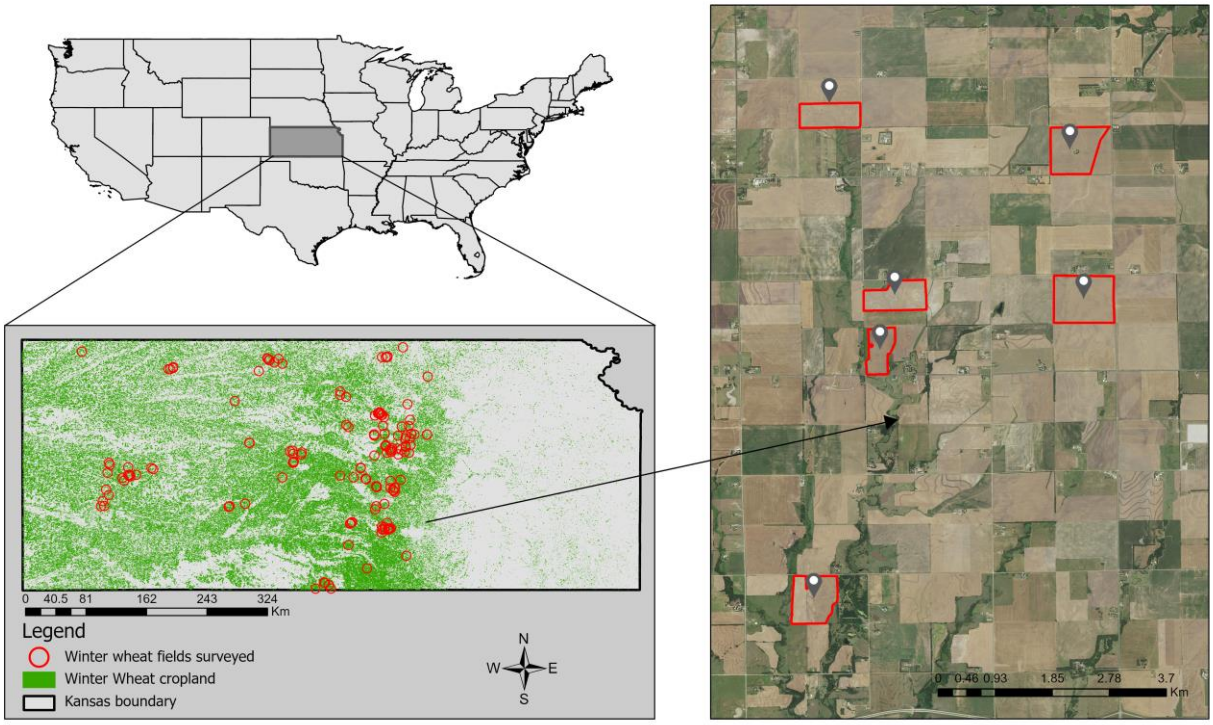

Figure 2-1 The Kansas map shows the winter wheat croplands in green. The red dots represent the 160 sample locations examined in the study. Overlaid on the aerial imagery are field boundaries for some of the winter wheat fields.

2.2.2.2. Yield data and Management data.

Grain yield from each field was collected in the same survey described above. Fields size ranged from 50,764 to 1,911,171 square meters approximately. Yields ranged from 0.4 to 7.05 Mg ha^{-1}, with a mean of 3.92 ha^{-1} and standard deviation of 1.18 Mg ha^{-1}. A simulated anthesis date was produced using the mechanistic crop simulation model Simple Simulation Model (SSM) – Wheat (Soltani & Sinclair, 2012), which is a process based model that simulates wheat growth and developments under non limiting conditions. This crop model has been validated for growing conditions in the U.S Great Plains (Lollato et al., 2017, 2019). Simulated anthesis date in the 160 fields ranged from DOY (day of year) 93 to 163 and averaged DOY 129.

2.2.3. Satellite data

Four satellite remote sensing datasets from January 2016 to July 2018 were used in this study: Landsat 8 Operational Land Imager (OLI) Collection 1 Level 1; Landsat 8 OLI Collection 2 Level 2; Sentinel-2 Multispectral Instrument (MSI) Level 1C; and Moderate Resolution Imaging Spectroradiometer (MODIS) Collection 6.

2.2.3.1. Landsat 8

Landsat 8 OLI captures images of the Earth's surface in nine spectral bands at a 30-m spatial resolution (15-m for panchromatic band). The dataset contains atmospherically corrected surface reflectance and land surface temperature. The study sites are covered by eight tiles (Table 2-1) for which Landsat 8 OLI Collection 1 data were downloaded from the United States Geological Survey (USGS) website (https://earthexplorer.usgs.gov/ accessed in January 2021). An alternative Landsat 8 OLI Collection 2 dataset (Wulder et al., 2019) hosted in the Google Earth Engine (GEE) platform was also used. Differences between the OLI collections are described in (USGS, 2022).

2.2.3.2. Sentinel-2

Sentinel-2 is a constellation that consists of twin satellites (2A and 2B) and is operated by the European Union (EU) Copernicus Program. Sentinel-2A was launched in June 2015 and Sentinel-2B in March 2017, with the satellites in the same orbit but situated 180 degrees apart to halve the revisit time. The Sentinel-2 data used in this study have a revisit frequency of 5-10 days and a spatial resolution of 10 m. The dataset was accessed through GEE with a total of 22 tiles covering the study area (Table 2-1). As Sentinel's Surface Reflectance (SR) data were not

available on GEE for the study period, we used the Top of Atmosphere (TOA) reflectance data instead. TOA reflectance data have shown effective performance in identifying spectral differences between crop types (Wang et al., 2020), instilling some confidence in their use for this study.

Table 2-1 - Tiles used in this study.

Tiles	ID
Landsat-8 OLI	028/032, 028/033, 028/034, 029/032, 029/033, 029/034, 030/032, 030/033, 030/034, 031/032, 031/033, 031/034
Sentinel-2	14SKJ, 14SKH, 13SGC,14SKG, 13SGB, 14TLK, 14SLJ, 14SLH, 14SMG, 14SMH, 14SMJ, 14TMK, 14TNK, 14SNJ, 14SNH, 14SNG, 14SPG, 14SPH, 14SPJ, 14TPK, 14SQG, 15STB.

2.2.3.3. MODIS

MODIS NDVI data were extracted from the USGS EROS Data Center's 250-m CONUS6 collection, which consists of weekly issued, biweekly maximum value composite imagery (Brown et al., 2015). Each field data sample was represented using a maximally interior pixel (Brown et al., 2013; Wardlow et al., 2007). Pixel-specific acquisition date information was used to precisely place (to the day) the raw time series values on the calendar, and these values were then linearly interpolated to create the regularly spaced, 7-day time series (calendar day 7, day 14, and so on) used in the analysis.

2.2.4. Methodology

2.2.4.1. Satellite data preprocessing

Detection and removal of ground-obscuring clouds and cloud shadows is essential for remote sensing data processing. For Landsat USGS, we applied a conditional using the Quality Assessment (QA) band (USGS, 2023), preserving only pixels with clear terrain conditions or

low to no confidence of cloud conditions. For Landsat GEE and Sentinel-2, we removed cells with cloud contamination or cloud shadow using the QA and QA60 bands, respectively.

2.2.4.2. NDVI time series

Time-series NDVI data are commonly used to monitor crop development throughout a growing season (Lai et al., 2018). For winter wheat grown in Kansas, the season starts between September and November of a year and finishes around June of the subsequent year. Still, the majority of crop growth takes place primarily during Jan-Jun (DOY 1-180) (Lollato et al., 2021; Lollato & Edwards, 2015) NDVI is computed using red (Red) and near-infrared (NIR) reflectance (Tucker,1974).

$$NDVI = \frac{NIR - Red}{NIR + Red} \quad (2\text{-}1)$$

Data from several Landsat and Sentinel tiles were required for this study (Figure 2-2). If a field had representation in multiple tiles and multiple concurrent (to the day) NDVI values were available, then the maximum NDVI was used, in favor of the greenest vegetation pixels.

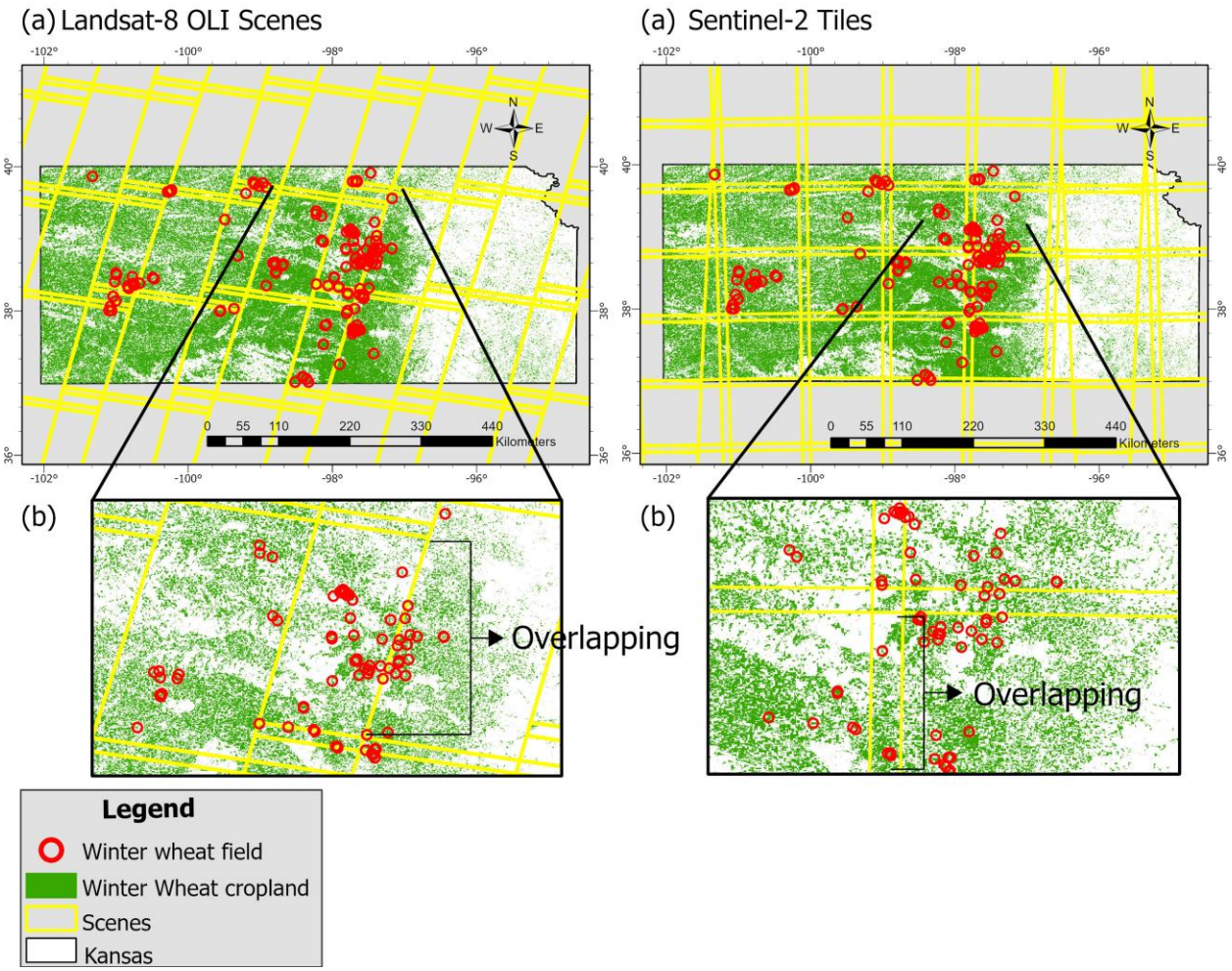

Figure 2-2. (a) Satellite tiles in yellow that are passing over the study area (Landsat-8 and Sentinel-2); (b) In detail, fields in red that are represented by multiple tiles (in overlapping tiles).

NDVI time series were visually accessed and a threshold NDVI value of 0.2 during April to May period was set. This threshold was defined because Landsat NDVI time-series showed lower NDVI values during the peak season compared to MODIS and Sentinel. Landsat NDVI time series with values higher than 0.2 during the peak season were capable to indicate the seasonal changes and winter wheat growth. As an additional constraint to bolster signal completeness, only fields with at least one monthly NDVI observation in the February-June period were included. January was not included since there is still influence of snow cover, thus

NDVI values are close to 0 or missing. These data selection criteria was imposed so that all sensors were evaluated using the same fields and timeframe in the dataset. Landsat USGS, Landsat GEE and MODIS shared the same number of winter wheat fields covering the years of 2016 to 2018 (n = 160). Since the NDVI time-series from the fields collected in 2016 using Sentinel did not match the selection criteria, the Sentinel dataset included only the years from 2017 to 2018 (n = 80).

2.2.4.3. Time series interpolation

VI time series obtained from remote sensing images are commonly affected by missing values (gaps). Using an up-sampling technique, we increased the frequency of the Landsat USGS, Landsat GEE, and Sentinel GEE to match with the weekly data from MODIS (Figure 2-3). Specifically, we used linear interpolation between straddling NDVI values to fill gaps. Since some samples had their earliest available February-June NDVI observation as late as DOY 56, we defined the study period to span DOY 56-182 (mid-February to end of June).

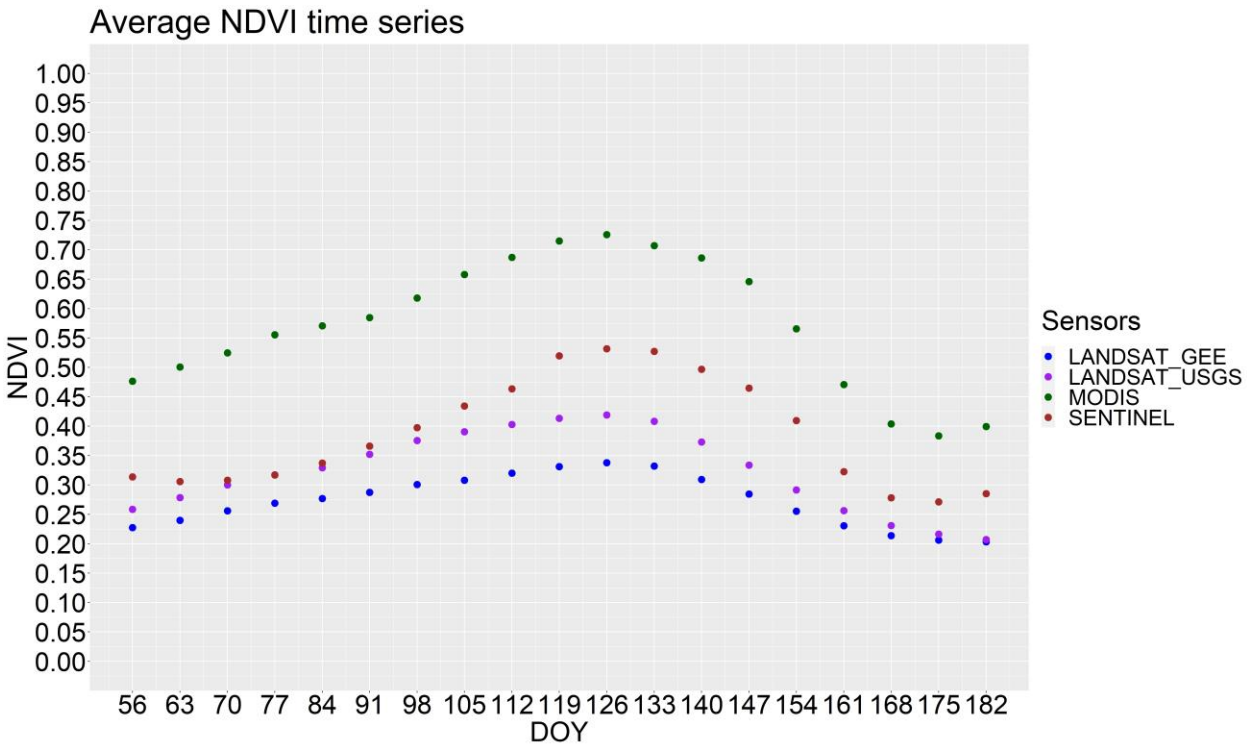

Figure 2-3- Sensor-specific, final NDVI profiles averaged across all samples (n = 160 for Landsat and MODIS; n = 80 for Sentinel).

2.2.4.4. NDVI predictor variables

Two-time intervals were analyzed, DOY 56-182 (full season, mid-February to June) covering post-dormancy tiller development, stem elongation, heading, anthesis, grain fill, and ripening, and DOY 105-154 (peak season, April to early June), representing the peak of NDVI greenness and the phenological stages of flag leaf emergence, heading, anthesis, and grain fill. Intervals follow the winter wheat and development stages in Kansas as showed in (Lollato, 2018). Accumulated NDVI (NDVI area under the curve, or AUC) and NDVI weekly data from the two-time intervals were used as independent variables and yields as the response variable. NDVI AUC was determined using the trapezoid rule for integral approximation. Thus, the independent variables for DOY 56-182 were: NDVI AUC and NDVI at DOY 56, 63, 70, 77, 84,

91, 98, 105, 112, 133, 140, 147, 154, 161, 168, 175, and 182. For interval DOY 105 to 154, independent variables were: NDVI AUC and NDVI at DOY 105, 112, 133, 140, 147, 154.

2.2.4.5. Empirical methods for estimating winter wheat yields

Least absolute shrinkage and selection operator (LASSO)

Adding more regressors in the model while having a limited number of observations (n=160), might lead to model overfitting, meaning that the model performance will improve on training data but will fail on testing (unseen) data. To prevent overfitting of the model with multiple regressors and decrease the effect of redundant features, the least absolute shrinkage and selection operator regression (LASSO) approach has been increasingly applied to improve the performance in crop yield models (Abbas et al., 2020; Correndo et al., 2021; Khaki & Wang, 2019). In short, LASSO adds penalty into parameter estimation to shrink the near zero regression coefficients to zero, thus removing them out of selection result (Tibshirani, 1996) . Here, NDVI predictor variables were input to a least absolute shrinkage and selection operator (LASSO) available in Scikit-learn for Python 3.9.

Although LASSO reduces redundant variables and overfitting, there may still be a need to remove remaining variables that are not statistically significant to the yield prediction model. Therefore, the final models (Linear regression and Random Forest) were built using only the most influential variables according to their influence in the final yield, selected by the regression coefficients from NDVI predictor variables. The NDVI predictor variables were selected by t-value score, p-value, lowest residual standard error, and largest coefficient of estimation (R^2) analysis. The greater the T-value and the smaller the P-value, the higher the evidence against the null hypothesis, i.e., predictors are significant. In addition to that, in some

cases, the selection was made by analyzing if the addition or removal of a variable could improve the results (R^2 and residual standard error) or not.

Linear Regression

Prediction models were performed using R programming language in R Studio (R Version 4.2.3). Linear regression used as input the NDVI predictor variables of each interval (DOY 56-182 and DOY 105-154) from the four remote sensing collections and related it to the survey yields. As a simple approach, linear regression models are commonly used in crop yield estimation studies in different regions (Johnson et al., 2021; Lobell, 2013; Lopresti et al., 2015).

The model equation is given by:

$$Yield = b_0 + b_1X_1 + b_2X_2 + \cdots + b_nX_n + \varepsilon \qquad (2\text{-}2)$$

Here, $\{b_0, b_1, \ldots\}$ are the regression coefficients, $\{X_1, X_2, \ldots\}$ are the NDVI predictor variables , and ε is the residual.

Random Forest Regression

Random Forest (RF) followed the same fashion as the linear regression, where the NDVI predictor variables were used as independent variables and the survey yields as the response variable. RF has been used in several yield prediction studies since its capability to handle high data dimensionality, outlier detection and robustness against overfitting (Lee et al., 2020; Luciano et al., 2021; Pang et al., 2022). The model is an ensemble of trees, or a combination of tree predictors, considered a strong learner more capable in terms of prediction power than a

decision tree (Breiman, 2001). Each tree depends on the values of a random vector sampled independently and with the same distribution for all trees in the forest. The generalization error converges to a limit as the number of trees in the forest becomes large and will depend on the strength of the individual trees in the forest and the correlation between them. Important RF hyperparameters, M_{try} (the number of variables randomly considered at each node) and N_{tree} (the number of random trees to be grown) were optimized by tuning approaches. Hyperparameter tuning and statistical performance evaluation were performed using the 'ranger' package (Wright & Ziegler, 2017) in RStudio.

2.2.4.6. Model Evaluation

With a limited size of samples, the training process may need every possible data to determine model parameters (Kuhn & Johnson, 2013). Thus, in our study, it was impossible to keep a significant percentage of the database for the validation and the testing dataset. The cross-validation approach is an effective and robust method to measure model generalization and goodness of fit of the yield models (Dinh & Aires, 2022). To tackle this limitation, several studies have applied a k-fold cross-validation procedure to obtain better accuracy and reduce overfitting (Fieuzal et al., 2020; Skakun et al., 2019; Zhao et al., 2020).

In this study, a 10-fold-cross validation was applied, where a single folder containing partial random sampling was retained as the cross-validation for testing the model, with the remnants samples in the nine folders used as training to fit the model. The cross-validation procedure was repeated 10 times resulting the average results from cross-validated coefficient of determination R^2 , Root Mean Squared Error (RMSE) and Mean Absolute error (MAE), defined as follows:

$$R^2 = 1 - \frac{\sum_{i=1}^{n}(y_{i-}\widehat{y_i})}{\sum_{i=1}^{n}(y_{i-}\bar{y})^2} \quad (2\text{-}3)$$

$$RMSE = \sqrt{\frac{\sum_{i=1}^{n}(y_{i-}\widehat{y_i})^2}{n}} \quad (2\text{-}4)$$

$$\text{MAE} = \frac{1}{n}\sum_{i=1}^{n}|y_{i-}\widehat{y_i}| \quad (2\text{-}5)$$

2.3. Results

2.3.1. NDVI time series of winter wheat

The NDVI time series from each of the four remote sensing collections are shown in (Figure 2-4). NDVI values ranged from 0.07-0.60 for Landsat USGS, 0.08-0.51 for Landsat GEE, 0.08-0.82 for Sentinel and 0.15-0.96 for MODIS. Observing the mean NDVI time-series Landsat GEE NDVI time-series profiles generally appeared flatter than Landsat USGS, Sentinel, and MODIS. Additionally, Sentinel NDVI time series showed flat NDVI values during DOY 56-70 while Landsat and MODIS showed an ascending pattern, perhaps reflecting increases in biomass after the winter dormancy period. Despite these discrepancies, the NDVI profiles from each sensor had roughly similar unimodal dynamics that correspond with the phenological development of winter wheat.

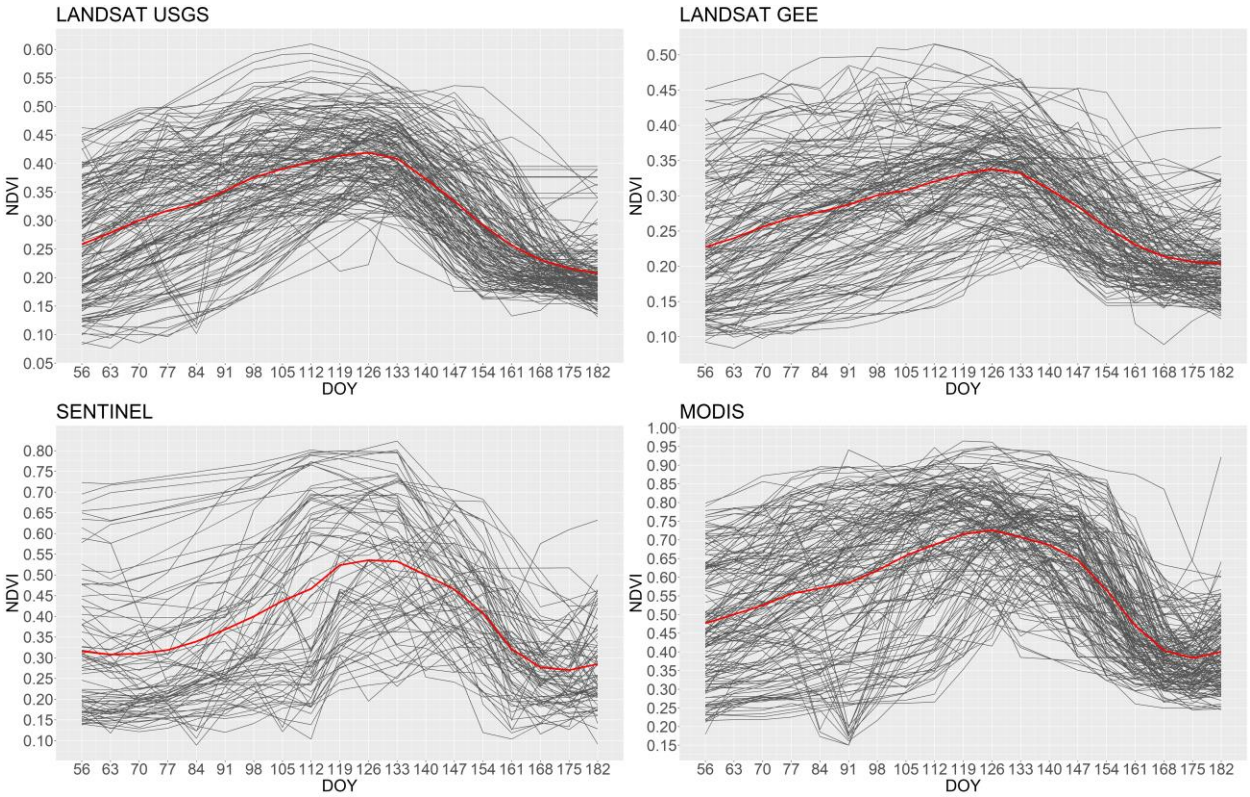

Figure 2-4 -Landsat USGS, Landsat GEE and MODIS NDVI time series profiles are shown for the 2016-2018 Kansas field samples (n=160). Sentinel NDVI time series profiles are shown for the 2017-2018 Kansas field samples (n=80). The red line represents the NDVI time-series average values.

Vegetation peak was noticed between DOY 119 and 133 (second half of Apr, usually when anthesis occurs), whereas ripening and harvest happened between DOY 154 and 168 (end of May to first half of June). Table 2-2 shows the descriptive statistics between DOY when simulated anthesis occurred and the NDVI peak DOY for each field by sensor. The average for simulated anthesis occurred in DOY 129, comparing to Landsat USGS, MODIS and GEE the average was earlier DOY 119, 124 and 122 respectively. Sentinel showed the most approximated result with mean DOY 131. Figure 2-5 shows the relationships between DOY simulated anthesis and DOY with the peak NDVI DOY for each field. R^2 ranged from 0.16 to 0.21 but with a significant relationship. Sentinel showed the highest relationship (R^2 =0.22) with the DOY simulated anthesis.

Table 2-2- Descriptive statistics of DOY when simulated anthesis occurred and DOY when the peak NDVI occurred for each field.

	Anthesis	***Vegetation peak DOY***			***Anthesis***	***Vegetation peak DOY***
Descriptive Statistics	*Simulated (N=160)*	Landsat USGS	MODIS	Landsat GEE	*Simulated (N=80)*	Sentinel
Min	*96*	70	77	56	*98*	105
Median	*132*	126	122.5	126	*134*	133
Mean	*129.2*	119.7	124.2	122.1	*130.8*	131
Max	*163*	182	182	182	*163*	182

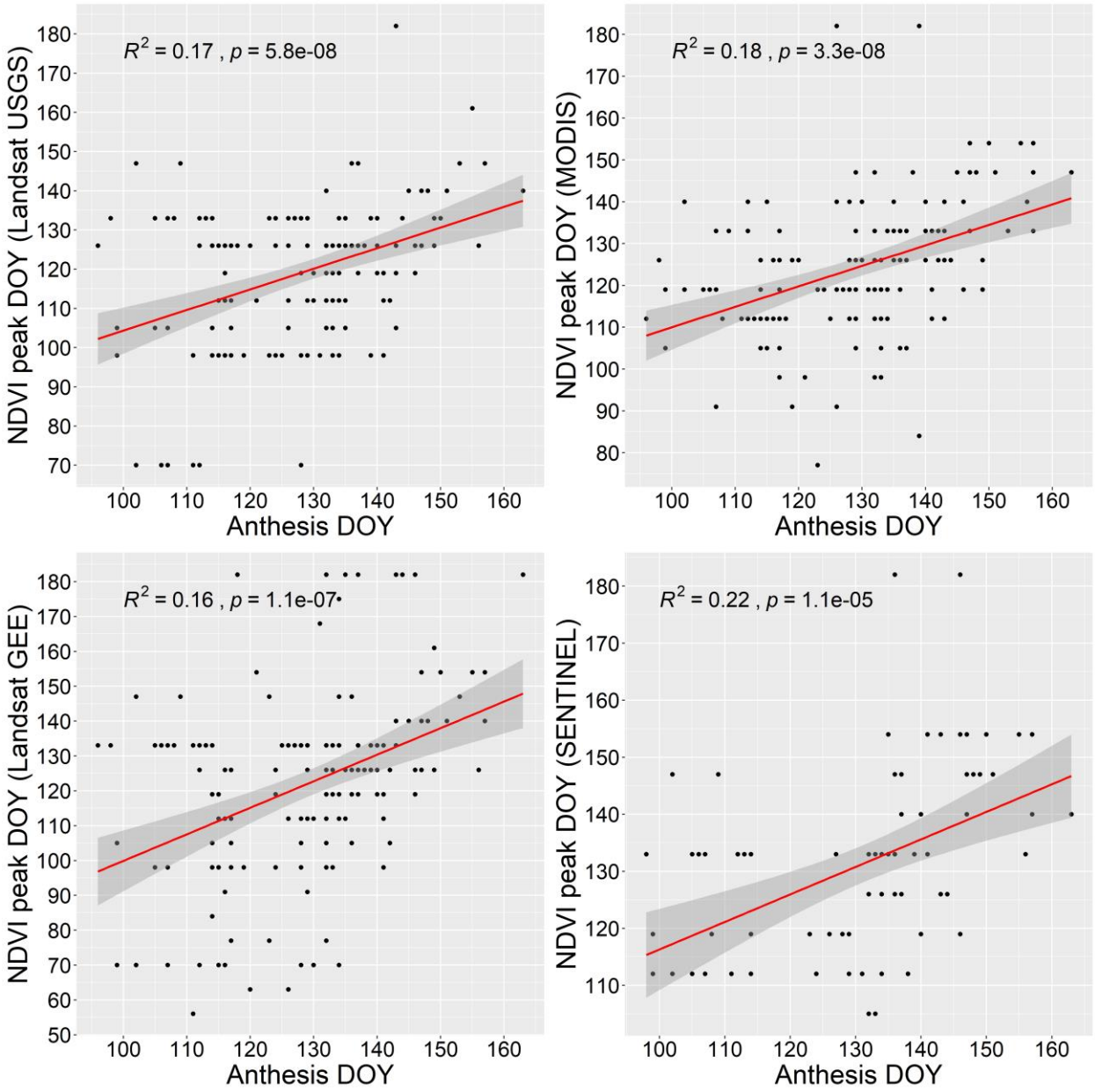

Figure 2-5 - Relationships between DOY when the peak NDVI occurred versus the DOY when simulated anthesis occurred for each field.

Figure 2-6 shows box plots illustrating yield and NDVI AUC distributions from 2016 to 2018. Large differences in wheat yields were observed from 2016 to 2018, yields were the highest in 2016 with a median of 4.57 Mg ha^{-1}, followed by 2017 with median yields of 4.03 Mg

ha^{-1}, and finally 2018, with median yields of 3.02 Mg ha^{-1}. Median yields and standard deviation from 2016 to 2018 was 3.90 Mg ha^{-1} and 1.18 Mg ha^{-1}. The variation in NDVI AUC across the years corroborates with the variation in winter wheat yields, as it was the highest in 2016 for all sensors and lowest in 2018.

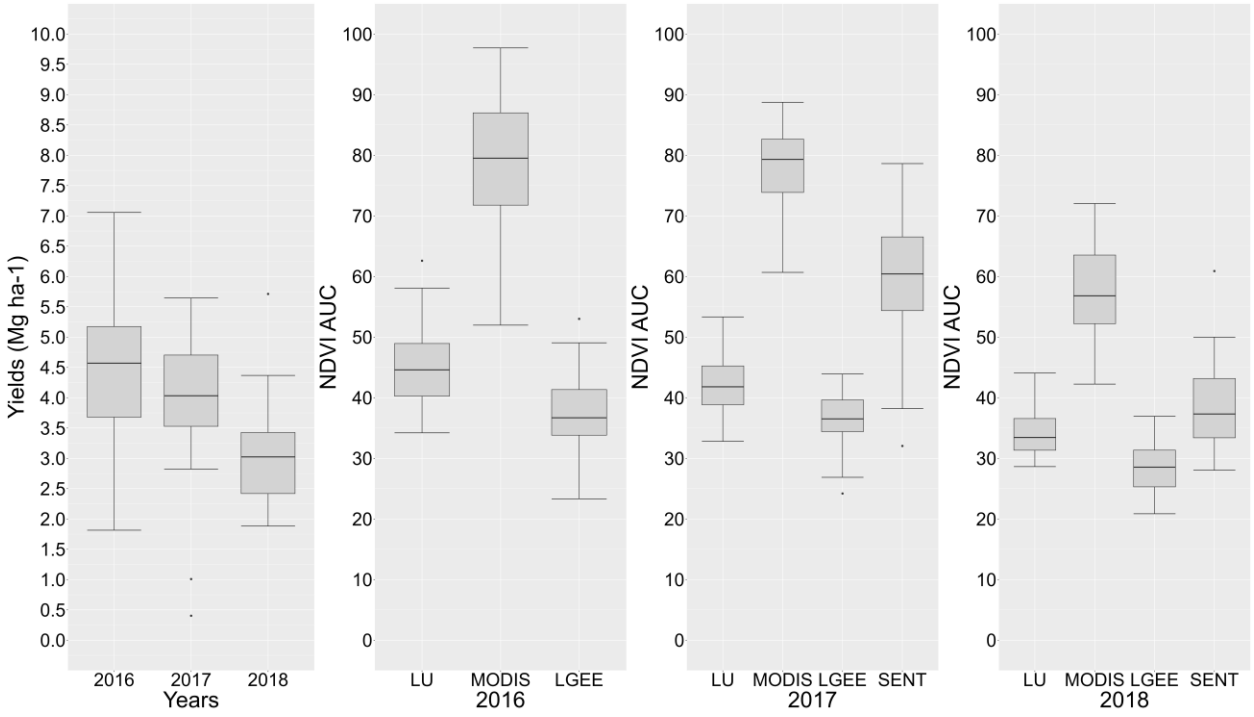

Figure 2-6 - Boxplot of winter wheat yield and NDVI AUC from 2016 to 2018. LU, LGEE and SENT refer to Landsat USGS, Landsat GEE and Sentinel, respectively.

2.3.2. Sensors estimation yield performance using Linear Regresson (LR) and Random Forest (RF) with LASSO and coefficient analysis

To compare how much LASSO improved the linear regression and RF model, Table 2-3 shows the training and testing dataset results from both models without the aid of LASSO. The results showed overfitting in the linear regression, especially in the RF model. The cross-validation results from RF were compared to the in-sample prediction RSME using all dataset, suggesting great overfitting in the RF model**.** MODIS had the best fit in the interval DOY 105-154 using linear regression with R^2 of 0.37 and RMSE of 0.96 Mg ha^{-1} in the training dataset and

R^2 of 0.37 and RMSE of 0.97 Mg ha^{-1}, mainly due to a higher degree of freedom, i.e., a smaller number of predictors by observations compared to interval DOY 56-182.

Table 2-3- Descriptive statistics of training dataset and testing dataset using Linear Regression and Random Forest without LASSO.

Linear Regression									
Intervals		**Landsat USGS**		**MODIS**		**Landsat GEE**		**Sentinel**	
	Metrics	**Train**	**Test**	**Train**	**Test**	**Train**	**Test**	**Train**	**Test**
DOY 56-182	R^2	0.406	0.303	0.399	0.316	0.326	0.2	0.436	0.236
	RMSE(Mg ha^{-1})	0.972	1.04	0.977	1.024	1.036	1.13	0.942	1.132
DOY 105-154	R^2	0.377	0.346	0.369	0.369	0.221	0.19	0.112	0.16
	RMSE(Mg ha^{-1})	0.961	0.98	0.964	0.968	1.076	1.103	1.042	1.06
Random Forest									
Intervals		**Landsat USGS**		**MODIS**		**Landsat GEE**		**Sentinel**	
	Metrics	***In-sample***	**Test**	***In-sample***	**Test**	***In-sample***	**Test**	***In-sample***	**Test**
DOY 56-182	R^2	0.914	0.322	0.915	0.298	0.933	0.191	0.936	0.253
	RMSE (Mg ha^{-1})	0.432	0.993	0.432	1.017	0.461	1.088	0.439	1.01
DOY 105-154	R^2	0.905	0.289	0.906	0.308	0.913	0.167	0.907	0.212
	RMSE (Mg ha^{-1})	0.461	1.024	0.446	1.011	0.492	1.108	0.484	1.058

Figure 2-7 and Figure 2-8 shows the statistical performance of each sensor using linear regression and RF without LASSO. In the interval DOY 56-182, RF presented slightly higher R^2, and the lower RMSE and MAE among sensors than linear regression. Landsat USGS presented the highest R^2 0.32, lowest prediction error RMSE of 0.99 Mg ha^{-1} and MAE of 0.79 Mg ha^{-1} in the RF model. In the linear regression model, MODIS presented the highest R^2 0.32 and lowest prediction error with RMSE of 1.02 Mg ha^{-1} and MAE of 0.79 Mg ha^{-1}. In the interval DOY 105 -154, MODIS presented the highest R^2 of 0.37 and lowest prediction error with a RMSE of 0.97

Mg ha^{-1} using linear regression. Sentinel and Landsat GEE presented the lowest R^2 (< 0.25) and the largest prediction errors with RMSE higher than 0.98 Mg ha^{-1} when predicting winter wheat yields in both intervals.

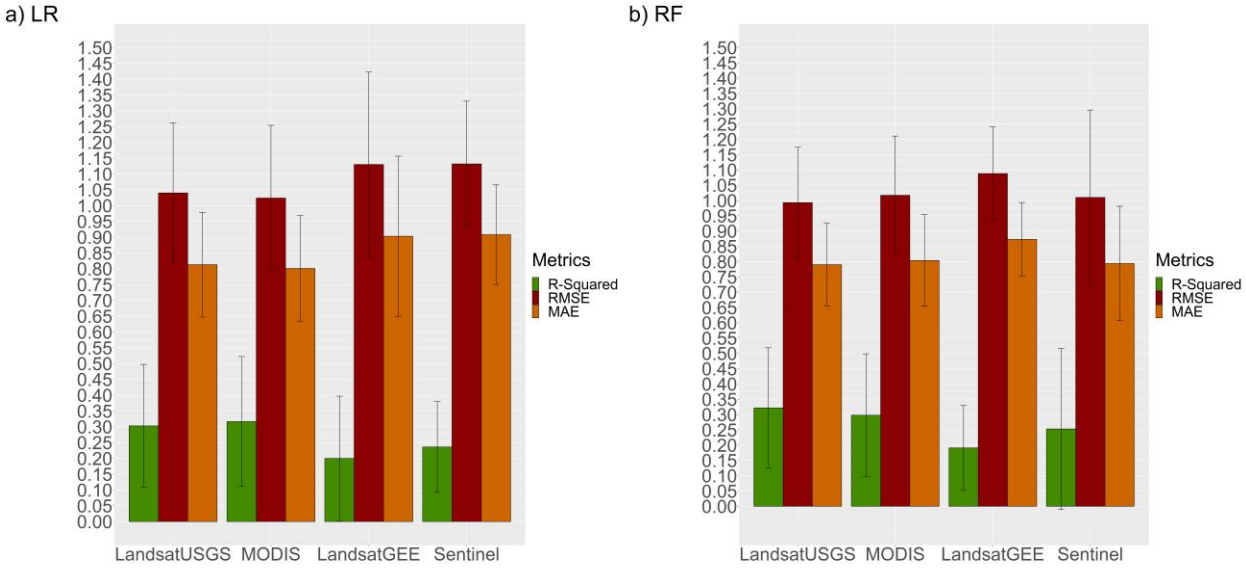

Figure 2-7- Statistical performance of each sensor using Linear Regression (LR) and Random Forest (RF) without using LASSO during the interval DOY 56-182.

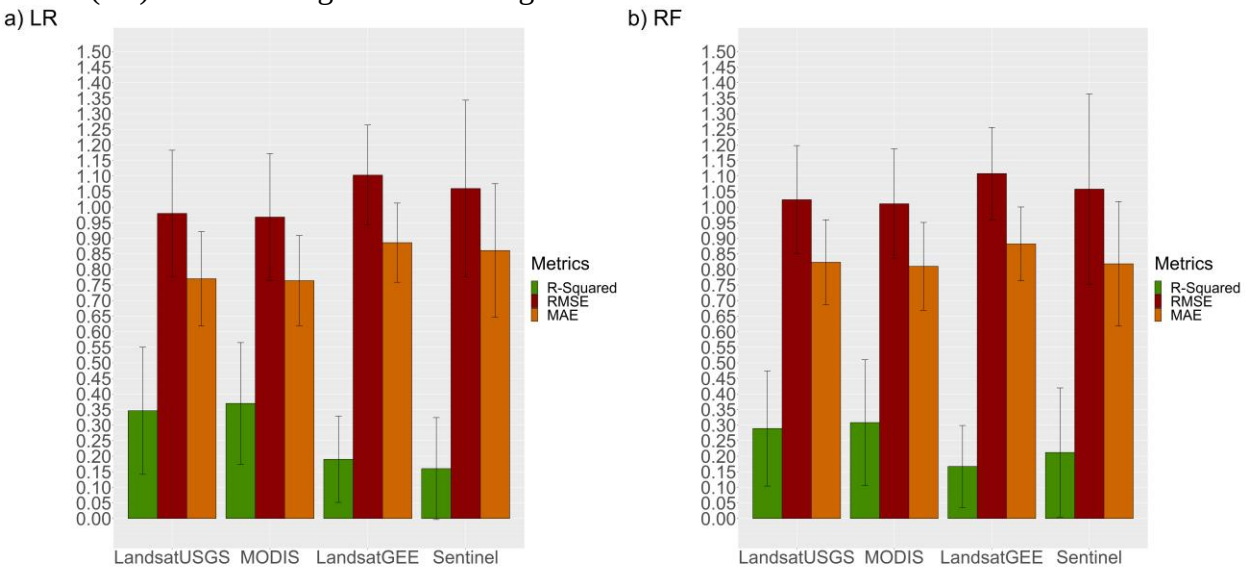

Figure 2-8 - Statistical performance of each sensor using Linear Regression (LR) and Random Forest (RF) without using LASSO during the interval DOY 105-154.

2.3.3. LASSO feature selection and coefficient analysis

The NDVI predictor variables included in the final model are shown in the tables (Table 2-4 to Table 2-17). For each sensor there is first a table showing the regression coefficients from NDVI predictor variables selected by LASSO. A second table presents regression coefficients from NDVI predictor variables included in the linear regression and RF prediction model. The NDVI predictor variables were selected by t-value score, p-value, residual error and coefficient of estimation analysis. . In addition, in some cases, the selection was made by analyzing if the addition or removal of a variable could improve the results. In the interval DOY 56-182, Landsat USGS NDVI predictor variables DOY 56 and NDVI 154 presented the highest significance and were included in the final models. With smaller significance compare to NDVI DOY 56 and NDVI 154, NDVI DOY 133 was also included since its addition improved the regression results (Table 2-4 and Table 2-5). For MODIS, NDVI DOY 98 presented the lowest significance and it was the only predictor variable removed, predictor variables NDVI DOY 91, DOY 105, DOY 140, DOY 154 were included in the linear and RF models (Table 2-6 and Table 2-7). NDVI predictor variables included in the final model from Sentinel were NDVI DOY 147 and DOY 182. Although with lower significance than DOY 182, when DOY 147 was removed, the model showed a higher residual standard error (Table 2-8 and Table 2-9).

For NDVI Landsat GEE (Table 2-10 and Table 2-11), NDVI DOY 147 showed the highest significance. NDVI DOY 147, NDVI DOY 168, and NDVI DOY 84 achieved the lowest residual error and highest R^2 and were included in the final models.

Table 2-4-Regression coefficients from Landsat USGS NDVI predictor variables selected by LASSO

	Estimate	**Std.Error**	**t value**	**Pr(>|t|)**
(Intercept)	0.082	0.526	0.157	0.875
AUC	0.013	0.032	0.434	0.664
DOY56	3.647	1.618	2.253	0.025
DOY133	2.418	2.389	1.012	0.313
DOY154	4.626	1.547	2.991	0.003
Residual standard error	0.963			
R²	0.354		***p-value***: <.001	

Table 2-5 - Regression coefficients from Landsat USGS NDVI predictor variables used in the linear regression and RF models

Final model predictors	**Estimate**	**Std.Error**	**t value**	**Pr(>|t|)**
(Intercept)	0.146	0.504	0.291	0.771
DOY56	4.226	0.916	4.612	<.001
DOY 133	3.081	1.834	1.680	0.094
DOY154	4.948	1.354	3.653	<.001
Residual standard error	0.961			
R²	0.353		***p-value***: <.001	

Table 2-6-Regression coefficients from MODIS NDVI predictor variables selected by LASSO.

	Estimate	**Std.Error**	**t value**	**Pr(>|t|)**
(Intercept)	1.045	0.696	1.5	0.135
DOY91	0.927	1.627	0.57	0.569
DOY98	0.710	2.743	0.259	0.796
DOY105	0.740	1.626	0.455	0.649
DOY140	1.372	1.164	1.178	0.240
DOY154	1.682	0.926	1.815	0.071
DOY182	-1.166	0.893	-1.306	0.193
Residual standard error	0.983			
R²	0.336		***p-value***: <.001	

Table 2-7-Regression coefficients from MODIS NDVI predictor variables used in the linear regression and RF models.

Final model predictors	**Estimate**	**Std.Error**	**t value**	**Pr(>|t|)**
(Intercept)	1.016	0.685	1.482	0.140
DOY91	1.295	0.790	1.638	0.103
DOY105	1.079	0.959	1.125	0.262
DOY140	1.403	1.155	1.215	0.226
DOY154	1.679	0.924	1.818	0.071
DOY182	-1.141	0.885	-1.289	0.199
Residual standard error	0.980			
R²	0.336		***p-value***: <.001	

Table 2-8- Regression coefficients from Sentinel NDVI predictor variables selected by LASSO

	Estimate	**Std.Error**	**t value**	**Pr(>|t|)**
(Intercept)	3.392	0.564	6.014	<.001
DOY140	1.192	1.8	0.662	0.509
DOY147	1.222	1.999	0.611	0.542
DOY182	-3.718	1.182	-3.145	0.002
Residual standard error	0.990			
R²	0.197		***p-value***: <.001	

Table 2-9- Regression coefficients from Sentinel NDVI predictor variables used in the linear regression and RF models.

Final model predictors	**Estimate**	**Std.Error**	**t value**	**Pr(>|t|)**
(Intercept)	3.529	0.522	6.749	<.001
DOY147	2.386	0.944	2.526	0.013
DOY182	-4.019	1.086	-3.699	<.001
Residual standard error	0.987			
R²	0.192		***p-value***: <.001	

Table 2-10 - Regression coefficients from Landsat GEE NDVI predictor variables selected by LASSO

	Estimate	**Std.Error**	**t value**	**Pr(>|t|)**
(Intercept)	1.961	0.624	3.143	0.002
DOY56	0.933	2.132	0.438	0.662
DOY84	2.472	6.590	0.375	0.708
DOY91	-1.025	5.924	-0.173	0.862
DOY147	9.284	1.822	5.094	<.001
DOY175	1.727	4.508	0.383	0.702
DOY168	-7.590	4.501	-1.686	0.093
Residual standard error	1.053			
R²	0.238		***p-value***: <.001	

Table 2-11- Regression coefficients from Landsat GEE predictor variables used in the linear regression and RF models.

Final model predictors	**Estimate**	**Std.Error**	**t value**	**Pr(>|t|)**
(Intercept)	2.068	0.544	3.799	<.001
DOY84	2.201	1.092	2.016	0.045
DOY147	9.013	1.727	5.218	<.001
DOY168	-6.1	2.115	-2.883	0.004
Residual standard error	1.044			
R²	0.236		***p-value***: <.001	

For interval DOY 105-154, NDVI predictor variables used for Landsat USGS in the linear regression and RF models were NDVI DOY 105 and DOY 154 (Table 2-12 and Table 2-13). NDVI DOY 133 was removed since NDVI predictor variables DOY 105 and DOY 154 presented a lower prediction error in the final models. As seen in Landsat USGS, MODIS NDVI predictor variable DOY 105 showed a high statistical relevance among the other variables, the predictor variables included in the models were DOY 105 and DOY 154 (Table 2-14 and Table 2-15). Sentinel NDVI predictors from LASSO were kept the same in the final models (Table 2-16) . Among all sensors Sentinel NDVI predictor variables in the interval DOY 105-154 were the only ones that did not show significant relationship with yields. NDVI Landsat GEE predictor variables DOY 105 and DOY 147 used in the final model were the same as the ones selected from LASSO (Table 2-17).

Table 2-12- Regression coefficients from Landsat USGS NDVI predictor variables selected by LASSO.

	Estimate	**Std.Error**	**t-value**	**Pr(>|t|)**
(Intercept)	0.0317	0.519	0.061	0.951
DOY105	4.485	1.278	3.508	<.001
DOY133	2.538	2.131	1.191	0.235
DOY154	3.844	1.335	2.88	0.004
Residual standard error	0.986			
R²	0.319		***p-value***: <.001	

Table 2-13 - Regression coefficients from Landsat USGS NDVI predictor variables used in the linear regression and RF models.

	Estimate	**Std.Error**	**t-value**	**Pr(>|t|)**
(Intercept)	0.379	0.430	0.883	0.379
DOY105	5.477	0.971	5.637	<.001
DOY154	4.879	1.015	4.804	<.001
Residual standard error	0.987			
R²	0.313		***p-value***: <.001	

Table 2-14- Regression coefficients from MODIS NDVI predictor variables selected by LASSO.

	Estimate	**Std.Error**	**t-value**	**Pr(>|t|)**
(Intercept)	0.209	0.473	0.442	0.658
DOY105	2.541	0.531	4.782	<.001
DOY140	1.684	1.127	1.494	0.137
DOY154	1.597	0.902	1.769	0.078
Residual standard error	0.990			
R²	0.313		***p-value:*** <.001	

Table 2-15- Regression coefficients from MODIS NDVI predictor variables used in the linear regression and RF models.

Final model predictors	**Estimate**	**Std.Error**	**t-value**	**Pr(>|t|)**
(Intercept)	0.519	0.427	1.215	0.226
DOY105	2.934	0.463	6.329	<.001
DOY154	2.635	0.578	4.554	<.001
Residual standard error	1.038			
R²	0.107		***p-value***: <.001	

Table 2-16- Regression coefficients from Sentinel NDVI predictor variables selected by LASSO and used in the linear regression and RF models.

Final model predictors	**Estimate**	**Std.Error**	**t-value**	**Pr(>|t|)**
(Intercept)	2.352	0.460	5.103	<.001
DOY112	0.924	0.719	1.286	0.202
DOY140	1.432	1.192	1.201	0.234
Residual standard error	1.086			
R²	0.168		***p-value***: 0.08	

Table 2-17- Regression coefficients from Landsat GEE NDVI predictor variables selected by LASSO and used in the linear regression and RF models.

Final model predictors	**Estimate**	**Std.Error**	**t-value**	**Pr(>|t|)**
(Intercept)	1.284	0.478	2.686	0.008
DOY105	2.831	1.120	2.527	0.012
DOY147	6.265	1.530	4.093	<.001
Residual standard error	0.990			
R²	0.313		***p-value***: <.001	

2.3.4. Winter wheat yield estimation by sensor using Linear Regresson (LR) and Random Forest (RF).

Table 2-18 shows the descriptive statistics of training dataset and testing dataset using linear regression and RF with the feature selection from LASSO. Surprisingly, satellite sensors NDVI predictor variables performed better using the linear regression model than RF in both intervals. The results show a decrease in prediction error in both models and reduced overfitting in linear regression. Although showing high RMSE and moderate R^2, Landsat USGS presented the best model fit among all the sensors in both intervals. With training R^2 of 0.35 and testing R^2

of 0.37 and training RMSE of 0.96 Mg ha^{-1} and RMSE of 0.95 Mg ha^{-1} using NDVI predictor variables in the interval DOY 56-182, and training R^2 of 0.31 and testing R^2 of 0.34 and training RMSE of 0.98 Mg ha^{-1} and RMSE of 0.976 Mg ha^{-1} using NDVI predictor variables in the interval DOY 105-154. Sentinel and Landsat GEE presented the largest discrepancies between train and test results.

Table 2-18- Descriptive statistics of training dataset and testing dataset using Linear Regression and Random Forest using LASSO.

Linear Regression									
Intervals		**Landsat USGS**		**MODIS**		**Landsat GEE**		**Sentinel**	
	Metrics	**Train**	**Test**	**Train**	**Test**	**Train**	**Test**	**Train**	**Test**
DOY 56-182	R^2	0.353	0.377	0.33	0.354	0.198	0.257	0.236	0.281
	RMSE(Mg ha^{-1})	0.961	0.953	0.981	0.977	0.99	1.044	1.045	0.971
DOY 105-154	R^2	0.313	0.345	0.295	0.342	0.168	0.204	0.107	0.219
	RMSE(Mg ha^{-1})	0.987	0.976	0.994	0.981	1.086	1.08	1.038	1.019
Random Forest									
Intervals		**Landsat USGS**		**MODIS**		**Landsat GEE**		**Sentinel**	
	Metrics	***In-sample***	**Test**	***In-sample***	**Test**	***In-sample***	**Test**	***In-sample***	**Test**
DOY 56-182	R^2	0.865	0.326	0.892	0.318	0.883	0.191	0.842	0.267
	RMSE(Mg ha^{-1})	0.505	0.991	0.479	0.998	0.545	1.08	0.534	1.007
DOY 105-154	R^2	0.847	0.264	0.863	0.273	0.868	0.149	0.845	0.15
	RMSE(Mg ha^{-1})	0.526	1.060	0.509	1.037	0.556	1.121	0.564	1.101

Figure 2-9 shows the statistical performance of each sensor using linear regression and RF during the interval DOY 56 -182. Landsat USGS presented the best performance (R^2 0.37, RMSE 0.95 Mg ha^{-1}, MAE 0.75 Mg ha^{-1}) among the other sensors using linear regression using the NDVI predictor variables DOY 56, DOY 133 and DOY 154. MODIS presented the second-best performance with R^2 0.35, RMSE 0.97 Mg ha^{-1}, MAE 0.77 Mg ha^{-1}. MODIS NDVI predictor variables used were DOY 91, DOY 105, DOY 140, DOY 154. Landsat GEE and

Sentinel presented the lowest performance with a R^2 0.25, RMSE 1.04 Mg ha^{-1}, MAE 0.84 Mg ha^{-1} and a R^2 0.28, RMSE 0.97 Mg ha^{-1}, MAE 0.78 Mg ha^{-1}, respectively.

In the same interval (Figure 2-9) the RF model showed a similar ranking of sensor performance, but overall reduced prediction accuracy than linear regression. Landsat USGS showed the highest R^2 of 0.32 and lowest prediction error (RMSE 0.99 Mg ha^{-1}) in the interval DOY 56-182. Again, MODIS showed the second-best performance with R^2 0.31, RMSE 0.99 Mg ha^{-1}, MAE 0.78 Mg ha^{-1}. Landsat GEE and Sentinel presented the lowest performance with a R^2 0.19, RMSE 1.08 Mg ha^{-1}, MAE 0.87 Mg ha^{-1} and a R^2 0.26, RMSE 1 Mg ha^{-1}, MAE 0.78 Mg ha^{-1}, respectively.

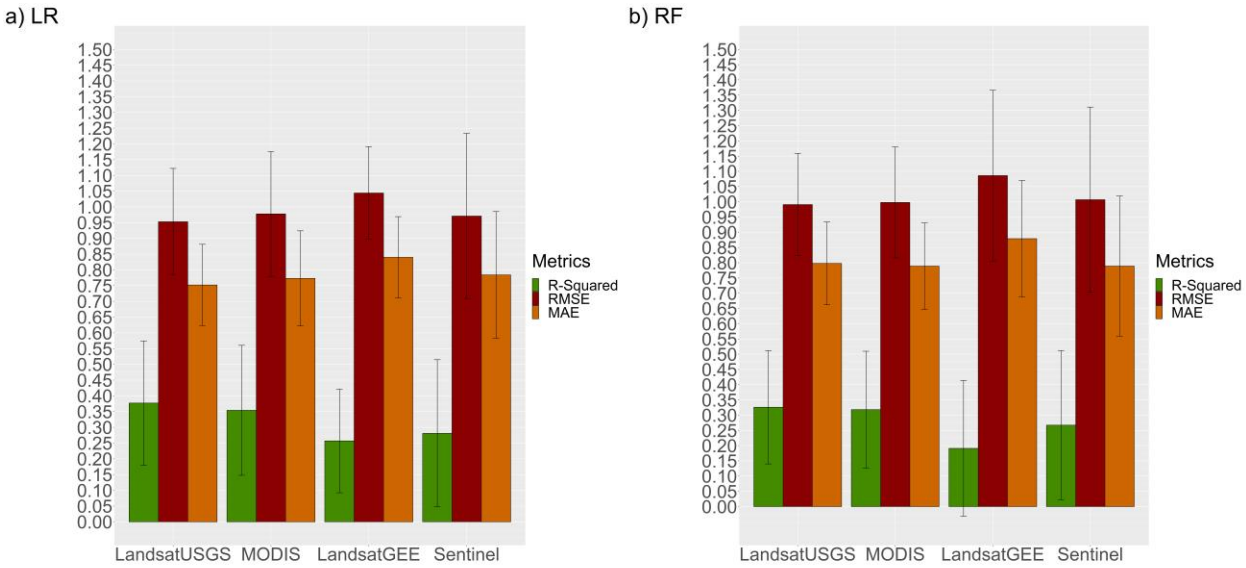

Figure 2-9 Statistical performance of each sensor using Linear Regression (LR) and Random Forest (RF) during the interval DOY 56-182**.** Error bars represent the standard devaition from CV results.

In interval DOY 154-105 (Figure 2-10), the linear regression attained the best results compared to RF. With the linear regression model, NDVI Landsat USGS achieved the best performance with a R^2 of 0.34, RMSE 0.97 Mg ha^{-1} and 0.77 Mg ha^{-1}, using NDVI predictor

variables DOY 105 and DOY 154. MODIS have the second-best result, with a R^2 of 0.34, RMSE of 0.98 Mg ha^{-1} and MAE 0.77 Mg ha^{-1}, using NDVI predictor variables DOY 105 and DOY 154. Landsat GEE and Sentinel presented the lowest performance, with a R^2 0.20, RMSE 1.08 Mg ha^{-1} and MAE 0.86 Mg ha^{-1} and R^2 of 0.21, RMSE of 1.01 Mg ha^{-1} and MAE of 0.79 Mg ha^{-1}, respectively.

RF results in interval DOY 105-154 showed that MODIS achieved the highest R^2 0.27 and the lowest RMSE of 1.03 Mg ha^{-1} and MAE 0.80 Mg ha^{-1}, followed by Landsat USGS with a R^2 of 0.26, RMSE of 1.06 Mg ha^{-1} and MAE 1.03 Mg ha^{-1}. Landsat GEE and Sentinel presented a R^2 of 0.14, RMSE of 1.21 Mg ha^{-1} and MAE 0.91 Mg ha^{-1} and R^2 of 0.15, RMSE of 1.10 Mg ha^{-1} and MAE 1.19 Mg ha^{-1}, respectively showing the lowest performance among all intervals and sensors. RF results indicated a higher standard deviation in Landsat GEE and Sentinel results (except for Landsat GEE in the interval DOY 105-154) compared to Landsat USGS and MODIS in both intervals.

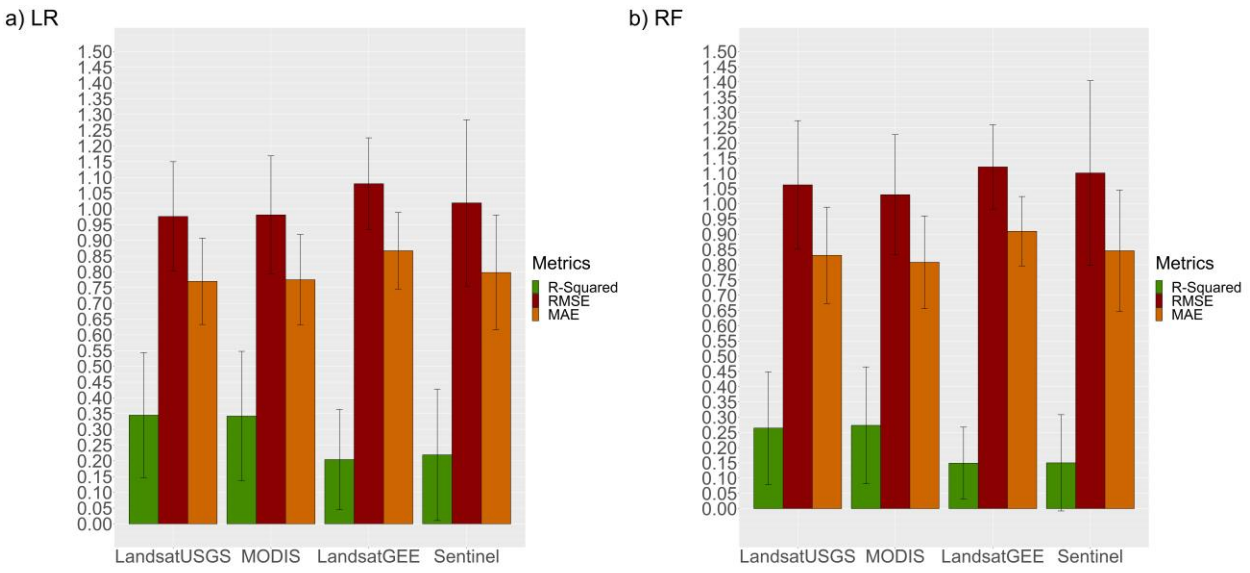

Figure 2-10 Statistical performance of each sensor using Linear Regression (LR) and Random Forest (RF) during the interval DOY 105-154.

2.4. Discussion

The results indicated an agreement between the NDVI time-series profiles and the phenological characteristics (growth stages) of winter wheat in Kansas, especially with Landsat USGS and MODIS. These dynamics include lower crop growth in the February-March timeframe, followed by an increase in crop growth until heading and anthesis, followed by a general decrease in NDVI as the crop senesces (Lollato et al., 2021; Lollato & Edwards, 2015). The yield distributions, including greater 2016 yield, followed by average 2017, and lower 2018, agree with USDA-reported yield data for Kansas (USDA-NASS, 2023a) are were mostly function of different precipitation averages across the state as previously reported (Jaenisch et al., 2021).

New in this study, the NDVI AUC distributions also appeared to behave consistently across the three independent data years and follow those patterns observed in the yield data. NDVI dynamics tracked seasonal changes and aided in monitoring winter wheat growth in

Kansas, agreeing with previous studies (Filippa et al. 2018; Mashonganyika et al. 2021; Wardlow et al. 2007). Compared to the simulated anthesis DOY for each field, the peak of NDVI appeared slightly earlier in the Landsat USGS, Landsat GEE and MODIS time-series, while sentinel mean NDVI peak DOY was the closest to the simulated anthesis DOY. From an agronomical perspective, these results align with curves of nitrogen uptake by the wheat crop which may maximize at anthesis depending on weather conditions during grain fill (Giordano et al., 2023; Lollato et al., 2021).

When observing the NDVI profiles and boxplots, Landsat GEE showed different results from Landsat USGS, with lower NDVI values. Landsat USGS dataset is part of Collection 1 where improvements were made in terms of radiometric and geometric parameters. Landsat GEE dataset is part of the latest improvements in Collection 2 Level-2, and it has improvements in radiometric calibration, enhanced quality assessment bands and atmospheric corrected data. However, the technique for cloud removal applied in the Landsat USGS dataset was different than in Landsat GEE, where we preserved only the pixels attributed to clear conditions as listed in Landsat Collection 1 Level 1 Quality band (USGS, 2023). In the Landsat GEE, a simple masking approach was utilized. This technique has been applied in previous studies using Google Earth Engine (Fink et al., 2022). The masking was based on the respective cloud detection and quality assessment bands where any pixel classified as cloud or cloud shadow was eliminated. The low NDVI values could have occurred by pixels containing atmospheric contamination that were not included in the masking method.

Although Sentinel-2 has the highest spatial resolution (10 m), only 2 fields in the year 2016 matched with the methodology criteria. Until March of 2017, Sentinel 2A was the only satellite in orbit, leaving Sentinel 2 data with a temporal resolution of ten days. The year 2016

(n=80) had the largest number of observations compared to 2017 (n=39) and 2018 (n=40). Thus, Sentinel was disadvantaged in terms of dataset availability. The small dataset 2017 and 2018 may have contributed to the low performance of Sentinel when predicting winter wheat yields compared to the other sensors. NDVI signal variability observed in the Sentinel NDVI time series (Figure 2-4) may be related to the application of the Sentinel 2 cloud mask band (QA60) which has been recently pointed out to underestimate the presence of clouds (Nguyen et al. 2020; Tiede et al. 2021). Overall, the performance of the QA60 cloud mask can be low, especially under critical conditions. These two aspects (data availability and cloud contamination) may explain the Sentinel NDVI poor performance when predicting winter wheat yields.

Regarding the feature selection from LASSO, improvements were observed in most cases, with the increase of R^2 and decrease of RMSE in most all results. In the linear regression, LASSO prevented overfitting and enhanced the model generalization ability in most all cases except using MODIS NDVI predictor variables in the interval DOY 105 to 154. In the RF, LASSO improved the estimation across all sensors in the interval DOY 56 to182. In interval 105-154, the RF model performed better without the feature selection approach.

RF model indicated a poor performance compared to the linear regression model. RF achieved the best performance using Landsat USGS during the interval DOY 56-182, with a RMSE of 0.99 Mg ha^{-1} compared to a RMSE of 0.96 Mg ha^{-1} using linear regression. RF is a non-linear model that handles unbalanced data and overfitting well. Many studies have used non-linear models especially when working with a combination of different types of data (e.g. satellite imagery, climate, soil) to estimating yields (Cai et al., 2019; Evans & Shen, 2021). The reason that the RF model did not show advantage in estimating yields over linear regression may be related to the small dataset in this study and the relationship of sensor NDVI predictor

variables and yields being essentially linear (Johnson et al., 2016). The results of Johnson et al.,(2016) showed that a linear regression using MODIS-NDVI predictor variables to predict barley (*Hordeum vulgare vulgare* L.), canola (*Brassica*) and spring wheat in the Canadian Prairies performed slightly better than non-linear models Bayesian Neural Networks and model-based recursive partitioning. Vannoppen et al., (2020) found similar performance when using only NDVI predictor variables to estimate winter wheat yields in Latvia, where linear regression presented a residual standard error of 0.55 Mg ha^{-1} and RF 0.58 Mg ha^{-1}.

Using the NDVI predictor variables from the interval DOY 56-182 in a linear regression model produced the best results, with Landsat USGS reporting the best performance (R^2 0.37, RMSE 0.95 Mg ha^{-1}, MAE 0.75 Mg ha^{-1}) among the other sensors. The most significant NDVI predictor variables were DOY 56 and DOY 154, with DOY 56 characterizing very early season NDVI and DOY 154 late grain filling stage. The benefit of higher early season NDVI (end of February and mid-March) may be related to different aspects regarding this specific dataset and the wheat crop in general. Regarding this specific dataset, the 2016 season was characterized by temperatures that were mostly above normal all winter, which resulted in an earlier dormancy break and initiation (Paulsen & Heyne, 1983) and sub-regional levels (Lollato et al., 2019; Lollato, Roozeboom, et al., 2020) .Regarding a strong signal of DOY 154 in predicting wheat yield, this reflects wheat growth in early June, where wheat is going through ripening stages of development when the grain test weight is determined and grain moisture decreases (Lollato, 2018). Greater levels of leaf area at this stage – here represented by greater NDVI – may associate with higher wheat yield due to practices associated with stay-green, such as greater N rates and the adoption of foliar fungicides (Cruppe et al., 2021; Jaenisch et al., 2019, 2022).

Disentangling the impacts of management practices on wheat yield and NDVI was beyond the scope of this work.

MODIS was the second most accurate sensor to predict winter wheat yields. The NDVI predictor variables from interval DOY 105-154, without feature selection, appeared to be the best for yield prediction using MODIS. The results showed that MODIS NDVI may perform better during the peak of crop development (i.e., flag leaf emergence, heading, anthesis, and grain filling). Using MODIS and AVHRR, Mkhabela et al., (2011) also found correlation between anthesis and grain filling period NDVI with grain yields. In another study in Argentina, MODIS NDVI during head emergence and anthesis stage appeared to be the best predictor for winter wheat yields (Lopresti et al., 2015). However, besides this individual result, MODIS presented a higher prediction error compared to Landsat USGS when analyzing all approaches and intervals. Coarser pixels, such as those in the MODIS dataset at a scale of 250 m, are often mixed and of questionable utility for field-scale analyses (Li et al. 2021).

MODIS and Sentinel presented 2 coefficients negative regarding the variable DOY 182 (Table 2-7 and Table 2-9), meaning a opposite relationship between NDVI and yields at the end of the season. This issue may be related to an agronomic issue such as the detection of late-emerging weed patches in wheat (Travlos et al., 2021), or noise from neighboring fields if the winter wheat field has a particular small size.

In this study, the lowest prediction error reported was a RMSE of 0.95 Mg ha^{-1} , which can produce uncertainties of winter wheat estimation at field scale. In previous research using Landsat imagery, Gaso et al., (2019) found that fields of smaller size had the highest values of RMSE, probably associated to low number of pixels and possible uncoordinated scales between yield estimated yield and the observed yield in the same grid of satellite image. As a result,

although the winter wheat NDVI signal was different from surrounding areas, they were calculated with neighboring pixels containing different land-uses.

While the results that we obtained were promising n that they suggested a good representation of crop growth and development dynamics by satellite-derived NDVI values, they also reflected the challenge of relatively low yield predictability as addressed in many studies using satellite imagery to estimate yields at field level over large areas (Engen et al., 2021; N. Zhang et al., 2017). We hypothesize that, because Kansas has environmental and agronomic characteristics that contrast among regions (Jaenisch et al., 2021) increasing the spatial heterogeneity of winter wheat yields (Dong et al., 2020), winter wheat yield variability was not fully captured by NDVI and it may require finer spatial information regarding climate, soil characteristics, used wheat varieties, and management practices to better represent yield at the field level. Another limitation was not fully exploring the higher temporal and spatial resolution from Sentinel-2 AB due to the dataset unavailability in 2016. In the future, adding new winter wheat field-yields in the dataset may improve the linear and RF algorithms.

Chapter 3 - Improving winter wheat yield estimation at field scale using Normalized Vegetation Difference Index metric from Landsat-8 OLI by homogenous subregions in Kansas, USA.

3.1. Introduction

Understanding the spatial differences of winter wheat yields (*Triticum aestivum* L.) and the environmental influencing factors are of great significance in increasing regional crop yields, promoting sustainable development of regional agriculture, and ensuring regional and national food security. Kansas is the largest winter wheat producing state in the U.S (Kansas Department of Agriculture, 2021) with the majority of wheat production located from central to western Kansas. The climate across these areas are affected by different physical features, including elevation, natural latitudinal and longitudinal gradients in temperature, precipitation and atmospheric evaporative demand (Lollato et al., 2017, 2020), proximity to lakes and rivers, and topography. The eastern part of the state is characterized by moderate elevations and abundant precipitation (more than 1,000 mm of annual precipitation) conditions of the lower Missouri basin and the western region by the drier High Plains lying along the eastern slope of the Rockies (with less than 500 mm of annual precipitation (Flora, 1948).

Since the environmental properties of agricultural areas in Kansas are heterogeneous, the growing condition for crops and the associated management practices adopted by producers can be highly variable (Jaenisch et al., 2021). The accurate yield information becomes indispensable and a challenge in major producing areas with high variable weather conditions (Kang et al., 2009). Currently, national and regional crop yield statistics are the commonly used to monitor

and evaluate causes of crop yield change, where the yield information is often collected by costly and time-consuming annual surveys, with limited spatial resolution and temporal frequency (Vannoppen & Gobin, 2021).

Satellite remote sensors offer a timely and cost-effective means of estimating the yield potential and understanding spatial-temporal yield variability enhancing the local, regional, and national production and helping to reduce environmental impacts (Evans & Shen, 2021). In addition, satellite remote sensor data has attracted attention by its capability in monitoring and mapping vegetation enabling the analysis of vegetation dynamics, such as phenological stages of crop development and the seasonal growth of crop types over different scales (Siachalou et al., 2015)

There are many choices of data sources estimation, ranging from handheld radiometers to drones, airborne and satellite platforms. High resolution sensors such as handheld radiometers, drones, airborne, and recently satellite sensors such as Quick Bird, SPOT5, Planet provide very fine details of crop growth monitoring and yield estimation within-field (Houborg & McCabe, 2016; Yang et al., 2009), however data processing may be costly and computationally intensive limiting their general use (Dorigo et al., 2007). Coarse resolution from MODIS (250m-1km) provides valuable historical dataset (17 years) and daily temporal resolution, key for regional, national, and global crop monitoring. However, the main drawback is that MODIS pixels has limited representative of finer pixels due saturation of mixed reflective signals, especially when investigating variability of crop yield at field (He et al., 2018; Meng et al., 2021; Zhang et al., 2019).

For instance, due to its moderate spatial resolution (10m - 30m) satellite sensors such as the Landsat series and Sentinel- 2 products have been commonly used in studies at field scale

across large areas (Fieuzal et al., 2020; Skakun et al., 2017). With global coverage at 30m resolution which is sufficient for within field monitoring, Landsat series has free availability and long-term record remote sensing data dating back to 1982 (Belward & Skøien, 2015). Sentinel-2 had its first satellite launched in June 2015 and its second in March 2017, both with a spatial resolution at 10m and revisit time of 10 days (resulting in 5 days), providing more opportunities in crop monitoring and yield estimation at a finer spatial-temporal resolution than Landsat (Sudmanns et al., 2020). Thus, Sentinel -2 AB are available for Kansas only since 2017 and cannot be used to produce long-term time series, its dataset availability and usability will depend on the period analyzed (Shen & Evans, 2021) .

Vegetation indices (VI's) derived from satellite data are the most used parameters to estimate yields due to their relationship to canopy architecture, biomass, and chlorophyll content (Moriondo et al., 2007; Shen & Evans, 2021). Among different vegetation indices, the normalized difference index (NDVI) is frequently used for crop growth and yield related research since is associated to crop net primary production, which can be defined as the amount of carbon taken by plants to create new biomass (Jiao et al., 2017; Parece & Campbell, 2017).

Methods to estimate crop yield using remote sensing data are diverse but empirical models and mechanistic models are the most commonly used in the literature (Gaso et al., 2019; Kern et al., 2018; Landau et al., 2000; Palosuo et al., 2011; Yao et al., 2015). Mechanistic models use weather, soil, crop, management information and vegetation indices as parameters to simulate plant development and growth. Aboveground biomass and grain yield are output variables of crop simulation models (Basso & Liu, 2019b). The main drawback of these models is that they require numerous crop specific inputs to simulate crop development. Empirical models don't require parameters from underlying plant biophysical mechanisms that drive crop

growth, instead, these are based on empirical relationships between historic yields and vegetation indices or other independent variables (Becker-Reshef, Vermote, et al., 2010; Johnson et al., 2021). The relationship between the predictor variables and the outcomes have traditionally been explored through linear regression, but non-linear approaches, such as machine learning (e.g., artificial neural network, support vector machine or random forest) can also be used too (Joshil Raj & SivaSathya, 2014; Lee et al., 2020). A fundamental requirement for the empirical approach is access to reliable and deep historical yield datasets, thus the limiting factor of empirical crop yield models is that it cannot be easily extrapolated to other areas (Schwalbert et al., 2018).

Crop yield models are challenged by very heterogeneous geographic areas, in this case, it is often necessary to recognize homogeneous areas with comparable initial conditions and parameters values (Gaso et al., 2019). Zonal schemes (FAO, 1978) such as agro-climatic crop zones (CZs) based on homogeneity in weather variables that have greatest influence on crop growth and yield, and agro-ecological zones (AEZs) based on geographic regions with similar climate and soils for agriculture have been used in several studies. For instance, CZs and AEZs have helped in identifying yield variability (Kouadio et al., 2014) and limiting factors for crop growth (Nabati et al., 2020), regionalize optimal crop management recommendations (Di Mauro et al., 2018; Heinemann et al., 2016), compare yield trends (Gupta & Mishra, 2019), determine suitable locations for new crop production technologies (Řezník et al., 2020; Taghizadeh-Mehrjardi et al., 2020), to maximize the impact of research and development efforts while minimizing costs(Rattalino Edreira et al., 2018), and to analyze impacts of climate change on agriculture (Fischer et al., 2005; Larina et al., 2022).

Long term weather data has been used to subdivide regions in crops grown in areas with smaller year-to-year variation (van Wart et al., 2013) For crops grown in regions with small year-to-year variability in gran yield, such as soybeans (*Glycine max* L.) in North Central U.S.A, this regional subdivision has accounted for up to 96% of the yield variability (Rattalino Edreira et al., 2017) .Kouadio et al., (2014) reduced 40% of mean absolute percentage error (MAPE) when forecasting winter wheat in Canada using MODIS NDVI and EVI and agroclimatic variables by ecodistricts (areas with distinct climate, soil, landscape, and ecological aspects). However, the same performance is unlikely to occur for crops grown in less predictable environments such as winter wheat in the U.S Great Plains, where the clustering based on long term annual weather only accounted for 46% of the yield variability (Jaenisch et al., 2021)

Recently some studies have tried to address this issue related to crops grown in heterogeneous environments, Chen et al., (2018) analyzed the similarity of phenological stages (dates of green-up and heading) using remote sensing data among winter wheat fields to subdivide a heterogeneous region in the North China Plain and improve regional winter wheat yield estimation data. Grouping crop fields into distinct levels of management adoption also helped identifying the causes of yield gap in a data-rich analysis in central Argentina (Di Mauro et al., 2018). Along with long-term weather data, sub-region specific management factors (e.g. seeding rate, previous crop and sowing date) were found important in determining winter wheat yield in Kansas (Jaenisch et al., 2021; Munaro et al., 2020). For example, in Kansas the range in sowing dates varies from an early and short sowing period in cooler, semi-arid, high altitude subregions (Northwestern Kansas), to a later and wider sowing period in warmer, subhumid, low altitude regions (South central Kansas) (Munaro et al., 2020). Jaenisch et al., (2021) identified the optimum sowing date of days of the year (DOY) 272, 284, and 268 for North Central (NC),

South Central (SC), and West Kansas; which is similar to optimum sowing date from previous work (275 in NC, 281 in SC, and 271 in the West) (Munaro et al., 2020).

Thus, this work explore the potential of using three subregions in Kansas (North Central, NC; South Central, SC; and West) based on their long-term climatology (long-term annual cumulative growing degree days, aridity index, and temperature seasonality) and regional-specific cropping systems (seeding rate, previous crop and sowing date) elaborated by Jaenisch et al., (2021) to estimate winter wheat yields at field scale. The main objective was to determine if the derived Landsat-8 NDVI estimates into a subregional model can result in improved crop yield estimation for winter wheat in Kansas. The main questions are:

(i) Is the subregional scheme helpful to show the spatial heterogeneity in winter wheat NDVI time-series dynamics in Kansas?

(ii) How much improvement the winter wheat yield models can obtain from a subregional analysis?

3.2 Material and Methods

3.2.1. Study Area

This study focused on central and western Kansas, where winter wheat is the predominant crop grown. Winter wheat is mostly non-irrigated (i.e. rainfed) representing 96 % of the wheat in the region (USDA-NASS, 2019). The climate in Kansas is subhumid in the east and semi-arid in the west (Barrow, 1992). Consequently, there are steep gradients in precipitation, elevation, and temperature across Kansas, with precipitation ranging from ~450 mm in the west and ~1100 mm in the east (Lollato et al., 2020) resulting in winter wheat growing season

precipitation ranging from ~200mm to 650mm. The average growing season temperature ranges from 7 to 12℃ from west to east due to elevation, which ranges from ~200 to 1200 m (Lollato et al., 2017). Common soil textures are silt loam and silty clay loam which possesses ideal qualities of a prairie soil with the best combination of physical and chemical characteristics for growing crops and grasses (USDA NRCS, 1993; USDA-NRCS, 2017)

3.2.2 Datasets

3.2.2.1. Field polygons

Using the survey field-specific geo-coordinates, was collected from a survey conducted by Jaenisch et al., (2021) during three consecutive seasons (i.e. 2016-2018). A total of 656 polygons were created representing the boundaries of each field. To assess the winter wheat field geolocations, the corresponding annual USDA Cropland Data Layer (CDL) datasets was retrieved (USDA National Agricultural Statistics Service Cropland Data Layer, 2023). After removing records that did not correspond with winter wheat in the CDL, 499 samples remained (205 in 2016, 179 in 2017, and 115 in 2018). After applying additional data screening (3.2.3.2. NDVI time series), the final dataset comprised 220 samples (field-yield pairs), with a total area of 87,854,542.5 square km (Figure 3-1).

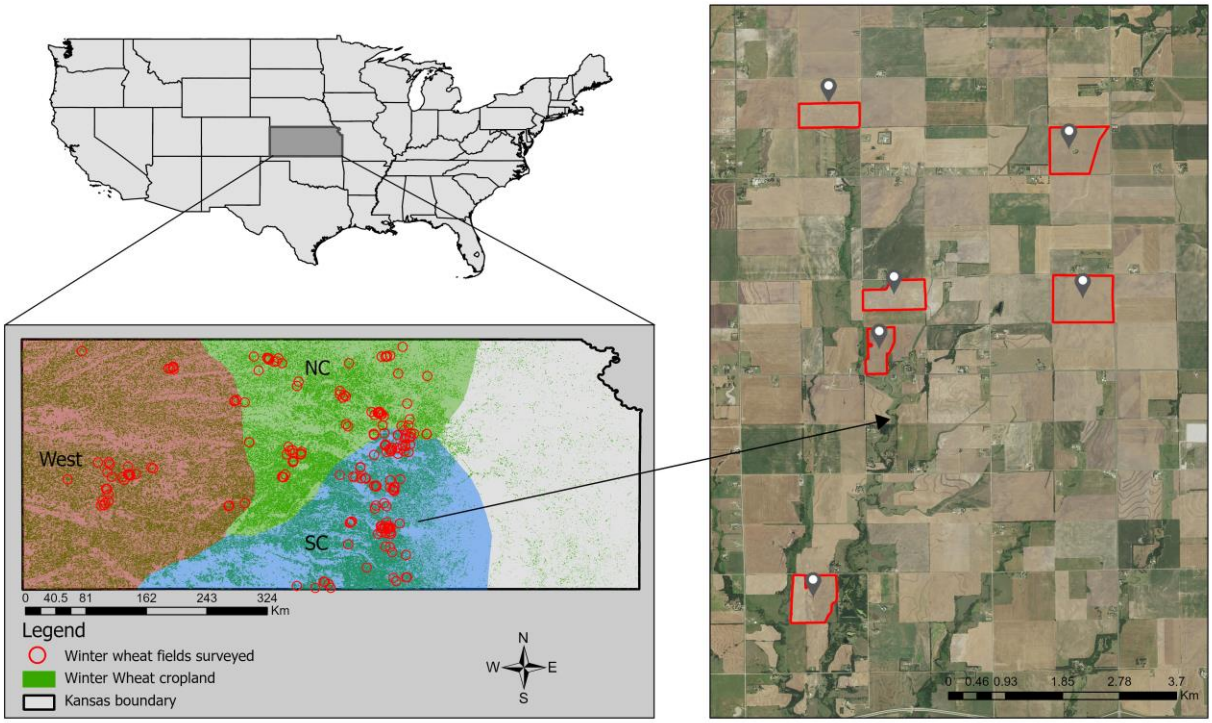

Figure 3-1- Kansas map shows the three sub- regions studied in Kansas (North Central, NC; South Central, SC; and West) as different colors. The red dots represent the 220 sample locations examined in the study. Overlaid on the aerial imagery are field boundaries for some of the winter wheat fields.

3.2.2.2. Yield and Management data

Grain yield (Mg ha^{-1}) and crop management (seeding rate, previous crop, and sowing date) data were collected in the field survey conducted by Jaenisch et al., (2021), and a simulated anthesis date by each field-yield was provided from the same study. The simulated anthesis date was processed using the using the Simple Simulation Model (SSM) – Wheat, (Soltani & Sinclair, 2012), which is a process based model that simulates wheat growth and developments under non limiting condition in the U.S Great Plains (Lollato et al., 2013).

3.2.2.3. Satellite data

Landsat 8-OLI

Landsat 8-OLI captures images of the Earth's surface in nine spectral bands at a 30-m spatial resolution (15-m for panchromatic band). Images are collected on a 16-day temporal cycle. The study sites are covered by eight tiles for which Landsat 8 OLI Collection 1 data were downloaded from the United States Geological Survey (USGS) website (https://earthexplorer.usgs.gov/ accessed in January 2021). The dataset contains atmospherically corrected surface reflectance and land surface temperature.

3.2.3. Methodology

3.2.3.1. Satellite data preprocessing

Detection and removal of ground-obscuring clouds and cloud shadows is essential for remote sensing data processing. A conditional was applied using the Quality Assessment (QA) band (USGS, 2023), preserving only pixels with clear terrain conditions or low to no confidence of cloud conditions. Satellite data processing and vegetation indices calculation developed using Python scripting in ArcGIS PRO.

3.2.3.2. NDVI time series

Time-series NDVI data are commonly used to monitor crop development throughout a growing season (Lai et al., 2018), which primarily takes place during January to June (DOY 1-180) for Kansas winter wheat. NDVI is computed using red (Red) and near-infrared (NIR) reflectance (Tucker,1974):

$$NDVI = \frac{NIR-Red}{NIR+Red} \quad (3\text{-}1)$$

Several Landsat tiles were required for this study (Figure 3-2), thus if a field had representation in multiple tiles and multiple concurrent (to the day) NDVI values were available, then the maximum NDVI was used.

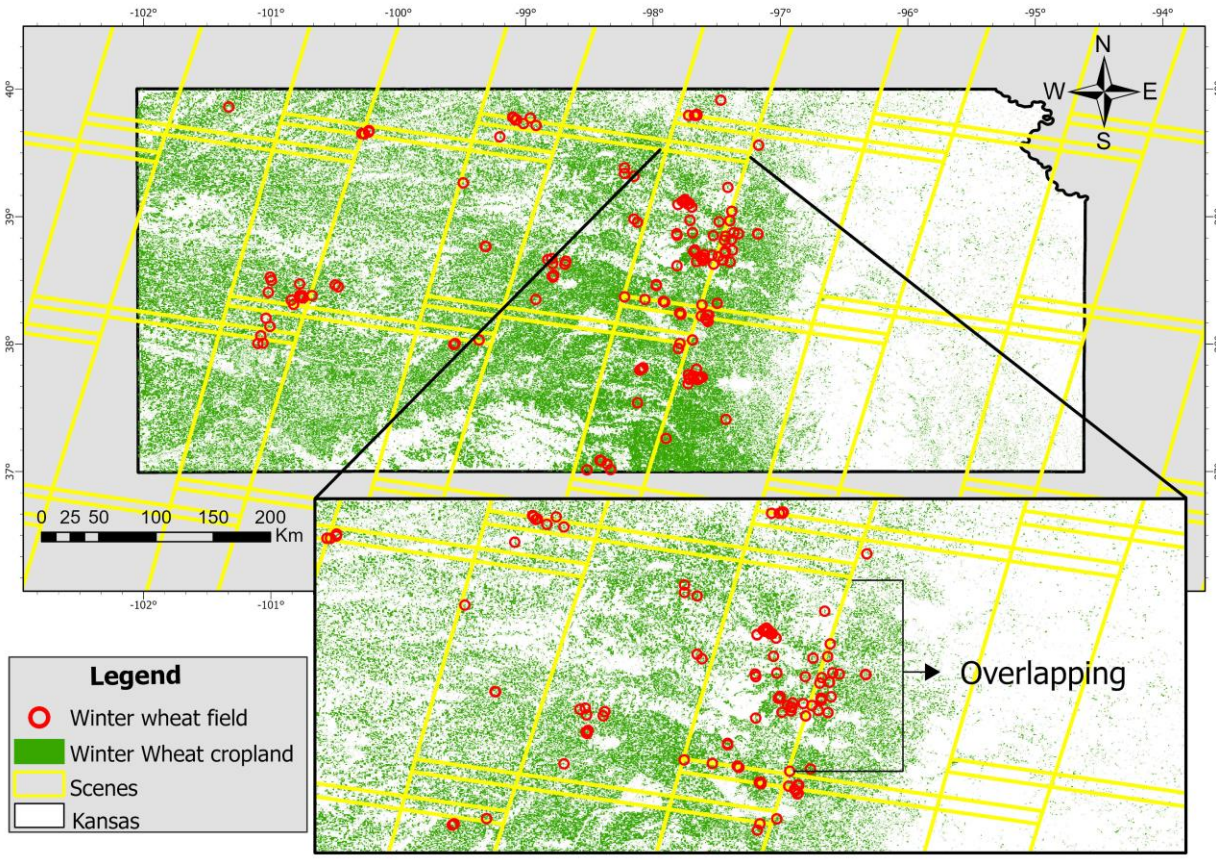

Figure 3-2 - (a) Landsat-8 scenes in yellow that are passing over the study area (b) In detail, fields in red that are represented by multiple scenes.

NDVI time series were visually accessed and a threshold NDVI value of 0.2 during April to May period was set. This threshold was defined because Landsat NDVI time-series showed lower NDVI values during the peak season compared to MODIS and Sentinel. Landsat NDVI time series with values higher than 0.2 during the peak season were capable to show the winter

wheat growing season. As an additional constraint to bolster signal completeness, only fields with at least one monthly NDVI observation in the February-June period were included. January was not included since there is still influence of snow cover, thus NDVI values are close to 0 or missing. In this chapter, NDVI predictor variables are from the satellite remote sensing dataset that exhibited the best performance in the previous Chapter 2 - . Without the need to compare to other sensors, we used all field samples (n=220) available that matched this selection criteria.

3.2.3.3. Time series interpolation

Landsat VI time series are commonly affected by missing values (gaps). Using an up-sampling technique, we increased the frequency of the Landsat NDVI observations by every 7 days(Figure 3-3). Specifically, we used linear interpolation between straddling NDVI values to fill gaps. Since some samples had their earliest available February-June NDVI observation as late as DOY 56, we defined the study period to span DOY 56-182 (mid-February to end of June).

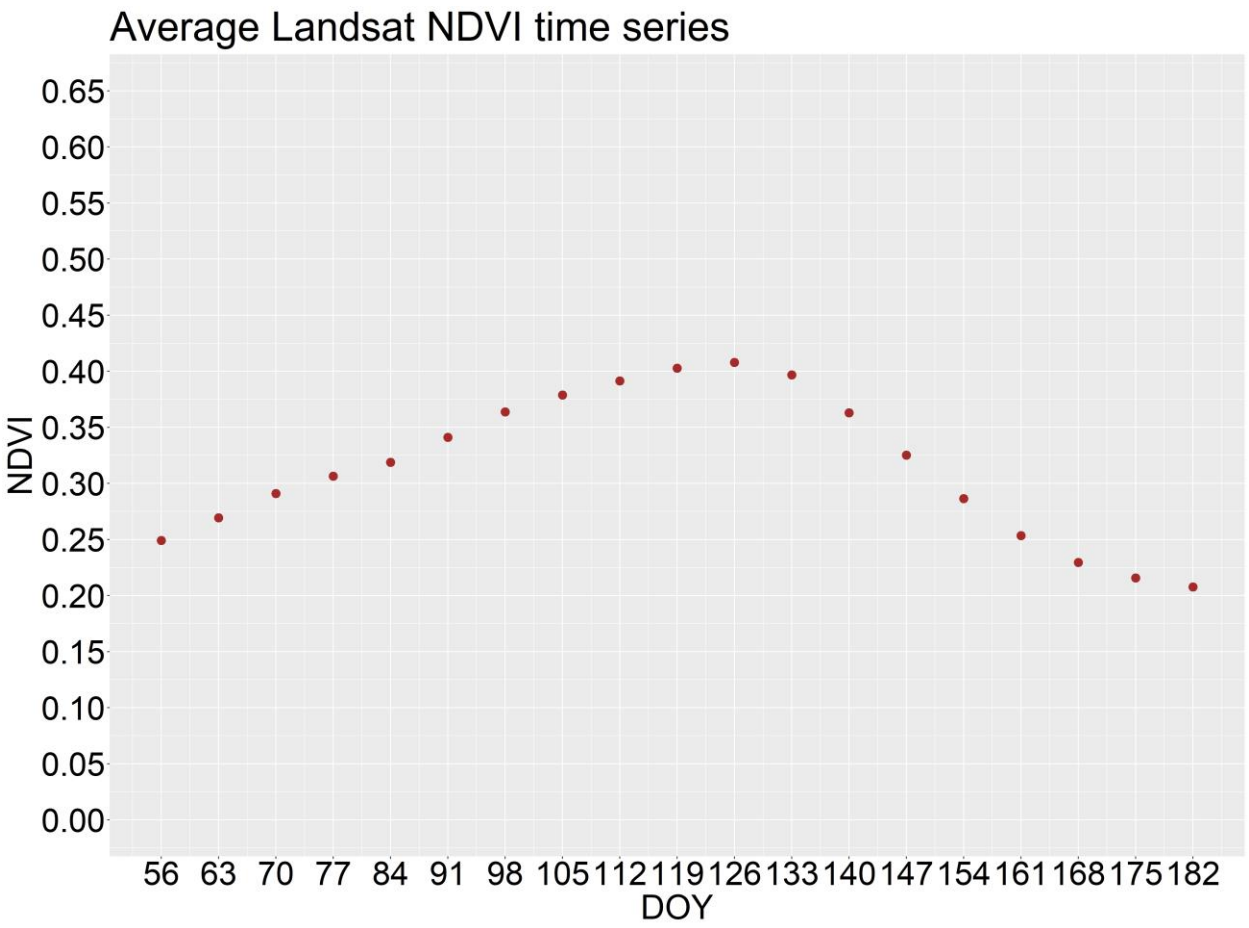

Figure 3-3- Final NDVI profiles averaged across all samples (n=220) with weekly DOY (56-182).

3.2.3.4. NDVI predictor variables

The interval of DOY 56-182 (*full season*, mid-February to June) covering post-dormancy tiller development, stem elongation, heading, anthesis, grain fill, and ripening defined the accumulated NDVI variable (NDVI area under the curve, or AUC). NDVI AUC was determined using the trapezoid rule for integral approximation. NDVI weekly values and NDVI AUC were used as independent variables. Thus, 20 independent variables were used as winter wheat yield predictor variables: NDVI AUC, DOY 56, .

3.2.3.5. Regional analysis

In this study, three subregions were used to subdivide field-specific data as previously established in Jaenisch et al. (2021). Briefly, winter wheat fields were clustered into three surveyed zones based on long-term climate data (long-term cumulative growing degree days, aridity index, temperature seasonality) and cropping systems, following a similar but coarser approach than that proposed by van Wart et al., (2013)). Subregions were clustered based on the following weather classification: North-central (635-890mm annual precipitation and 3,792-4,829 °C annual thermal units), south-central (635-890mm, 4,830-5,949 °C annual thermal units), and west (<625mm, 3,792-4,829°C annual thermal units).

We also note that these intrinsic weather characteristics among regions result in different management practices adopted by winter wheat growers within each region, as summarized in Jaenisch et al., (2021). For example, (i) the optimal sowing dates are earlier in in NC and West as compared to SC (DOY 275 and271 versus 281); (ii) seeding rate are greater in NC and SC (90-95 kg ha^{-1} and 88-95 kg ha^{-1}, respectively) than West (68 kg ha^{-1}); (iii) row spacing are narrower in SC and NC versus the West (19 cm or less to 25.4 cm or 30.5 cm, respectively); (iv) no-till adoption, occurring in 75%, 52%, and 40% of the fields in NC, SC and West; and (v) crop sequence, where 75% of winter wheat fields were in a fallow-crop rotation in the West, and the majority of previous crop in NC and SC were soybeans (44 and 30%) or wheat (42 and 51%). This division resulted in 75 field-yields in NC, 109 in SC and 38 in West Kansas.

3.2.3.6. Empirical methods for estimating winter wheat yields

Least absolute shrinkage and selection operator (LASSO)

LASSO was used as a method to remove variables that are redundant and reduce overfitting. In short, LASSO adds penalty into parameter estimation to shrink the near zero regression coefficients to zero, thus removing them out of selection result (Tibshirani, 1996) . Lambda is the hyperparameter that tunes the intensity of the penalty term, the larger the parameter of lambda the greater number of coefficients will be shrunk to zero (Fonti & Belitser, 2017). Values between 0.01 and 10 were evaluated using cross-validation to find the best lambda value. NDVI predictor variables were input to a least absolute shrinkage and selection operator (LASSO) available in Scikit-learn for Python 3.9.

Although LASSO greatly reduces redundant variables and overfitting, there may still be a need to remove remaining variables that are not statistically significant to the yield prediction model. Therefore, the final models (Linear regression and Random Forest) were built using only the most influential variables according to their influence in the final yield, selected by the regression coefficients from NDVI predictor variables. The NDVI predictor variables were selected by t-value score, p-value, residual error and coefficient of estimation analysis. In addition to that, in some cases, the selection was made by analyzing if the addition or removal of a variable could improve the results or not.

Linear Regression

Prediction models were performed using R programming language in R Studio (R Version 4.2.2). Linear Regression was trained to predict winter wheat yields using the NDVI predictor variables across all field-yields and fields by subregion. As a simple approach, linear regression models are commonly used in crop yield estimation studies in different regions (Johnson et al., 2021; Lobell, 2013; Lopresti et al., 2015).

The model equation is given by:

$$Yield = b_0 + b_1X_1 + b_2X_2 + \cdots + b_nX_n + \varepsilon \quad (3\text{-}2)$$

Here, $\{b_0, b_1, \ldots\}$ are the regression coefficients, $\{X_1, X_2, \ldots\}$ are the NDVI predictor variables , and ε is the residual.

Random Forest

Random Forest (RF) regression followed the same scheme from linear regression to estimate winter wheat yields. RF model is an ensemble-based learning algorithm where each tree comprises random set of variables and samples of the dataset. RF is an ensemble learning technique elaborated by (Breiman, 2001) constructed by a large set of decision trees, with each tree being built using a random set of features and samples.

The generalization error converges to a limit as the number of trees in the forest becomes large and will depend on the strength of the individual trees in the forest and the correlation between them. RF then calculates the average of prediction from the terminal nodes to make the final prediction. Important RF hyperparameters, M_{try} (the number of variables randomly

considered at each node) and N_{tree} (the number of random trees to be grown) were optimized by tuning approaches. Hyperparameter tuning and statistical performance evaluation were performed using the 'ranger' package (Wright & Ziegler, 2017) in RStudio.

3.2.3.7. Model Evaluation

Linear regression and RF models were evaluated using a repeated 10-fold cross validation (CV). In K-fold CV, the entire available data is randomly partitioned into folds of equal size, then the training of the model is done on k-1 parts and one part is left out for testing. This process is repeated k times, where each of the folds is used once to measure the prediction accuracy. The resulting error measures of each interaction is averaged to calculate the final error (Hastie et al., 2009). K-fold CV estimation has a variation due to randomness of partitioning the sample into k-folds (Efron & Tibshirani, 1997). To reduce the internal variance the whole process of partitioning and estimating was repeated 10 times (Kim, 2009).

Model performance was assessed using the coefficient of determination (R^2) to estimate how much variation in the observations was explained by the model, Root Mean Squared Error (RMSE) as an average squared errors-based statistic that penalizes large errors, and Mean Absolute error (MAE) as an average magnitude of the errors, defined as follows:

$$R^2 = 1 - \frac{\sum_{i=1}^{n}(y_{i-} \hat{y}_i)}{\sum_{i=1}^{n}(y_{i-} \bar{y})^2} \quad (3\text{-}3)$$

$$RMSE = \sqrt{\frac{\sum_{i=1}^{n}(y_{i-} \hat{y}_i)^2}{n}} \quad (3\text{-}4)$$

$$\text{MAE} = \frac{1}{n}\sum_{i=1}^{n}|y_{i-} \hat{y}_i| \quad (3\text{-}5)$$

3.3 Results

3.3.1. Subregional winter wheat NDVI time series

The NDVI time series from each subregion are shown in Figure 3-4. NDVI values ranged from 0.07-0.60 using all fields, 0.07-0.56 for NC fields, 0.09 -0.53 for SC fields and 0.08-0.60 for West fields. Landsat NDVI time series were capable of detecting distinct patterns from each sub-region. Observing the mean NDVI time-series, NC presented flatter shaped curve from DOY 56 to 91 compared to SC and West Kansas which showed an ascending pattern during the early growing season. The vegetation peak across all fields was noticed between DOY 119 and 133 (second half of April, usually when anthesis occurs), whereas ripening and harvest happened between DOY 154 and 168 (end of May to first half of June). SC NDVI time-series presented an earlier vegetation peak DOY 119 compared to NC NDVI time-series and West NDVI time-series, close to DOY 126. After vegetation peak, NDVI values appeared to decrease earlier in SC, compared to NC and West, suggesting earlier ripening and harvest.

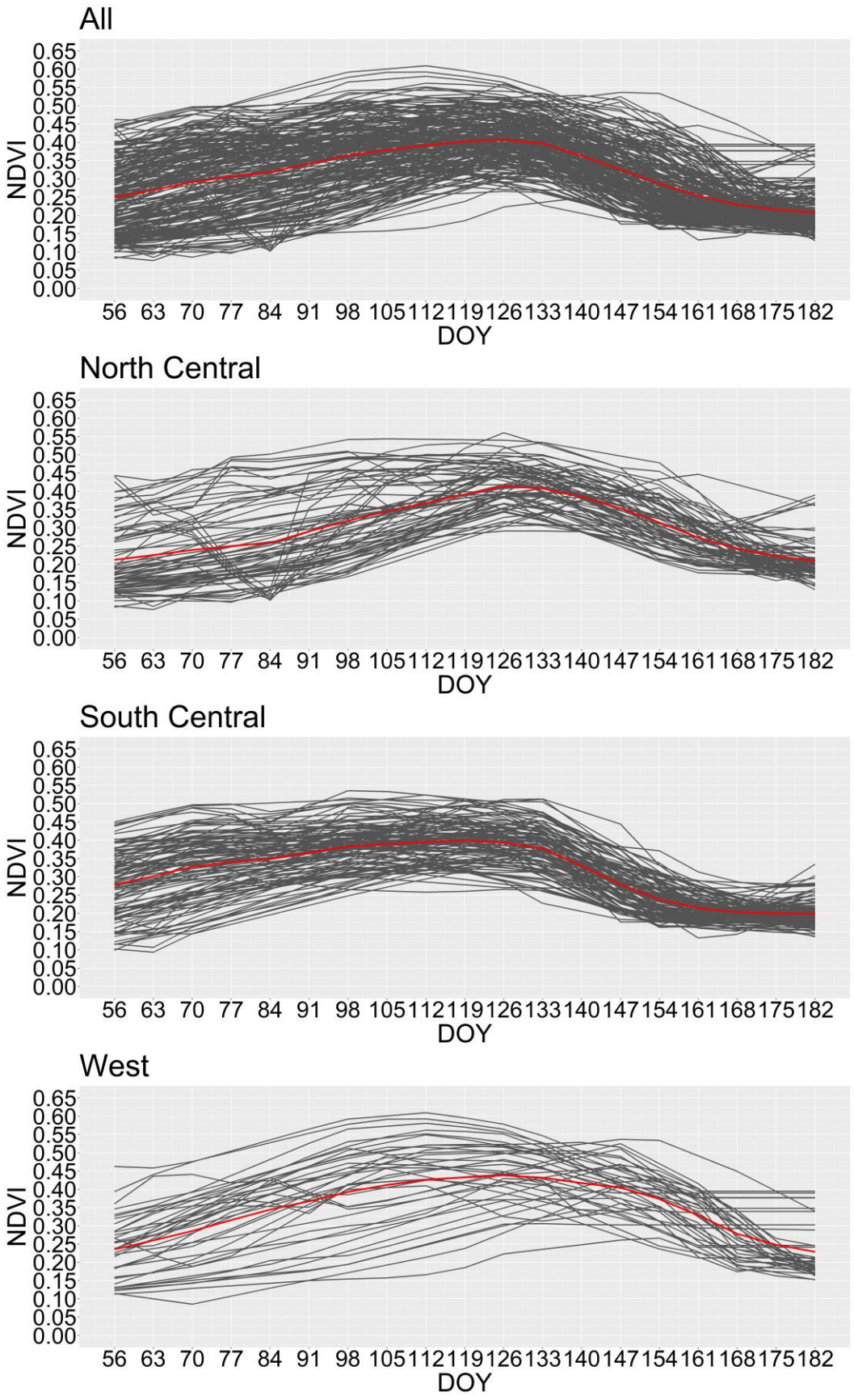
All
North Central
South Central
West
NDVI
0.65
0.60
0.55
0.50
0.45
0.40
0.35
0.30
0.25
0.20
0.15
0.10
0.05
0.00
56 63 70 77 84 91 98 105 112 119 126 133 140 147 154 161 168 175 182
DOY

Figure 3-4- Landsat NDVI time series profiles are shown using all field-yields samples (n=220), NC field samples (n=73), SC field samples (n=109) and West field samples (n=38) from 2016-2018.

Table 3-1 shows the descriptive statistics between DOY when simulated anthesis occurred and the NDVI peak DOY for each field by region. The average for simulated anthesis across all fields occurred in DOY 128, compared to when the NDVI peak occurred the average was earlier, DOY 120. In NC, SC, and West the average NDVI peak DOY occurred DOY 128, DOY 112, and DOY 126, earlier than the simulated anthesis, DOY 134, DOY 122, DOY 135, respectively. NC showed the most approximated result with mean DOY 128. Average NDVI peak DOY occurred earlier in SC (DOY 122) than in NC and West (DOY 128 and DOY 126). Figure 3-5 shows the relationships between DOY simulated anthesis and DOY and the peak NDVI DOY for each field by subregions. R^2 was low and ranged from 0.08 to 0.17, with a significant relationship in all regions, expect West. All fields and NC showed the highest relationship (R^2 =0.17 and R^2 =0.12) with the DOY simulated anthesis.

Table 3-1- Descriptive statistics of DOY when simulated anthesis occurred and DOY when the peak NDVI occurred for each field.

Descriptive Statistics	Simulated Anthesis (All)	All	Simulated Anthesis (NC)	NC	Simulated Anthesis (SC)	SC	Simulated Anthesis (West)	West
Min	80	70	96	98	80	70	102	98
Median	132	126	136	126	125	119	134	126
Mean	128	120	134	128	122	112	135	126
Max	163	182	163	182	146	133	157	154

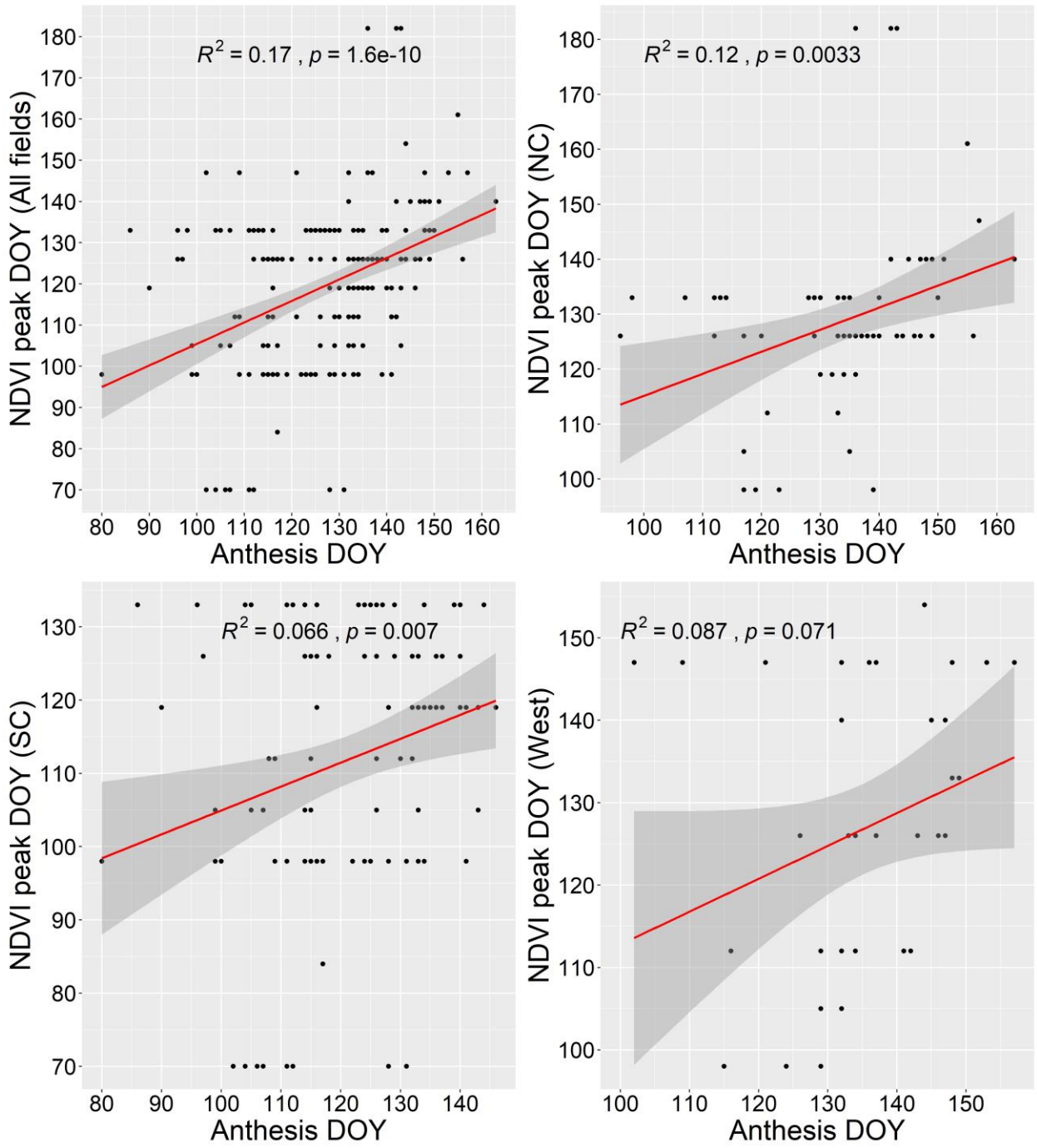

Figure 3-5-Relationships between DOY when the peak NDVI occurred versus the DOY when simulated anthesis occurred for each field all fields and by subregions (NC, SC, West) Kansas.

Table 3-2 shows the statistical summary of yields in all fields in Kansas and by subregions. Yields were the highest in the West with a median of 4.64 Mg ha^{-1}, followed by SC

with median yields of 3.76 Mg ha^{-1} and NC 3.66 Mg ha^{-1}. Figure 4 shows box plots illustrating yield and NDVI AUC distributions by subregions. The variation in NDVI AUC across the subregions corroborates with the subregional variation in winter wheat yields. NDVI AUC was the highest in West, followed by SC and NC (Figure 3-6).

Table 3-2-Statistical summary of winter wheat yields from 2016 to 2018, using all fields and by subregions (NC, SC, West) Kansas.

Yields statistical summary	**Regions**			
	ALL	*NC*	*SC*	*West*
Max	7.056	6.048	5.913	7.056
Min	0.403	1.949	0.403	1.210
Mean	3.866	3.664	3.827	4.364
Median	3.830	3.427	3.763	4.637
SD	1.156	0.960	1.143	1.403

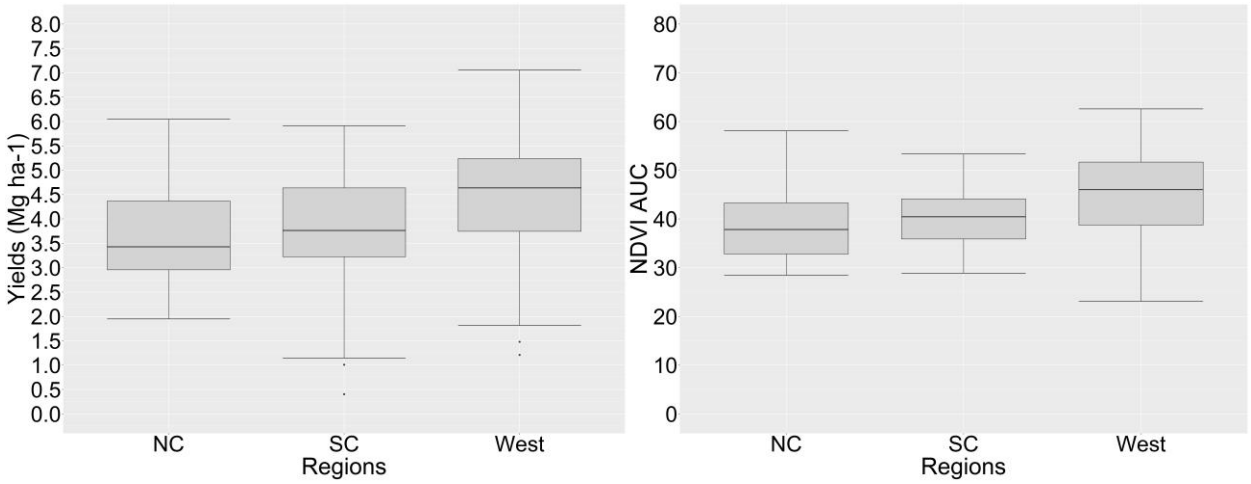

Figure 3-6 - Boxplot of winter wheat yield and NDVI AUC from fields in NC, SC, and West .

3.3.2 LASSO and coefficient analysis for feature selection

As a final examination, regression coefficients from the NDVI predictor variables selected by LASSO were analyzed and only the most significant variables influencing grain yield

were included in the linear regression and RF model prediction. For each sensor there is first a table showing the regression coefficients from NDVI predictor variables selected by LASSO. A second table presents regression coefficients from NDVI predictor variables included in the linear regression and RF prediction model. The NDVI predictor variables were selected by t-value score, p-value, residual error and coefficient of estimation analysis. In addition to that, in some cases, the selection was made by analyzing if the addition or removal of a variable could improve the results or not. NDVI predictor variables when using grain yield from all fields across Kansas included in the prediction models were NDVI AUC, DOY 56, DOY 105, DOY 154. NDVI predictor variable DOY 105 was discarded due its low t-value and p-value >.05 (Table 3-3 and Table 3-4) .

In NC, the NDVI predictor variables remained the same from LASSO selection and NDVI predictor variables DOY 56, DOY 105, DOY 154 were included in the linear regression and RF models (Table 3-4 and Table 3-5). In SC, NDVI DOY 63, DOY 133, DOY 154 prediction variables combination presented the lowest Residual standard error and were included in the prediction models (Table 3-6 and Table 3-7). In West Kansas, NDVI predictor variables DOY 133 and DOY 140 selected from LASSO results were the same used in the final models (Table 3-8).

Table 3-3- Regression coefficients from all field-yields NDVI predictor variables selected by LASSO.

Predictors	**Estimate**	**Std.Error**	**t value**	**Pr(>|t|)**
(Intercept)	0.180	0.430	0.419	0.675
AUC	0.048	0.041	1.164	0.245
DOY56	2.413	1.347	1.79	0.074
DOY105	0.031	2.563	0.012	0.990
DOY154	3.853	1.624	2.372	0.018
Residual standard error	0.946			
R^2	0.343		***p-value:*** <.001	

Table 3-4- Regression coefficients from all field-yields NDVI predictor variables included in the linear regression and RF models.

Final model predictors	**Estimate**	**Std.Error**	**t value**	**Pr(>|t|)**
(Intercept)	0.178	0.406	0.44	0.660
AUC	0.049	0.020	2.43	0.015
DOY56	2.409	1.312	1.837	0.067
DOY154	3.841	1.255	3.06	0.002
Residual standard error	0.943			
R^2	0.343		***p-value***: <.001	

Table 3-5- Regression coefficients from NC NDVI predictor variables included in the linear regression and RF models.

Final model predictors	**Estimate**	**Std.Error**	**t value**	**Pr(>|t|)**
(Intercept)	0.677	0.541	1.251	0.215
DOY56	1.555	2.134	0.729	0.468
DOY105	3.231	2.401	1.346	0.182
DOY154	4.904	1.559	3.145	0.002
Residual standard error	0.773			
R^2	0.377		***p-value***: <.001	

Table 3-6- Regression coefficients from SC NDVI predictor variables selected by LASSO.

Predictors	**Estimate**	**Std.Error**	**t value**	**Pr(>|t|)**
(Intercept)	-0.109	0.6516	-0.169	0.866
DOY56	0.010	5.5533	0.002	0.998
DOY63	4.573	5.4791	0.835	0.405
DOY133	3.155	2.0381	1.548	0.124
DOY154	5.731	2.5629	2.236	0.027
Residual standard error	0.954			
R²	0.328		***p-value***: <.001	

Table 3-7- Regression coefficients from the SC NDVI predictor variables included in the linear regression and RF models

Final model predictors	**Estimate**	**Std.Error**	**t value**	**Pr(>|t|)**
(Intercept)	-0.110	0.616	-0.179	0.858
DOY63	4.583	1.078	4.252	<.001
DOY133	3.155	2.028	1.556	0.122
DOY154	5.732	2.507	2.286	0.024
Residual standard error	0.949			
R²	0.328		***p-value***: <.001	

Table 3-8- Regression coefficients from West NDVI predictor variables included in the linear regression and RF models.

Final model predictors	**Estimate**	**Std.Error**	**t value**	**Pr(>|t|)**
(Intercept)	-1.695	0.991	-1.71	0.096
DOY133	10.004	5.133	1.949	0.059
DOY140	4.178	5.546	0.753	0.456
Residual standard error	0.987			
R²	0.532		***p-value***: <.001	

3.3.3. Subregional winter wheat yield estimation with NDVI predictor variables.

Table 3-9 shows the descriptive statistics of training dataset and testing dataset using linear regression and RF. As seen in Chapter 2 - , NDVI predictor variables performed better using the linear regression model than RF. LASSO and the coefficient analysis helped in preventing overfitting in the linear regression. The training results below from RF are the in-sample R^2 and RMSE from RF prediction using all dataset and shows a R^2 of 0.88 and low RMSE of 0.45, the results from 10-fold cross validation using all fields show a R^2 of 0.30 and high RMSE of 0.98 suggesting great discrepancy between results and that overfitting is occurring in the RF model. In the linear regression, NDVI predictors variables from all fields presented the best fit in training and testing data (R^2 of 0.34 and 0.35 and RMSE of 0.94 and 0.93, respectively). NC and SC showed a good fit in training and testing prediction error, with RMSE of 0.77 and 0.76 in NC, RMSE of 0.949 and 0.934 in SC. West presented the largest discrepancies between train and test results with R^2 of 0.53 and 0.61 and RMSE of 0.98 and 0.953, respectively.

Table 3-9- Descriptive statistics of training dataset and testing dataset using Linear Regression and Random Forest using LASSO.

		Regions							
Models	**Metrics**	**ALL**		**NC**		**SC**		**West**	
		Train	**Test**	**Train**	**Test**	**Train**	**Test**	**Train**	**Test**
Linear Regression	R^2	0.343	0.359	0.373	0.419	0.328	0.376	0.532	0.617
	RMSE(Mg ha^{-1})	0.943	0.939	0.770	0.761	0.949	0.934	0.986	0.953
		In-sample	**Test**	*In-sample*	**Test**	*In-sample*	**Test**	*In-sample*	**Test**
Random Forest	R^2	0.886	0.302	0.86	0.422	0.874	0.324	0.981	0.554
	RMSE(Mg ha^{-1})	0.456	0.984	0.393	0.764	0.489	0.974	0.502	1.037

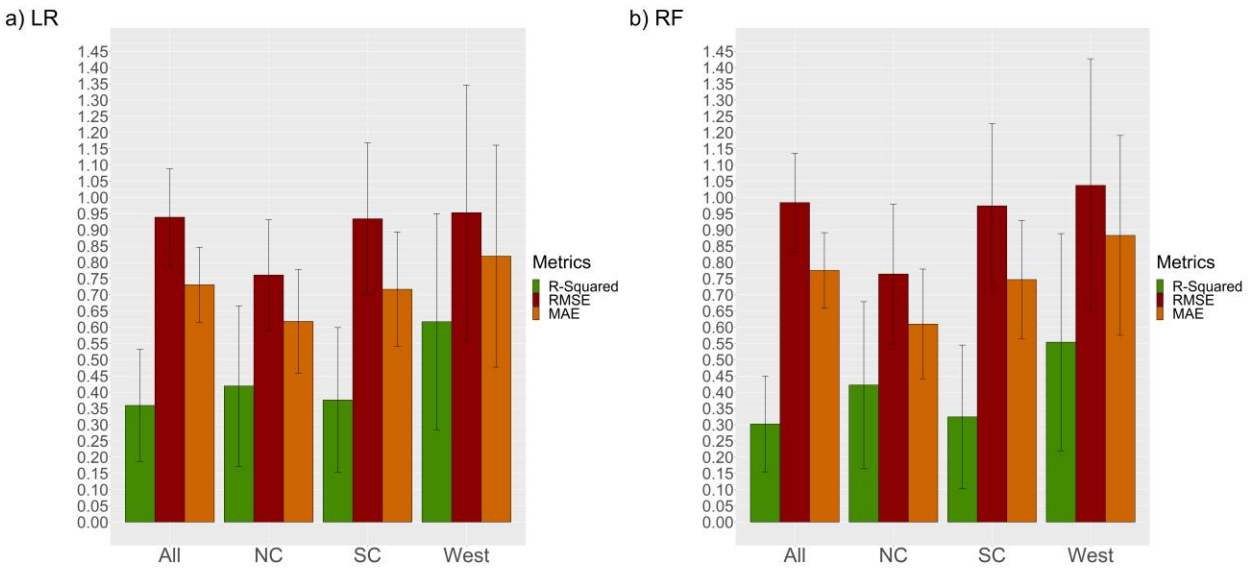

Figure 3-7 shows the subregional statistical performance of Linear Regression (LR) and Random Forest (RF) yield prediction model.

Linear regression outperformed the RF model when using NDVI predictor variables from all fields and subregions. Linear regression results showed that the yield estimation using all fields NDVI predictor variables achieved lower performance compared to NC and SC, with a R^2 of 0.30, RMSE of 0.98 Mg ha^{-1} and MAE of 0.77 Mg ha^{-1}. NDVI predictor variables in NC obtained the best results with a R^2 of 0.41, RMSE of 0.76 Mg ha^{-1} and MAE of 0.60 Mg ha^{-1}, followed by SC NDVI predictor variables with a R^2 of 0.37, RMSE of 0.93 Mg ha^{-1} and MAE of 0.71 Mg ha^{-1}.

RF presented similar ranking in terms of region performance. NC obtained the best prediction results, with a R^2 of 0.42, RMSE of 0.76 Mg ha^{-1} and MAE of 0.609Mg ha^{-1} followed by SC R^2 of 0.32, RMSE of 0.97 Mg ha^{-1} and MAE of 0.74 Mg ha^{-1}. NDVI predictor variables from all fields achieved a R^2 of 0.30, RMSE of 0.98 Mg ha^{-1} and MAE of 0.77 Mg ha^{-1} .West

reported poor performance in both models (RMSE > 0.95 Mg ha^{-1}) and high standard deviation, possibly due its relatively small sample (n=39) causing more overfitting.

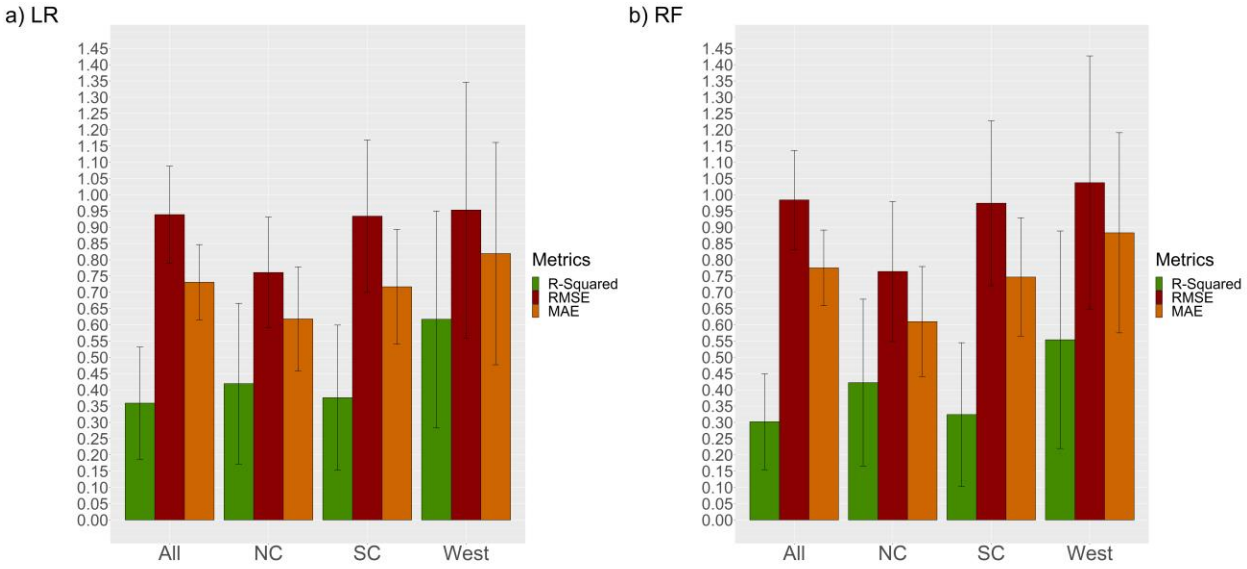

Figure 3-7- Subregional statistical performance of Linear Regression (LR) and Random Forest (RF) yield prediction model.

3.4. Discussion

NDVI time series tracked seasonal changes and detected distinct patterns of winter wheat growth by subregions (NC, SC and West) in Kansas. Distinct spectral-temporal differences were observed in green-up, vegetation peak and maturity timing in NC, SC and West. For instance, SC presented higher green-up NDVI values than NC and West. Vegetation peak occurred earlier in DOY 119, while in NC and West, DOY 126 respectively. After vegetation peak, SC experienced a faster decline in NDVI values than the other regions. For example, the mean SC NDVI values in DOY 133 were 0.37 and decreased to 0.27 in DOY 147. NC and West showed more gradual decrease in NDVI after reaching maturity, in NC NDVI values were 0.40 and in DOY 147, 0.35 and West DOY 133 mean NDVI values were 0.43 and DOY 147, 0.40. In a study using crop phenology and long-term weather data in the U.S Southern Great Plains, Lollato et al., (2020)

showed that the heading of winter wheat follows a strong latitudinal and less apparent longitudinal gradient, increasing from south to north , whereas maturity followed an east-west gradient, which may explain the early development in the SC NDVI time series and late development in West NDVI time-series. These results also align well with previous simulation studies using long-term weather data (Lollato et al., 2017) and more regional studies on wheat heading dates (Zhao et al., 2020). The earlier crop maturity in south central Kansas as opposed to northwest Kansas is multi-faceted, owing to: (i) lower latitudes resulting in warmer temperatures and thus accelerated crop phenology (Lollato et al., 2020); (ii) lower elevation (thus, warmer nights) inducing shorter maturity, and (iii) choice of adapted varieties which are naturally shorter-cycled than those adopted in the west (Jaenisch et al., 2021).

Some of the NDVI time series in NC presented a distinct pattern compared to the other regions, with increasing NDVI values in DOY 63 (early March), sharp drop in DOY 84 (mid-March) followed with a great increase in DOY 91 (end of March). These NDVI time series refer to fields clustered in the northernmost area in NC Kansas (Figure 3-8). By mid- March wheat enters the greening up state after dormancy, causing the NDVI to increase rapidly. Such pattern was observed in previous work using MODIS NDVI time series in the US Central Great Plain (Masialeti et al., 2010; Wardlow et al., 2007) and NDVI winter wheat in China (Ren et al., 2008). However, the severe decrease in NDVI values in Mid- March seems atypical although freeze still can happen this time of the year (Lingenfelser et al., 2018). Another reason is clouds and poor atmospheric conditions, each of these reduces NDVI values. Although the conditional masking technique performed effectively in removing sources of signal error in most of the imagery dataset, in this scene a small portion of pixels flagged as “clear conditions” remained

neighboring or within-field causing the low values in NDVI. Figure 3-8 shows the winter wheat fields and the masked NDVI imagery in DOY 84.

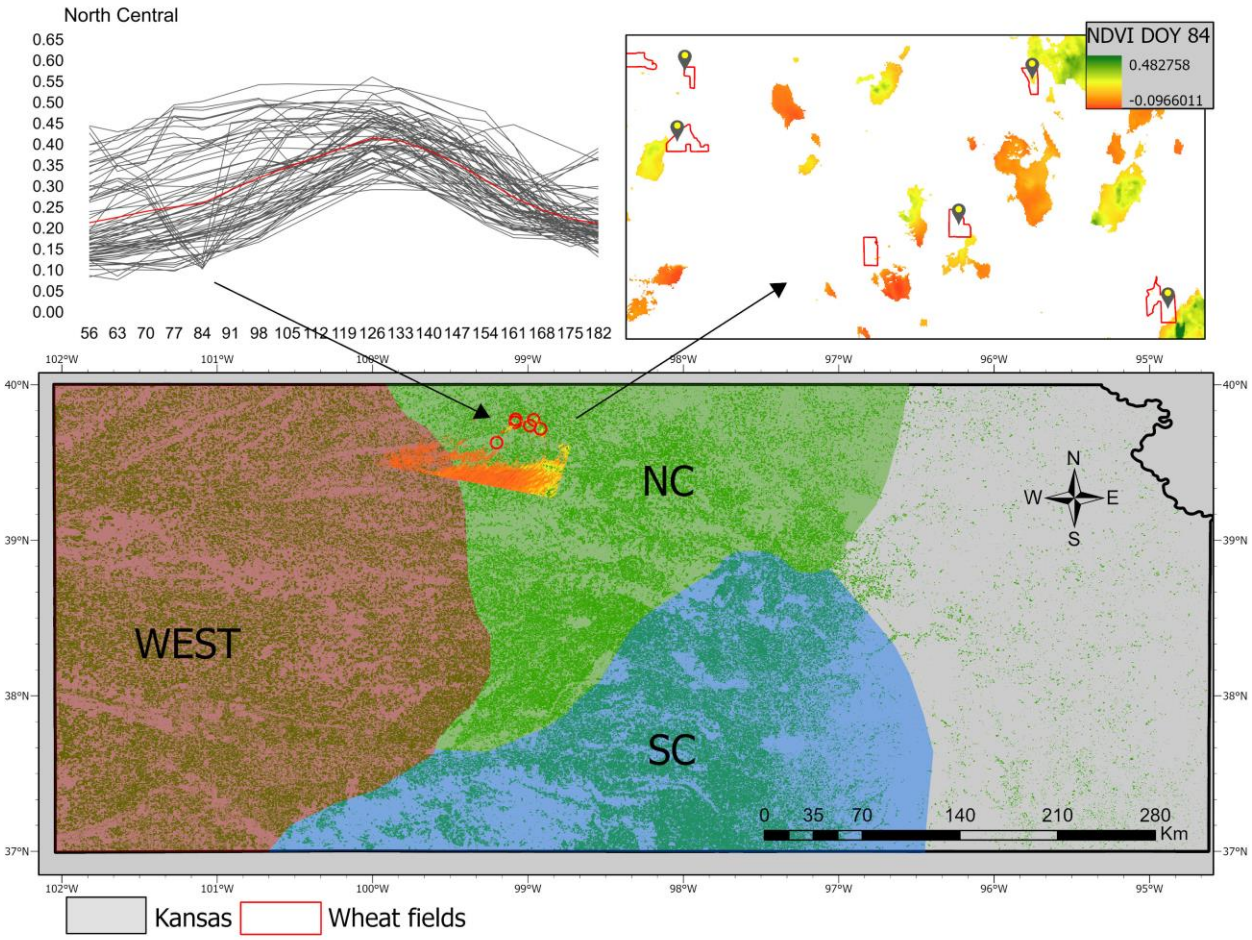

Figure 3-8- The map above shows the fields in NC Kansas with low NDVI value in DOY 84 and the masked NDVI imagery overlayed (orange/yellow color). On top, the NC NDVI time series (in the left) and the fields boundaries overlaying the masked NDVI imagery from Landsat-8

Winter wheat yield estimation using NDVI predictor variables performed better in linear regression than in RF. Non-linear methods (i.e., RF, Support Vector Machine, and Artificial Neural Networks) are known to outperform the linear methods when most relationships between yield and different variables (e.g., satellite imagery, climate, soil, management). are non-linear (Sun et al., 2022; Y. Wang et al., 2020). The small dataset and the linear relationship between

NDVI and yields (Lopresti et al., 2015) could potentially explain why simple regression was better at capturing this relationship than the RF (Johnson et al., 2016; Mallick et al., 2021)

When analyzing all fields NDVI predictor variables, the linear regression achieved a RMSE of 0.93 Mg ha^{-1}, a higher prediction error than NC and SC, except for West. NDVI AUC and NDVI weekly predictor variables DOY 56 and DOY 154 were the most significant variables and included in the model. The presence of NDVI AUC as one of the best predictor variables agrees with many studies that have successfully used NDVI AUC to estimate crop yields (Azadbakht et al. 2022; Skakun et al. 2019). NDVI predictor variables around DOY 56 and 63 may be related to different aspects regarding this specific dataset and the wheat crop in general. Regarding this specific dataset, the 2016 season was characterized by temperatures that were mostly above normal all winter, which resulted in an earlier dormancy break and initiation (Paulsen & Heyne, 1983) and sub-regional levels (Lollato et al., 2019; Lollato, Roozeboom, et al., 2020). Regarding a strong signal of DOY 154 in predicting wheat yield, this reflects wheat growth in early June, where wheat is going through ripening stages of development when the grain test weight is determined and grain moisture decreases (Lollato, 2018). Greater levels of leaf area at this stage – here represented by greater NDVI – may associate with higher wheat yield due to practices associated with stay-green, such as greater N rates and the adoption of foliar fungicides (Cruppe et al., 2021; Jaenisch et al., 2019, 2022). Disentangling the impacts of management practices on wheat yield and NDVI was beyond the scope of this work.

NC NDVI predictor variables presented the best performance in predicting winter wheat yields using linear regression with the lowest prediction error RMSE of 0.76 Mg ha^{-1}. The NDVI prediction variables in NC represented three distinct stages of winter wheat growth: DOY 63 and DOY 154 indicating green-up and ripening stage (as mentioned previously), and DOY 105

representing heading and anthesis stage. The strongest correlation was seen in using DOY 154 NDVI predictor variables (early June), in NC wheat was harvest between June 11th and July 5th from 2016 to 2018 (Jaenisch et al., 2021). Studies have shown NDVI has a good prediction ability of wheat grain in late growing stages. For example, using LASSO regression for spring wheat yield prediction, Shafiee et al., (2021) showed that NDVI achieved the highest prediction ability for grain yield at dates toward maturity.

SC NDVI predictor variables showed the second lowest prediction error, with a RMSE of 0.93 Mg ha^{-1}. Among the NDVI predictor variables DOY 56, DOY 154 and DOY 133 included in the SC model, the strongest correlation was seen in using DOY 56 NDVI predictor variables (early Spring). These findings align with the widespread use of early-season NDVI to forecast winter wheat grain yield potential to help guide the determination of nitrogen rates in this region (Raun et al., 2001; Stone et al., 1996; see discussion Beres et al., 2020 for full history). Using Sentinel-2 in Morocco, Imanni et al., (2022) found strong correlation in tillering and maturity stages with wheat yields. Panek and Gozdowski, (2021) found a strong relationship between grain yields and the NDVI from the very early growth stages in Central Europe. A limitation in using NDVI at early stages is that anything that happens to the crop after the forecast date is not reflected in the crop yield estimate. For example, if after the forecasting date a drought, freeze events, or pests outbreak happens, especially during the critical period of development, the model would most likely to show erroneous crop yield forecasting results (Lopresti et al., 2015; Mkhabela et al., 2011) .

Uncertainty in prediction using early NDVI in more homogeneous environments with moderate climates, such as the study in Central Europe, is lower than in heterogeneous environment regions such as Kansas, vulnerable to freezes and severe heat during anthesis and

grain-filling stages, respectively (Paulsen, 1997). For instance, from 2016 to 2018, SC Kansas experienced freezing temperatures and hailstorm during the months of April and May and heat stress in early June in Western Kansas (Lingenfelser et al., 2017, 2018). Since anthesis represents the reproductive stage of winter wheat, very low temperatures can result in sterility which has an impact on yields (Paulsen, 1997; Shroyer et al., 1995; Y. Zhang et al., 2022). Stress caused by extreme temperatures has a stronger impact during the grain-fill stage reducing grain moisture and size (Lollato, 2018).

West showed the lowest accuracy (RMSE=0.93 Mg ha^{-1}) possibly due to the small number of samples reducing linear regression and RF model effectiveness. However, the prediction model presented the highest R^2, where the predictors could explain 61% of yield variability. The NDVI predictor variables used to predict yields in West Kansas were DOY 133 and DOY 140, which falls into the flowering and grain-filling periods.

Overall, the results showed that is possible to predict in earlier stages of the growing season; however, its accuracy will depend on weather conditions. NDVI also performed well during late growing stages, agreeing with other studies that have indicated that yield estimation accuracy reaches the maximum in the late stage of growth (Sun et al., 2022). Since forecasting crop production differs from prediction as it requires interpreting future observations only using the past data (Griffiths et al., 2010), considering only the late growing stages to use a forecast model to inform farmers may not be sufficient (Shahhosseini et al., 2020).

The results in NC and SC indicated the potential of using more homogeneous regions to predict winter wheat yields using satellite imagery, especially in heterogenous environments, such as Kansas. Lastly the results support the original contribution in subdividing Kansas into smaller and more homogeneous crop zones using long-term weather conditions and since

weather interacts with management, taking in account the agronomic practices that are region-specific (Jaenisch et al., 2021).

Chapter 4 - Improving winter wheat yield estimation at field scale using management and climate data by homogeneous subregions in Kansas, USA.

4.1. Introduction

Crop yield is strongly influenced by numerous variables including environment (e.g. climate, soil properties), genetics, and management (Mathieu & Aires, 2018). In Kansas, the largest producer of winter wheat (*Triticum aestivum* L.) in the U.S.A, improvements in winter wheat crops were made through the development and adoption of technological advances in genetics, agronomic and resource use practices (Jaenisch et al., 2022; Maeoka et al., 2020; Rife et al., 2019). Still, winter wheat is a long duration crop that can face different temperatures ranges and experience damage during the growing season, thus weather and climate are the prominent drivers of yield variability (Obembe et al., 2021b). Rainfed winter wheat grown in Kansas is impacted by high precipitation variability and increased temperatures during critical wheat development spring and grain filling period (Nelson et al., 2022; Tack et al., 2015). All of which could become more frequent and intense under climate change (Lollato et al., 2020), reinforcing the need for accurate and timely predictions of crop yield in an uncertain climate.

Climate data and soil properties describe the environmental information that constrains the growing condition of the crop, and it has been extensively used as parameters in crop yield models (Alvarez, 2009; Hammer et al., 2000; Morell et al., 2016). Satellite remote sensing provides timely and accurate information to monitor crop growth and have the ability to collect radiances in the visible and near-infrared portions of the electromagnetic spectrum which are

useful for vegetation monitoring (Tucker,1979). In the last decades, research focused on using vegetation indices (Vis) (García-Martínez et al., 2020; Kouadio et al., 2014; Moriondo et al., 2007) and biophysical parameters, such as the leaf area index (LAI) and photosynthetically active radiation (FPAR), (Cammalleri et al., 2022; D. M. Johnson, 2016; Tripathy et al., 2013) derived from satellite images have proven a potential improvement of crop yield estimations.

Vegetation indices can serve as potential proxies of plant biomass, identifying vegetation health status variations at both small (within-field) and large scales (regional scales, national and global). For large scale studies, VIs have been mainly obtained from Moderate Resolution Imaging Spectroradiometer (MODIS) (Johnson et al., 2021; Kouadio et al., 2014; Lopresti et al., 2015). At smaller scales, Landsat imagery and recently Sentinel have been the most used (Fieuzal et al., 2020; Shen & Evans, 2021; Yli-Heikkila et al., 2022). Among different indices, NDVI is frequently used for crop growth and yield-related research as a remote sensing parameter due its relationship with net primary production and biomass (Kogan et al., 2012; Lai et al., 2018; Moriondo et al., 2007).

Commonly modeling approaches using remotely sensed data for predicting crop yield are mechanistic models (process-based) and empirical models (de Wit et al., 2012; Gaso et al., 2019; Lai et al., 2018; Luciano et al., 2021). In mechanistic models, remotely sensed data is usually assimilated as one of the parameters in the model to simulate physiological processes of crop growth and development in response to environmental conditions and management practices. For example, Chen et al., (2018) assimilated leaf area index (LAI) to a crop model (MCWLA-Wheat) to improve its reliability in estimating winter wheat yields, producing more accurate yield estimates at regional scale than without assimilation.

Empirical modeling estimates direct relationships between VIs and crop yield in a given data set without considering the underlying processes in crop physiology and ecology. Skakun et al., (2019), used vegetation indices to derive different metrics to build empirical regression winter wheat models at regional scale in Ukraine. Recently, new machine learning approaches capable of capturing the nonlinear relationships between crop yield and large set of predictors have shown significant improvement in empirical modeling. For instance, Schwalbert et al., (2020) used vegetation indices and precipitation independent variables to estimate soybean yields in Brazil and found a better performance using LTSM neural networks than other regression algorithms (random forest and ordinary linear squared regression).

Although encouraging results have been achieved by using VI and biophysical parameters from satellite imagery data, other intrinsic driving factors in weather, or variability in soil properties and management operations still pose an obstacle for widespread use of remote sensing for yield estimation and have not been yet fully explored in crop yield models (Huang et al., 2019; Lee et al., 2020). Very recently, researchers started to assess multi-source data to address these issues. For example, Wang et al., (2020) found that combining multiple sources (satellite images, climate data, soil maps, and historical yield records) outperformed single source satellite data, with the highest accuracy being obtained when the four data sources were all considered in the model development. In a multi-source data analysis using Random Forest, Sun et al., (2022) achieved a better winter wheat yield forecasting using satellite data, climate data and geographic information (spatial information data).

In this study, different types of data, including satellite imagery, climate, soil and management data were used as the predictors to forecast the winter wheat yield at the field scale

in Kansas. Two linear regression methods, multiple linear regression and Random Forest were built and compared. The goal of the study was to answer the following two questions*:*

(i) How much improvement can be obtained by combining different data types (satellite, management, and climate)?

(ii) How much improvement can be obtained in prediction at field scale by combining satellite, management, and climate data and by analyzing three homogeneous subregions in Kansas?

4.2. Material and Methods

4.2.1.Study Area

This study focused on central and western Kansas, located in the U.S Central Great Plains, the largest contiguous area of low-precipitation winter wheat in the world (T. Fischer et al., 2014) (Figure 4-1). Winter wheat is the predominant crop cultivated in this area, grown continuously or in rotation with other cereal (e.g. corn [*Zea mays* L]) or legumes (e.g. soybeans [*Glycine max* (L.)]), or after a fallow period that can range from 3 months in central Kansas to 11-14 months in western Kansas. Usually, winter wheat sowing happens from mid-September until mid-November, and harvest occurs from early June to early July, depending on location and crop sequence (Munaro et al., 2020). Kansas's major soil is Harney silt loam, which possesses the ideal qualities of a prairie soil with the best combination of physical and chemical characteristics for growing crops and grasses (USDA NRCS, 1993)

Given the mid latitude and mid continental location, pronounced thermal and hydrologic seasonality characterizes the climate of Kansas. For example, a steep spatial gradient in average

precipitation is present ranging from ~450 mm in the west and ~1100 mm in the east (Lollato et al., 2020) resulting in winter wheat growing season precipitation ranging from ~200 to 650mm. The climate is semi-arid in the west and humid subtropical in the east with most of the precipitation occurring in spring and summer. The annual average temperature in Kansas is between 11◦C and 13◦C. The average growing season temperature ranges from 7 to 12℃ from west to east due to elevation, which ranges from ~200 to 1200 m (Lollato et al., 2017).

4.2.2 Datasets

4.2.2.1. Survey Data

Field-level grain yield, management practices, and environmental data (weather and soil data) were collected and processed from a field survey conducted by Jaenisch et al., (2021) during the winter wheat harvest seasons of 2016, 2017 and 2018 in Kansas, USA. The survey data focused on non-irrigated fields, which represent 96% of the wheat in the region (USDA-NASS, 2019)

Yield and Management data

Field-specific management practices data collected from each field are shown in Table 4-1. For more details about data collection and processing, please see Jaenisch et al., (2021). Briefly, a total of 48 field specific management variables were collected either directly or indirectly calculated. Nitrogen (N) was divided by the first application and second application, with different sources (Urea, urea ammonium nitrate, or anhydrous ammonia), timing (during tillering, joint or pre sowing), and application methods (streamer nozzle, broadcast, or knife) characterizing the full nitrogen management of a field. Variety names were asked from growers

and this nominal variable was translated into more biologically relevant varietal ratings for given agronomic characteristics, using a 1-to-9 scale, where one is highly resistant (StripeRust, LeafRust, WSM and Drought), early maturity (Maturity), and short (Height); and nine is highly susceptible, late maturity, and tall.

Table 4-1- List of agronomic management variables collected from commercial wheat fields in Kansas during three crop seasons (2016-2018).

Agronomic management data	**Units (or classes)**
Sowing date	Day of year
Variety or blend name	Unitless, used to retrieve different seven variety traits
Pre-plant control of volunteer wheat	Yes/No
Row spacing	cm
Seeding rate	Kg ha^{-1}
Fungicide seed treatment	Yes/No
Insecticide seed treatment	Yes/No
Both seed treatment	Yes/No
Grazing	Yes/No
Manure	Yes/No
Tillage	Conventional or no-till
In-furrow phosphorus	Yes/No
Broadcast or banded phosphorus	Yes/No
Phosphorus rate	Kg ha^{-1}
First Nitrogen source	Urea, urea ammonium nitrate, or anhydrous ammonoia
First Nitrogen rate	Kg ha^{-1}
First Nitrogen application method	Streamer nozzle, broadcast, or knife
First Nitrogen timing	Pre-plant, Zadoks' 20 or 31
Second Nitrogen source	Urea, urea ammonium nitrate, or anhydrous ammonoia
Second Nitrogen rate	Kg ha^{-1}
Second Nitrogen application method	Streamer nozzle, broadcast, or knife
Second Nitrogen timing	Pre-plant, Zadoks' 20 or 31
Total Nitrogen rate	Kg ha^{-1}
Sulfur	Yes/No
Chloride	Yes/No
Zinc	Yes/No
Fungicide application (jointing stage) (Zadoks 25− 31)	Yes/No
Fungicide application (flag leaf stage) (Zadoks 39− 55)	Yes/No

Table 4-1. Continued.

Previous Crop	Corn	Yes/No
	Fallow	Yes/No
	Soybean	Yes/No
	Wheat	Yes/No
	Other	Yes/No
Varieties	Leaf rust variety resistance	1-9
	Stripe rust variety resistance	1-9
	WSM variety resistance	1-9
	Maturity - variety maturity rating	1-9
	Height - variety maturity rating	1-9
	Drought - variety drought tolerance rating	1-9
	Straw strength-variety rating	1-9

Environmental data

Climate data: Mean maximum temperatures (Tmax), and minimum temperatures (Tmin), and precipitation data were collected from the National Weather Service Cooperative Observer Program and Automated Surface Systems in Kansas, which includes 455 stations. Daily solar radiation and reference evapotranspiration were collected from 62 Kansas Mesonet stations. The daily dataset was filtered for the following conditions: (i) outliers were characterized as presenting more than 3.5 standard deviations away from climatological mean temperature for the day (Frich et al., 2002); (ii) daily homogeneity of temperature and precipitation observations were observed visually by the monthly average time series. Site weather data were then interpolated by using natural neighbor interpolation method (Amidror, 2002) on a daily step.

Weather variables included in this study were cumulative rainfall and mean daily Tmax and Tmin for the growing season and for the grain filling period, cumulative solar radiation for the growing season, and the photothermal quotient (PTQ, the ratio between incident solar radiation and average temperature) for the critical period (20 days before anthesis until 10 days after anthesis) using a $T_{base} = 0$℃.

Soil data: included available water capacity (AWHC) at the 0-20cm and 20-200cm depths and simulated initial plant available water at sowing, the initial moisture conditions. The dataset includes soil depth and available water capacity and was retrieved from the Web Soil Survey database (USDA-NRCS, 2015). Dataset collection followed the steps: (i) creating an area of interest using the field boundaries, (ii) quantifying the percentage of each different soil class within each field, and (iii) calculating the weighted-average AWHC across the different soil types for each depth. Soil curve number, albedo, bulk density, and drainage factor were retrieved from Soltani and Sinclair (2012) and Ratliff et al., (1983). The initial plant available water was

calculated using the Simple Simulation Model (SSM) – Wheat, (Soltani & Sinclair, 2012) depending on the previous crop harvested. When wheat was sown following fallow, the model initiated at 50% available water and the soil water balance component estimated the available water at wheat sowing (Lollato et al., 2016). When wheat was sown immediately after a summer crop, the initial plant available water was calculated preceding soybeans or maize modules of the SSM model.

4.2.2.2. Field polygons

Initially, the survey field provided 656 field-specific geo-coordinates and 656 polygons were created representing the field boundaries. To evaluate the winter wheat field geolocations, we used corresponding annual USDA Cropland Data Layer (CDL) datasets (USDA National Agricultural Statistics Service Cropland Data Layer, 2023). Some of the survey geo-coordinates provided did not correspond with winter wheat in the CDL and were removed from the analysis, 499 samples remained (205 in 2016, 179 in 2017, and 115 in 2018). After applying additional data screening (4.2.4.2. NDVI time series), the final dataset comprised 220 samples (field-yield pairs) (Figure 4-1).

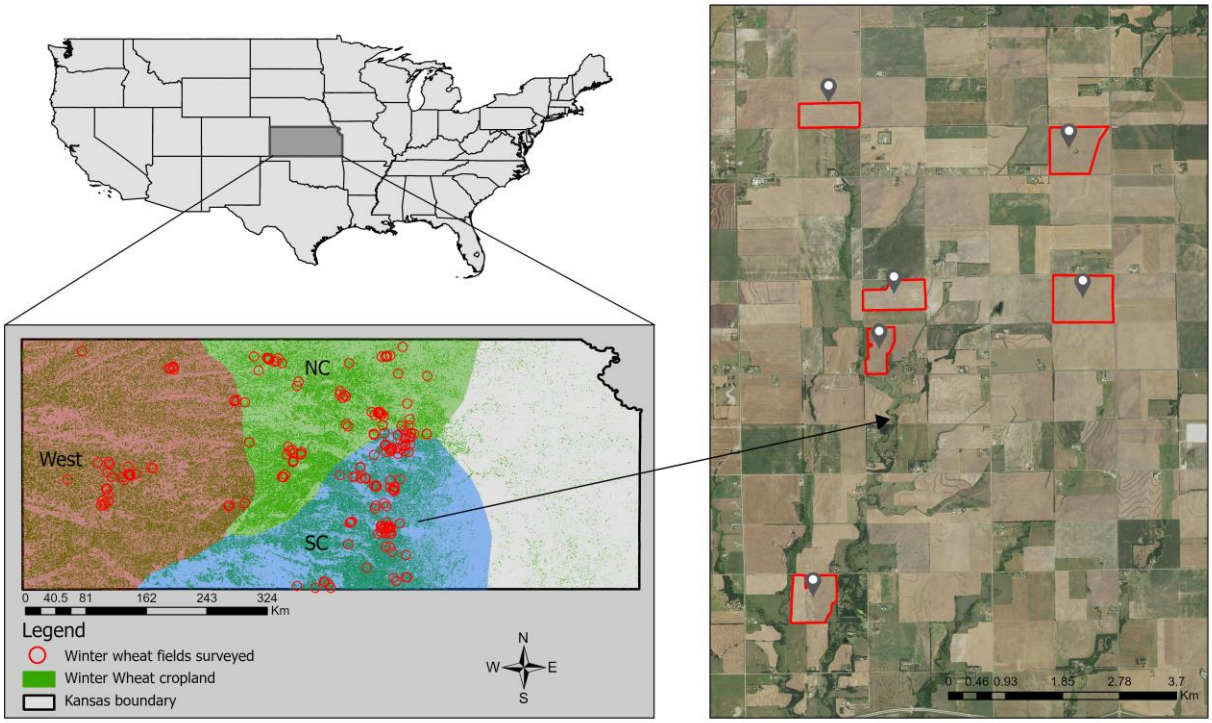

Figure 4-1- Kansas map shows the three sub- regions studied in Kansas (North Central, NC; South Central, SC; and West) as different colors. The red dots represent the 220 sample locations examined in the study. Overlaid on the aerial imagery are field boundaries for some of the winter wheat fields.

4.2.3. Satellite data

Landsat 8 OLI captures images of the Earth's surface in nine spectral bands at a 30-m spatial resolution (15-m for panchromatic band). The dataset contains atmospherically corrected surface reflectance and land surface temperature. The study sites are covered by eight tiles for which Landsat 8 OLI Collection 1 data were downloaded from the United States Geological Survey (USGS) website (https://earthexplorer.usgs.gov/ accessed in January 2021).

4.2.4 Methodology

4.2.4.1. Satellite data preprocessing

Detection and removal of ground-obscuring clouds and cloud shadows is essential for remote sensing data processing. For Landsat USGS, we applied a conditional using the Quality Assessment (QA) band (USGS, 2023), preserving only pixels with clear terrain conditions or low to no confidence of cloud conditions.

4.2.4.2. NDVI time series

Time-series NDVI data are commonly used to monitor crop development throughout a growing season (Lai et al., 2018; Shammi & Meng, 2021; Shen & Evans, 2021), which is for winter wheat in Kansas displayed from January to June (DOY 1-180) (Masialeti et al., 2010; Wardlow et al., 2007). NDVI is calculated by the difference of red (Red) and near-infrared (NIR) reflectance bands (Rouse and Haas, 1974; Tucker, 1974), according to equation 1:

$$NDVI = \frac{NIR-Red}{NIR+Red} \quad (4\text{-}1)$$

Data from several Landsat scenes were required for this study. If a field had representation in multiple tiles and multiple concurrent (to the day) NDVI values were available, then the maximum NDVI was used (Figure 4-2).

NDVI time series were visually accessed and a threshold NDVI value of 0.2 during April to May period was set. This threshold was defined because Landsat NDVI time-series showed lower NDVI values during the peak season compared to MODIS and Sentinel. Landsat NDVI time series with values higher than 0.2 during the peak season were capable to represent the winter wheat growing season. As an additional constraint to bolster signal completeness, only fields with at least one monthly NDVI observation in the February-June period were included.

January was not included since there is still influence of snow cover, thus NDVI values are close to 0 or missing. In total, 220 fields matched this criteria and were used in this analysis.

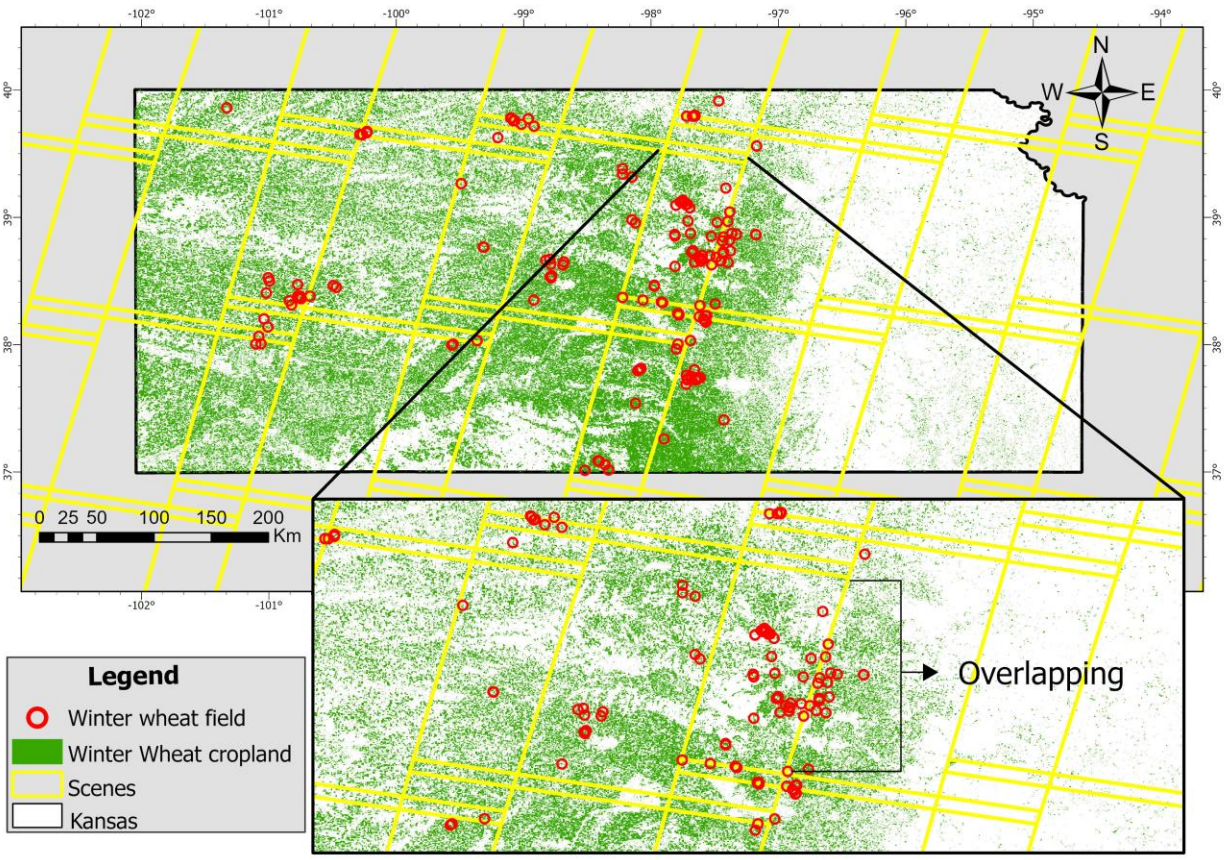

Figure 4-2- (a) Landsat-8 scenes in yellow that are passing over the study area (b) In detail, fields in red that are represented by multiple scenes.

4.2.4.3. Time series interpolation

Landsat VI time series are commonly affected by missing values (gaps). Using an up-sampling technique, we increased the frequency of the Landsat NDVI observations by every 7 days(Figure 4-3). Specifically, we used linear interpolation between missing NDVI values to fill

gaps. Since some samples had their earliest available February-June NDVI observation as late as DOY 56, we defined the study period to span DOY 56-182 (mid-February to end of June).

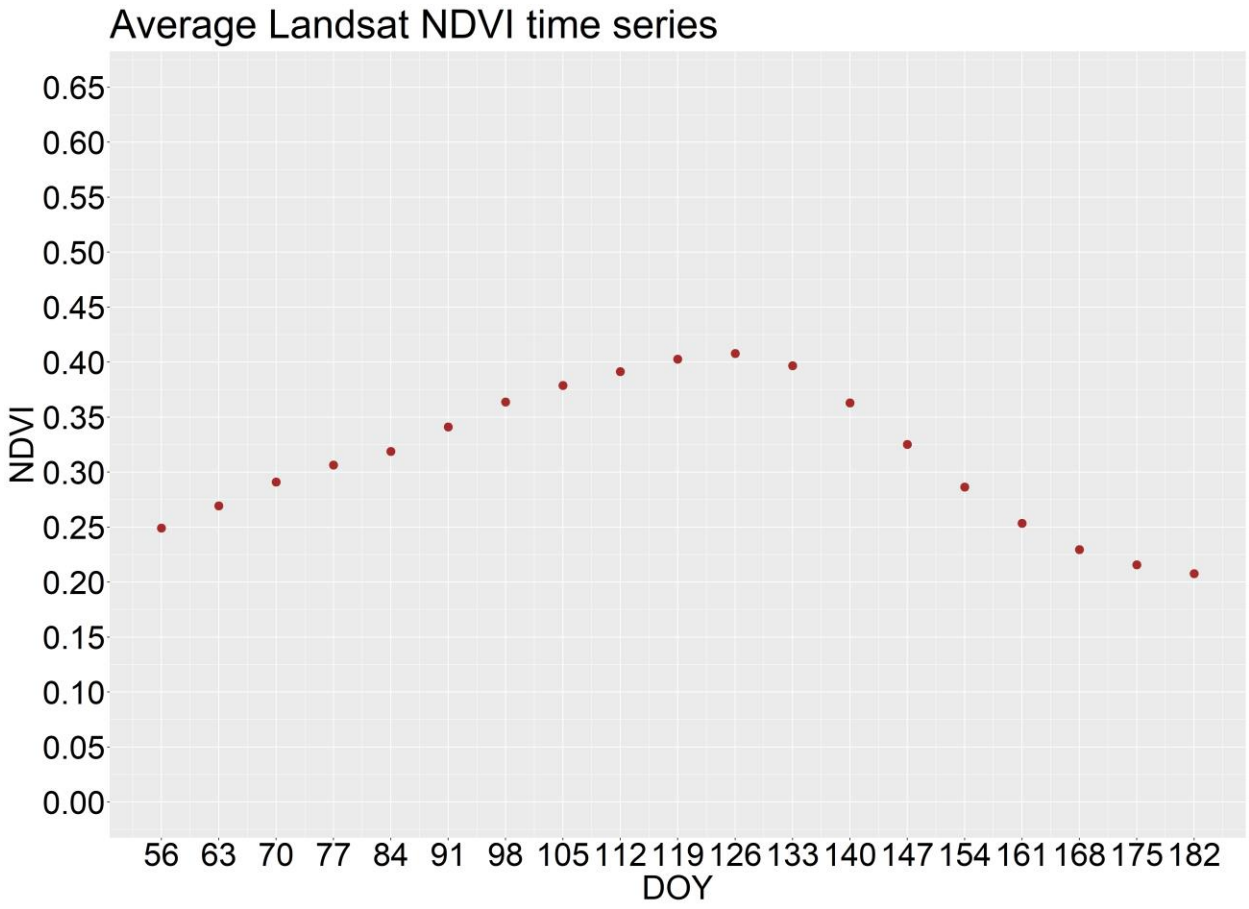

Figure 4-3 - Final NDVI profiles averaged across all samples (n =220).

4.2.4.4. NDVI predictor variables

NDVI area under the curve (or AUC) and NDVI weekly data were selected to serve as potential predictors of winter wheat yields. We selected the interval DOY 56-182 to define the accumulated NDVI predictor variables (NDVI AUC). DOY 56- 182 covers the *full season*, (mid-February to June), comprising post-dormancy tiller development, stem elongation, heading, anthesis, grain fill, and ripening. NDVI AUC was determined using the trapezoid rule for integral

approximation. Consequently, 20 independent variables were used as winter wheat yield predictor variables: NDVI AUC, DOY 56, .

4.2.4.5. Regional analysis

Regional heterogeneity in Kansas poses challenges for winter wheat yield prediction. Subdividing a heterogenous region into smaller, more homogeneous subregions considering the biophysical determinants can potentially improve winter wheat yield prediction (Rattalino Edreira et al., 2020; Wardlow et al., 2007). In this study, three subregions were used to subdivide field-specific data as previously established in Jaenisch et al. (2021). Briefly, winter wheat fields were clustered into three surveyed zones based on long-term climate data (long-term cumulative growing degree days, aridity index, temperature seasonality) and cropping systems, following a similar but coarser approach than that proposed by van Wart et al., (2013) Subregions were clustered based on the following weather classification: North-central (635-890mm annual precipitation and 3,792-4,829 °C annual thermal units), south-central (635-890mm, 4,830-5,949 °C annual thermal units), and west (<625mm, 3,792-4,829°C annual thermal units).

4.2.4.6. Empirical methods for estimating winter wheat yields.

Least absolute shrinkage and selection operator (LASSO)

LASSO was applied to minimize overfitting and prediction error. The model performs regularization and feature selection and it was first formulated by Tibshirani, (1996). LASSO applies a shrinkage (or regularization) process where it penalizes the coefficient of regression variables, shrinking some of them to zero. The variables that still have non-zero coefficients after the shrinkage process are selected to be part of the model. In this study, the tuning parameter to

of shrinkage penalty was determined using 10-fold cross validation. The length of the path (min lambda and max lambda) was chosen to be 0.01 and 10 default values along the regularization pass were tested to find the best lambda value. LASSO was performed using Scikit-learn in Python 3.9.

Although LASSO greatly reduces redundant variables and overfitting, there may still be a need to remove remaining variables that are not statistically significant to the yield prediction model. Therefore, the final models (Linear regression and Random Forest) were built using only the most influential variables according to their influence in the final yield, selected by the regression coefficients from NDVI predictor variables. The NDVI predictor variables were selected by t-value score, p-value, residual error and coefficient of estimation analysis. In some cases, the selection was also made by analyzing if the addition or removal of a variable could improve the results or not.

Linear Regression

Linear regression is a popular and straightforward technique in crop yield prediction studies, often used as a benchmark with other models. Linear regression predicts the dependent variable Y_i (Yields) using a set of independent variables X_{ij}(NDVI, management and weather). The model is expressed by:

$$Yield = \sum_{j=1}^{k} B_j X_{ij} + \varepsilon_i \qquad (4\text{-}2)$$

Where k is the number of independent variables, $B_j$is a regression coefficient, X_{ij} is the j value for the observation i, and $\varepsilon_i$is the residual error.

Random Forest

The same data used for training the linear regression model was used in the Random Forest (RF) model for comparison purposes. Along with linear regression, RF is one of the most used models for crop yield prediction (Everingham et al., 2016; Pang et al., 2022; van Klompenburg et al., 2020) RF is an ensemble learning technique elaborated by (Breiman, 2001) constructed by a large set of decision trees, with each tree being built using a random set of features and samples.

The generalization error converges to a limit as the number of trees in the forest becomes large and will depend on the strength of the individual trees in the forest and the correlation between them. RF then calculates the average of prediction from the terminal nodes to make the final prediction. Important RF hyperparameters, M_{try} (the number of variables randomly considered at each node) and N_{tree} (the number of random trees to be grown) were optimized by tuning approaches. Hyperparameter tuning and statistical performance evaluation were performed using the 'ranger' package (Wright & Ziegler, 2017) in RStudio.

4.2.4.7. Model Evaluation

Linear regression and RF models were evaluated using a repeated 10-fold cross validation (CV). In K-fold CV, the entire available data is randomly partitioned into folds of equal size, then the training of the model is done on k-1 parts and one part is left out for testing. This process is repeated k times, where each of the folds is used once to measure the prediction accuracy. The resulting error measures of each interaction is averaged to calculate the final error (Hastie et al., 2009). K-fold CV estimation has a variation due to randomness of partitioning the

sample into k-folds (Efron & Tibshirani, 1997). To reduce the internal variance the whole process of partitioning and estimating was repeated 10 times (Kim, 2009).

RF model performance was assessed using the coefficient of determination (R^2) to estimate how much variation in the observations was explained by the model, Root Mean Squared Error (RMSE) as an average squared errors-based statistic that penalizes large errors, and Mean Absolute error (MAE) as an average magnitude of the errors, defined as follows:

$$R^2 = 1 - \frac{\sum_{i=1}^{n}(y_{i-} \hat{y}_i)}{\sum_{i=1}^{n}(y_{i-} \bar{y})^2} \quad (4\text{-}3)$$

$$RMSE = \sqrt{\frac{\sum_{i=1}^{n}(y_{i-} \hat{y}_i)^2}{n}} \quad (4\text{-}4)$$

$$\text{MAE} = \frac{1}{n}\sum_{i=1}^{n}|y_{i-} \hat{y}_i| \quad (4\text{-}5)$$

4.3. Results

4.3.1. LASSO and coefficient analysis for feature selection

Using all field-yields (Table 4-2 and Table 4-3), NDVI predictor variables, NDVI AUC and DOY 140, along with the management variables flag leaf foliar fungicide, seed fungicide application, total N, initial plant available water, variety leaf rust resistance, manure fertilizer, second N application stage (during tillering) and first N source (urea); and the weather variable cumulative rainfall during growing season were the most significant variables. All variables presented positive impact in yields, except for the first nitrogen source using urea and seed fungicide application.

In NC (Table 4-4 and Table 4-5), the NDVI predictor variables DOY 105 and DOY 154 along with the management variables previous corn crop, variety height, phosphorus (P) rate, total N rate, chloride (Cl) application, zinc (Zn) application, and the weather variables mean

maximum temperature and initial plant available water were the most significant and included in the prediction models. Among all variables, only Zn application and previous crop corn had an negative correlation with winter wheat yields.

In SC (Table 4-6 and Table 4-7), the only NDVI predictor variable included was DOY 133, among the management and weather variables, insecticide seed treatment, flag leaf foliar fungicide, total N rate, manure fertilizer, urea as the first N source, broadcast as the first nitrogen method, second N stage (during joint), mean maximum temperature during grain filling and water holding capacity of the soil in the upper 20 cm layer were incorporated in the prediction model. Seed insecticide application, first N source (urea), first N method (broadcast), second N stage (during joint), and mean maximum temperature during grain filling had negative impact in the yields. Lastly, in the West (Table 4-8 and

Table 4-9)**,** the most significant variables were NDVI predictor variable DOY 133, sowing date, initial plant available water and mean maximum temperature. Sowing date and maximum temperate had a negative effect on the winter wheat yields.

Table 4-2- Regression coefficients from all field-yields using NDVI, climate, and management predictor variables selected by LASSO.

Predictors	**Estimate**	**Std.Error**	**t value**	**Pr(>|t|)**
(Intercept)	1.081	1.413	0.765	0.445
AUC	0.030	0.017	1.782	0.076
DOY133	-0.341	2.750	-0.124	0.901
DOY140	3.606	2.341	1.54	0.125
Leaf rust variety resistance	0.063	0.029	2.165	0.031
Total Nitrogen rate	0.006	0.002	2.973	0.003
Fungicide seed treatment (yes)	-0.305	0.138	-2.215	0.027
Fungicide application - flag leaf stage (yes)	0.484	0.135	3.571	<.001
First Nitrogen source -urea (yes)	-0.248	0.133	-1.863	0.063
Second Nitrogen timing (tiller)	0.206	0.129	1.592	0.112
Initial plant available water	0.001	0.0004	4.664	<.001
Cumulative rainfall	0.0009	0.0005	1.692	0.092
Max temp during grain-fill	-0.051	0.040	-1.276	0.203
Manure (yes)	0.493	0.286	1.721	0.086
Residual standard error	0.778			
R^2	0.578	***p-value:*** <.001		

Table 4-3- Regression coefficients from all field-yields NDVI predictor variables included in the linear regression and RF models.

Predictors	**Estimate**	**Std.Error**	**t value**	**Pr(>|t|)**
(Intercept)	-0.632	0.442	-1.431	0.153
AUC	0.037	0.012	3.085	0.002
DOY140	2.420	1.083	2.233	0.026
Fungicide application - flag leaf stage (yes)	0.531	0.130	4.08	<.001
Initial plant available water	0.001	0.0004	4.529	<.001
Cumulative rainfall	0.001	0.0005	2.384	0.018
Total Nitrogen rate	0.006	0.001	3.566	<.001
Leaf rust variety resistance	0.060	0.028	2.094	0.037
Fungicide seed treatment (yes)	-0.316	0.137	-2.302	0.022
Manure(yes)	0.506	0.285	1.771	0.078
Second Nitrogen timing (tiller)	0.213	0.129	1.645	0.101
First Nitrogen source -urea (yes)	-0.243	0.132	-1.83	0.068
Residual standard error	0.773			
R^2	0.575	***p-value:*** <.001		

Table 4-4- Regression coefficients from NC predictor variables selected by LASSO.

Predictors	**Estimate**	**Std.Error**	**t value**	**Pr(>|t|)**
(Intercept)	-6.445	3.666	-1.758	0.0842
DOY105	2.541	1.428	1.779	0.080
DOY154	2.514	1.467	1.714	0.092
Previous crop – other(yes)	0.394	0.634	0.622	0.536
Previous crop -corn (yes)	-1.019	0.439	-2.318	0.024
Height	0.112	0.057	1.971	0.053
Phosphorus rate	0.020	0.009	2.287	0.026
Total nitrogen rate	0.011	0.005	2.166	0.034
Broadcast or banded phosphorus (yes)	0.135	0.202	0.669	0.506
Chloride application (yes)	1.036	0.463	2.236	0.029
Zinc application (yes)	-0.387	0.200	-1.932	0.058
Second Nitrogen application method (streamer)	-0.219	0.288	-0.76	0.450
Initial plant available water	0.001	0.0007	1.4	0.167
Max Temp	0.337	0.218	1.547	0.127
Min Temp	-0.065	0.160	-0.408	0.684
PTQ during critical period	0.713	0.863	0.826	0.412
Residual standard error	0.569			
R^2	0.721	***p-value:*** <.001		

Table 4-5- Regression coefficients from NC predictor variables included in the linear regression and RF models.

Predictors	**Estimate**	**Std.Error**	**t value**	**Pr(>|t|)**
(Intercept)	-5.446	1.693	-3.216	0.002
DOY105	2.8951	0.959	3.019	0.003
DOY154	3.028	1.264	2.394	0.019
Previous crop -corn (yes)	-1.016	0.426	-2.382	0.020
Height	0.128	0.052	2.468	0.016
Phosphorus rate	0.022	0.007	2.99	0.003
Total nitrogen rate	0.010	0.004	2.294	0.025
Chloride application (yes)	0.945	0.436	2.165	0.034
Zinc application (yes)	-0.487	0.164	-2.953	0.004
Initial plant available water	0.001	0.0006	2.349	0.022
Max Temp	0.302	0.101	2.972	0.004
Residual standard error	0.555			
R²	0.712	***p-value:*** <.001		

Table 4-6- Regression coefficients from SC predictor variables selected by LASSO.

Predictors	Estimate	Std.Error	t value	Pr(>|t|)
(Intercept)	3.911	4.27	0.914	0.363
AUC	5.42E-05	0.027	0.002	0.998
DOY133	1.672	2.5123	0.666	0.507
DOY154	1.156	2.263	0.511	0.610
Leaf rust	0.020	0.042	0.476	0.635
Drought	-0.086	0.089	-0.972	0.333
Total nitrogen rate	0.003	0.003	1.09	0.278
Insecticide seed treatment (yes)	-0.736	0.335	-2.193	0.030
Manure (yes)	0.413	0.385	1.073	0.286
Sulfur application (yes)	-0.15	0.199	-0.752	0.454
First Nitrogen source – urea (yes)	-0.528	0.264	-1.998	0.048
First Nitrogen application method – broadcast (yes)	-0.265	0.228	-1.162	0.248
Second Nitrogen timing – tiller (yes)	0.077	0.201	0.384	0.702
Second Nitrogen timing – joint (yes)	-0.668	0.271	-2.46	0.015
Fungicide application (flag leaf stage)	0.731	0.183	3.987	0.0001
Max temp during grain-fill	-0.137	0.079	-1.731	0.086
Soil water holding capacity (upper 20 cm layer)	0.296	0.108	2.726	0.007
Initial plant available water	0.001	0.0008	1.575	0.118
Cumulative rainfall	7.73E-05	0.001	0.064	0.949
PTQ during critical period	0.881	1.807	0.488	0.626
Residual standard error	0.662			
R²	0.723	***p-value:*** <.001		

Table 4-7- Regression coefficients from SC predictor variables included in the linear regression and RF models.

Predictors	**Estimate**	**Std. Error**	**t value**	**Pr(>|t|)**
(Intercept)	5.838	1.356	4.305	<.001
DOY133	1.836	1.255	1.463	0.146
Total nitrogen application	0.006	0.002	2.378	0.019
Insecticide seed treatment (yes)	-0.847	0.295	-2.872	0.005
Manure (yes)	0.682	0.320	2.129	0.035
First Nitrogen source – urea (yes)	-0.423	0.213	-1.988	0.049
First Nitrogen application method – broadcast (yes)	-0.390	0.188	-2.068	0.041
Second Nitrogen timing – joint (yes)	-0.935	0.224	-4.16	<.001
Fungicide application (flag leaf stage)	0.692	0.160	4.322	<.001
Max temp during grain-fill	-0.181	0.042	-4.227	<.001
Soil water holding capacity (upper 20 cm layer)	0.333	0.101	3.286	0.001
Residual standard error	0.650			
R^2	0.706		***p-value:*** <.001	

Table 4-8- Regression coefficients from West predictor variables selected by LASSO.

Predictors	Estimate	Std. Error	t value	Pr(>|t|)
(Intercept)	20.049	8.262	2.427	0.021
DOY133	9.833	3.879	2.535	0.016
DOY140	1.516	4.289	0.353	0.726
Previous crop – other (yes)	-0.164	0.671	-0.245	0.808
Fungicide application (flag leaf stage)	0.240	0.329	0.73	0.471
Sowing date	-0.043	0.022	-1.897	0.067.
Initial plant available water	0.002	0.0009	2.281	0.030
Max temp	-0.546	0.216	-2.519	0.017
Cumulative rainfall during grain-filling	-0.001	0.004	-0.478	0.636
Residual standard error	0.735			
R^2	0.784	***p-value:*** <.001		

Table 4-9 - Regression coefficients from West predictor variables included in the linear regression and RF models.

Predictors	Estimate	Std. Error	t value	Pr(>|t|)
(Intercept)	23.866	7.139	3.343	0.002
DOY133	11.087	1.775	6.246	<.001
Sowing date	-0.052	0.019	-2.651	0.012
Initial plant available water	0.002	0.0007	3.558	0.001
Max temp	-0.638	0.159	-4.006	<.001
Residual standard error	0.706			
R^2	0.773	***p-value:*** <.001		

4.3.2. Predicting winter wheat yields using NDVI, climate, and management predictor variables.

Table 4-10 shows the descriptive statistics of training dataset and testing dataset using linear regression and RF. The subregional approach with additional use of management practices and environmental data along with NDVI greatly benefited the prediction models, although

overall linear regression still performed better than RF. Prediction error was higher using all field-yields than in subregions NC, SC and West, with a RMSE of 0.78 Mg ha^{-1}. For instance, NC Kansas presented the lowest prediction error among all regions (RMSE=0.58 Mg ha^{-1}). Contrasting the results from the previous Chapter 3 - , SC Kansas achieved the best fit between training and testing data with training results of R^2 of 0.70 and RMSE 0.65 Mg ha^{-1} and testing results R^2 0.70 and RMSE 0.66 Mg ha^{-1}.West presented the third best performance with prediction error of 0.69 Mg ha^{-1}.

In the RF the prediction performance across all fields was slightly higher than linear regression, with a R^2 0.57 and RMSE 0.78 Mg ha^{-1}. While better than the previous results from Chapter 2 - and Chapter 3 - , RF persisted with overfitting. The RF training results are the in-sample R^2 and RMSE from the prediction results using all dataset and shows high R^2 (>0.9) and low RMSE (<0.46 Mg ha^{-1}), whereas the results from 10-fold cross validation overall showed a $R^2 < 0.71$ and RMSE > 0.59 Mg ha^{-1}, this discrepancy between results suggest that great overfitting is occurring in the model.

Table 4-10. Descriptive statistics of training dataset and testing dataset using Linear Regression and Random Forest.

		Regions							
Models	**Metrics**	**ALL**		**NC**		**SC**		**West**	
		Train	**Test**	**Train**	**Test**	**Train**	**Test**	**Train**	**Test**
Linear Regression	R^2	0.575	0.545	0.712	0.663	0.706	0.704	0.773	0.736
	RMSE (Mg ha^{-1})	0.773	0.786	0.555	0.584	0.6505	0.662	0.706	0.693
Random Forest	R^2	0.931	0.576	0.925	0.658	0.924	0.680	0.93	0.711
	RMSE (Mg ha^{-1})	0.370	0.787	0.307	0.593	0.373	0.711	0.461	0.834

Figure 4-4 shows the results from linear regression and RF yield prediction model in all field-yields and by subregions NC, SC and West in Kansas using NDVI, climate, and management predictor variables. Since the objective is prediction yield performance, the major focus is on the prediction error, the RMSE and MAE rather than R^2. Linear regression results showed that the yield estimation using all fields NDVI predictor variables achieved lowest performance compared to the subregions NC, SC and West. NC obtained the best results with a R^2 of 0.66, RMSE of 0.58 Mg ha^{-1} and MAE of 0.48 Mg ha^{-1}, followed by SC with a R^2 of 0.70, RMSE of 0.66 Mg ha^{-1} and MAE of 0.52 Mg ha^{-1}. West achieved a R^2 of 0.73, RMSE of 0.69 Mg ha^{-1} and MAE of 0.59 Mg ha^{-1}. Although with better results than all fields in Kansas, West showed the highest standard deviation from the 10 K-Fold cross-validation results, which may be related to its limited dataset (n=39).

NC showed the lowest prediction error in the RF model with RMSE of 0.59 Mg ha^{-1}, followed by SC with RMSE of 0.77 Mg ha^{-1}, and when using all field-yields RMSE of 0.78 Mg ha^{-1}. West Kansas showed the lowest performance in the RF model with a R^2 of 0.71, RMSE of 0.83 Mg ha^{-1} and MAE of 0.69 Mg ha^{-1}. All fields and NC Kansas presented similar performance than the linear regression results, however with slightly lower R^2 and higher RMSE and MAE.

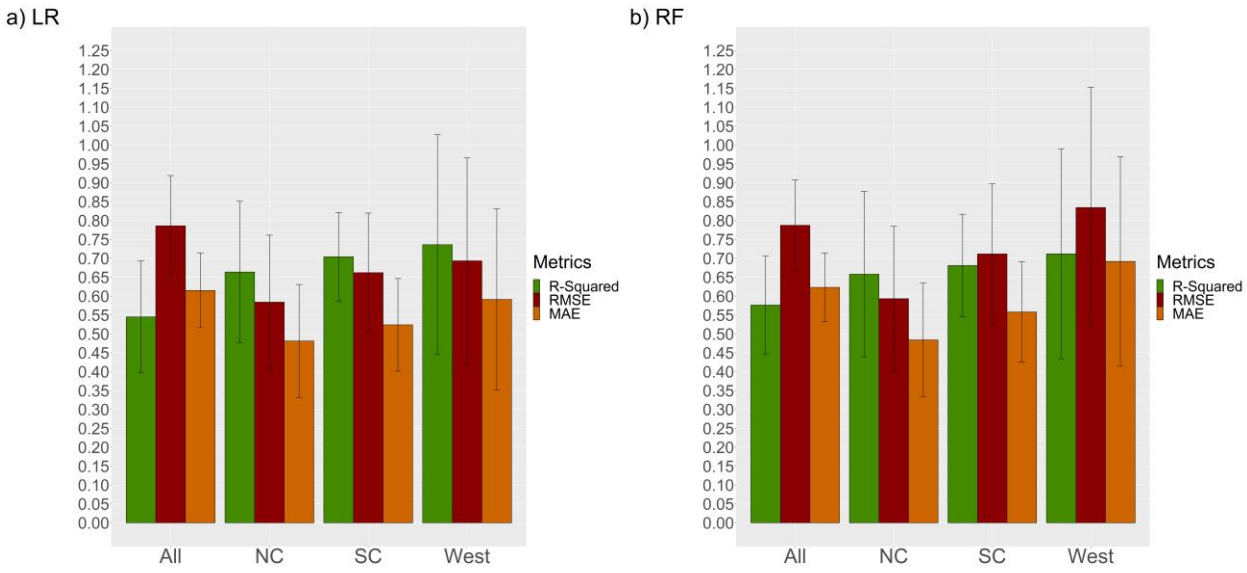

Figure 4-4- Statistical performance of Linear regression (LR) and Random Forest (RF) yield prediction model in all field-yields and by subregions NC, SC and West in Kansas using NDVI, climate, and management predictor variables.

Figure 4-5 compare the linear regression predicted and observed yield for all fields, and NC, SC and West subregions, respectively. There was a close clustering of data around the reference line for all field-yields between 3 to 4.5 Mg $ha^{-1,}$ while this was seen for the NC between 2.5 to 3.5 Mg ha^{-1}. In NC, linear regression performed better predicting field with lower yields than higher yielding ones. SC the data was clustered between 3.5 Mg ha^{-1} and 4.5 Mg ha^{-1}. Lastly, West displayed quite widely dispersed data, although some points are slightly clustered around 4 and 5.5 Mg ha^{-1}.

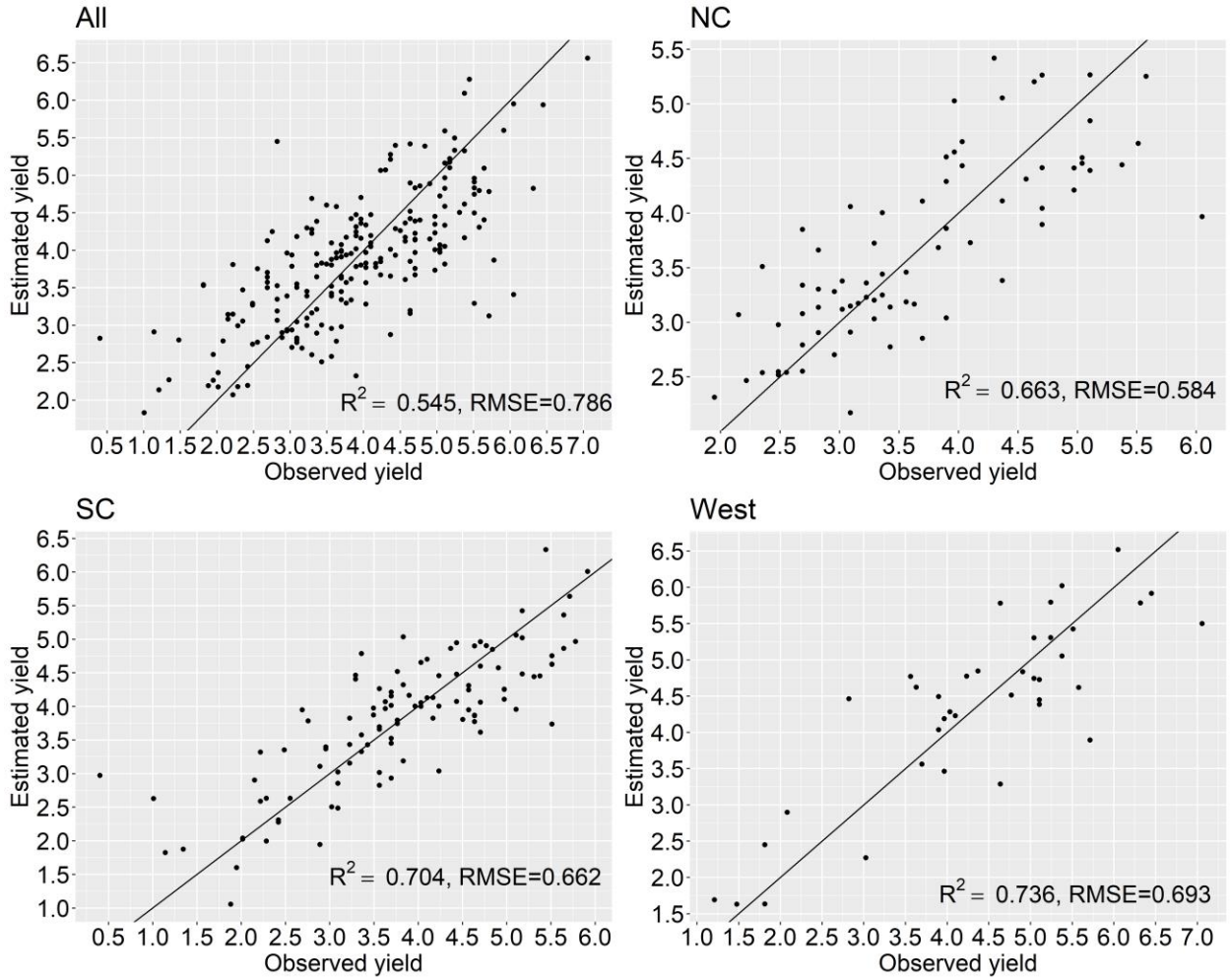

Figure 4-5 - Comparison of predicted vs. observed yield for all field-yields; NC ; SC and West.

4.4. Discussion

Linear regression and RF using the combinations of multiple sources (NDVI, climate and management) by subregions outperformed the single data source results in Chapter 3 - . Although machine learning models have been shown to outperform traditional linear regression models in explaining variability in data and for crop yield predictions (Cai et al., 2019; Schwalbert et al., 2018; Sun et al., 2022). In this study, linear regression performed better than RF. Some of the reasons related to the lack of improvement in the RF may be related to (i) the number of predictors for the given sample size, which may have driven down the effective

degrees of freedom of the RF modeling framework, (ii) the small number of observations due the lack of Landsat records matching with the criteria (see section 4.2.4.2. NDVI time series), which limited the study from 656 field-yields to 220 field-yields, with smaller observations by subregions, NC (n=73), SC(n=109) and West (n=38), (iii) the level of complexity of the dataset . In this case, if the relationship between predictors and yields is mainly linear, that may affect the relative performance of the RF algorithm and lead the model to overfit.

When analyzing all field-yields, RMSE was the highest compared to the other subregions with a 0.78 Mg ha^{-1}, showing the best prediction for fields with yields between 3 to 4.5 Mg ha^{-1}. Using a linear mixed-effects model, Lai et al., (2018) found that the integrated Landsat NDVI was useful to estimate wheat yield at within-field scale in Australia across large spatial regions. In contrast, Vannoppen and Gobin (2021) found weak relationship between integral NDVI and yields when predicting winter wheat yields in northern Belgium, differing from previous work where the integral NDVI along with climate data could explain up to 95% of variance in a regional approach in Latvia (Vannoppen et al., 2020).

Foliar fungicide, precipitation and initial plant water storage were also observed in previous studies as important variables to determine wheat yields in Kansas. Using a parsimonious CIT approach, Jaenisch analyzed the full survey dataset (n=656 field-yields) used in this chapter, and the results indicated cumulative growing season rainfall as the most important factor associated with increased winter wheat yields. According to the authors, in fields receiving more than 388mm of precipitation, yields ranged from 3.0 to 5.6 Mg ha^{-1}, with the highest yields related to foliar fungicide application during flag leaf. When receiving less precipitation, fields ranged from 2.5 to 3.0 Mg ha^{-1} and depended more on initial plant water storage. In a different study, Munaro et al.,(2020) used winter wheat variety performance trails

from U.S central Great Plains to quantify effects of management practices on crop yields variability and found that foliar fungicides were the variable more consistently associated with wheat yields across the region. For total N, the estimate coefficient showed that a smaller change in the mean of yield given one unit shift in the N variable than the other variables mentioned previously, however it shows as an important management fertilizer and potential predictor for winter wheat yields across the region.

NC achieved the highest accuracy among all subregions and better prediction than using all field-yields across Kansas, with a prediction error of 0.593 Mg ha^{-1}, and performing better in predicting in fields with yields between 2.5 to 3.5 Mg ha^{-1}. The NDVI DOY 105 predictor variable presented the strongest significance with wheat yields with the highest t-value among all variables. DOY 105 is identified as the period of ascending NDVI values in the NC NDVI time series (Figure 3-4) and may be related to flag leaf and heading stages before it reaches the vegetation peak around DOY 126, close to anthesis. According to Lollato, (2018) the flag leaf period and the next last leaf is a key stage that accounts for 70 to 90 percent of the photosynthates used for grain fill, a main source of energy for grain development and growth (Kong et al., 2010). Previous studies have indicated the good performance of NDVI during heading stage to predict winter wheat yields. For example, Magney et al., (2016) found that using NDVI data during heading stage reduced the model RMSE error from 1.44% to 1.09%. Ren et al., (2008) could achieve a good prediction at the booting-heading stage with a relative error of yield estimation from 4.62% to 5.40% . Among the weather variables, mean maximum temperature during growing season had a positive effect in winter wheat yields. Lollato et al., (2020) found strong latitudinal gradients in temperatures from southern to northern locations in the U.S Great Plains, with mean maximum temperature and minimum temperature decreasing

from 26.2 and 11.0 ◦C in southern locations to 17.4 and 2.5 ◦C in northern locations. Thus, assuming the colder weather in northern Kansas than the other subregions, mean maximum temperatures during growing season still a positive factor related to increasing winter wheat yields, while rising temperatures in southern areas are often related to reduced yields (Hatfield et al., 2018; Lollato et al., 2017). In addition, increased yields due warmer temperatures in northern areas of the US Great Plains have been related to an increase of growing degree days during critical growth stages that can be beneficial for winter wheat yields (Stewart et al., 2018).Some studies have mentioned that rising temperatures is making winter wheat production more challenging in southern areas than in northern areas of the U.S Great Plains (Barkley et al., 2014; Zhao et al., 2022).

Management of fertilizer, P,N and Cl presented a positive association with yields showing as good predictors of winter yields in NC. Curiously, Zn presented a negative influence on wheat yields. Some studies indicated that yield may affect mineral concentrations though the dilution effect in high yielding fields or concentration effect in low yielding fields (Fan et al., 2008; Liu et al., 2014). Thus, high concentration of Zn in lower yielding fields in NC may explain the negative relationship with yields and does not necessarily imply that reducing Zn application overall could produce gains in yields (Morgounov et al., 2007) . Plant height was also associated with final yield. In a study using different biological measurements from a long-term winter wheat study in Oklahoma, USA, Girma et al., (2006) indicated that mid-season measurements of NDVI, chlorophyll content, total nitrogen uptake and plant height was found as good predictors of final winter wheat grain yield.

NC showed greater predominance of predictor variables related to management fertilizers, while SC and West presented predictor variables, accounting with the management

ones, more related to weather as the most important for predicting winter wheat yield. SC and West regions are typically more exposed to heat stress and water deficit stress, respectively while NC presents a more favorable environment and cooler weather (Couëdel et al., 2021). As mentioned in (Jaenisch et al., 2021), the results provide insights about the greater importance in management practices and NDVI in determining yields in less erratic environments.

SC achieved the second-best result with RMSE of 0.66 Mg ha^{-1}.With the best prediction in fields with yields between 3.5 Mg ha^{-1} and 4.5 Mg ha^{-1}.NDVI predictor variable DOY 133 was not as significant as weather variables and management variables. The most important predictors in SC were fungicide application during flag leaf, mean maximum temperature during grain filling, soil water holding capacity and second N application timing (during joint). Maximum temperature during grain filling showed a negative correlation with wheat yields. In SC Kansas winter wheat is often threatened by high temperatures, precipitation and evapotranspiration, a combination that supports the results of mean maximum temperature during grain fill and soil water capacity as good predictors of grain yield (Couëdel et al., 2021).

SC greater moisture levels during growing season can also induce fungal disease development in winter wheat (Byamukama et al., 2019). Thus, fungicide application during flag leaf was positively related to grain yield and a potential good predictor for winter wheat yields. Nonetheless, application of foliar fungicide should be based on current weather conditions since drought stress during early spring is also a common phenomenon in the U.S Southern Great Plains (Cruppe et al., 2022). In this regard, although not included in the final model since it did not increase the prediction performance, drought was one of the variables previously selected from LASSO, presenting negative impact on yields in SC. The variable second N timing (during jointing) showed a significant negative impact in winter wheat yields in SC. However, due to the

already small dataset in SC, the number of observations of fields that applied second N during jointing stage was very small n=12, a larger dataset would provide more assertive results regarding the potential of estimation from this particular variable. Same results were observed for insecticide seed treatment and first application of N using urea, there was only 8 observations that applied seed treatment and 24 observations across the 109 samples.

The result in SC shows that early NDVI predictor variables were removed from LASSO feature selection when adding weather and management predictor variables. These results emphasize that using NDVI at earlier stages of the growing season to predict winter wheat yields may provide misleading prediction of grain yields, especially in vulnerable environments, since extreme weather conditions during anthesis and grain-filling stages can negatively impact the final yields (Kadam et al., 2014; Vallentin et al., 2022). An accurate prediction will depend on meteorological and management conditions that will occur during grain fill and harvest. Unlike crops whose production consists of total above-ground biomass, wheat grain is contained in storage organs and its yield is sensitive to meteorological conditions at critical growth stages. Consequently, there is uncertainty of yield prediction, since the above-ground biomass may be high, but the grain yield may not be commensurately large (Reeves et al., 2005).

In the West, the results showed that the NDVI predictor variable DOY 133, along with mean maximum temperature during growing season, initial plant available water and sowing were the most important variables for winter wheat yield prediction. The linear regression presented a RMSE of 0.69 Mg ha^{-1} and the highest R^2 among the other subregions, where the predictors could explain 73% of yield variability. The NDVI predictor variable DOY 133 showed the strongest relationship with yields compared to the other variables. During DOY 133, the NDVI values were still high and the descending NDVI values shows in a slower pace than

the other subregions (Figure 3-4), perhaps describing a late development and maturity. The results agree with Jaenisch et al., (2021), that also found later maturity varieties related to higher yields than early maturity ones in West Kansas. Mean maximum temperature during growing season was the second most influential variable and had a negative impact in winter wheat yields in West Kansas. A handful of studies have indicated winter wheat yield loss due extreme temperatures and water supply variability in the semi-arid Western Kansas (Lin et al., 2017; Lollato et al., 2017). Analyzing hot-dry-windy (HDW) events in the U.S Great Plains, Zhao et al., (2022) found that HDW has increased from 1982 to 2020 and were the most impactful drivers for wheat yield loss, especially in the southwest Kansas and the panhandle areas of Oklahoma and Texas.

Initial plant water storage appeared as an important component in predicting winter wheat yields in the West. Since West Kansas is a drought prone area, water supply is a key component for winter wheat growth, explaining 82% of yield variability in this region (Lollato et al., 2017). Lastly, sowing date had a negative effect in winter wheat yields in West. Optimum sowing dates are often earlier in the West than in NC and SC subregions in Kansas (Jaenisch et al., 2021; Munaro et al., 2020). Due the cooler air and soil temperatures, sowing starts earlier in the northwest around September 10th and lasts until the end of September, while in Southeastern Kansas it can start as late as October 5th. Thus, sowing in colder soils can delay wheat emergence and impact tiller development reducing winter hardiness during winter (Shroyer, 1996).

Overall, empirical winter wheat yield modeling using NDVI predictor variables in Kansas is environmentally dependent, especially in SC and West Kansas. Nevertheless, the use of management region-specific variables provided important information, where NC showed management of fertilizers (N, P, Cl) as good predictors and could be used along with NDVI to

estimate yields. SC and West predictor variables relied more on variables related environmental conditions, such as fungicide application, soil water storage, sowing data. For future work, a larger sample size could potentially improve machine learning modeling and prediction accuracy using NDVI, especially in NC and West Kansas.

Chapter 5 - Conclusion

This dissertation focused on analyzing the potential of using satellite imagery to predict winter wheat yields at the field scale in Kansas. The study is quite unique since it uses remote sensing to predict yield at field scale across a large region that is environmentally heterogeneous. The work involved evaluating different satellite sensors, from coarse to moderate resolution, using Normalized Vegetation Index Data, and assessing winter wheat yields by more homogeneous regions using different types of data (NDVI, climate, and weather).

In Chapter II, the study aimed to investigate the potential of satellite imagery of different resolutions to predict field-level winter wheat in Kansas. The results indicated an agreement between the NDVI time-series profiles and the phenological characteristics (growth stages) of winter wheat in Kansas, especially with Landsat USGS and MODIS. Landsat USGS presented the lowest prediction error among all sensors analyzed with an RMSE of 0.95 Mg ha^{-1} using linear regression. Generally, the NDVI predictor variables were not enough to explain field-scale winter wheat yield variability across much of Kansas. Nevertheless, the chapter presented interesting outcomes, such as using the NDVI weekly data as predictor variables, indicating that Landsat USGS NDVI variables performed better in the early season DOY 56 and near the end of the growing season (DOY 154) while MODIS NDVI variables performed better at peak season (from DOY 105-154). Overall, the results show the challenge in predicting winter wheat yields at field scale over a very heterogeneous region. Thus, when the NDVI is not enough to detect yield variability, it may require more spatial information regarding climate, soil characteristics, and management practices. In addition, it is important to highlight challenges and limitations in this chapter, such as the small dataset caused by mismatching field geolocations that reduced the number of winter wheat samples and missing data from satellite imagery; and not fully exploring

the higher temporal and spatial resolution, from Sentinel-2 AB due the dataset unavailability in 2016.

In Chapter 3, the main objective was to evaluate improvements in winter wheat yield estimation by more homogeneous regions using satellite imagery at the field scale in Kansas. NDVI time series presented to be capable of tracking seasonal changes and detect distinct patterns of winter wheat growth in NC, SC, and West Kansas. The results proved more accurate when using NDVI variables to predict winter wheat yields in more homogeneous regions (NC, SC, and West) than when using fields across all three regions combined. For instance, NC performed best with an RMSE of 0.71 Mg ha^{-1} followed by SC with a RMSE of 0.93 Mg ha^{-1} . SC presented a high prediction error, however, lower than when using all field-yields. NDVI during late growing season stages was the most associated with yields, showing that yield estimation accuracy reaches the maximum in the late growth stage. Wheat yield estimates made at the end of the growing season might allow state agencies to improve the accuracy of regional yield forecasting, however they are too late for promoting early to mid-season farm management decisions. The prediction model also showed that is possible to predict in the earlier stages of the growing season; however, its accuracy will depend on weather conditions. The results indicated that the improved performance in NC may be related to its favorable environment compared to SC and Western Kansas. Overall, the results confirmed the importance of using more homogeneous regions in Kansas to predict winter wheat yields using satellite imagery.

In the fourth chapter different types of data, including satellite imagery, climate, soil, and management data, were used as the predictors to forecast the winter wheat yield by subregions at the field scale in Kansas. A zonal approach (NC, SC, West) that includes weather and management variables along with NDVI was found to improve field-scale yield estimation in

Kansas. NC, SC, and West Kansas performed better than when estimating yields using all field yields. NC achieved the highest accuracy among all subregions and better prediction than using all field-yields across Kansas, with a prediction error of 0.59 Mg ha^{-1} . In addition, the use of management region-specific variables provided important information, where NC showed management of fertilizers (N, P, Cl) as good predictors and could be used along with NDVI to estimate yields. SC predictor variables relied more on environmental conditions, such as soil water storage and management practices associated with weather conditions (fungicide application). Although also relying on weather variables, West Kansas showed the potential of using NDVI predictor variables during grain filling stages and the importance of management region-specific variables such as showing date. In Chapter 3, the Linear regression model showed that it is possible to predict in earlier stages of the growing season; however, its accuracy will depend on weather conditions. Thus, empirical winter wheat yield modeling using NDVI predictor variables in Kansas is environmentally dependent, especially in SC and West Kansas.

Linear regression performed better than RF across all studies, in chapters 2 to 4. Some of the reasons related to the lack of improvement in the RF may be related to (i) the number of predictors for the given sample size, which may have driven down the effective degrees of freedom of the RF modeling framework, (ii) the small number of observations of satellite imagery data matching the criteria, which limited the study to 160 fields when comparing satellite sensors and 220 fields when using only Landsat, consequently with smaller observations by subregions, NC (n=73), SC(n=109) and West (n=38), (iii) the level of complexity of the dataset. In this case, if the relationship between predictors and yields is mainly linear, that may affect the relative performance of the RF algorithm and lead the model to overfit.

Although there is still plenty of room for improvement, the main contribution from this work is showing that the NDVI is environmentally dependent, that means even though climate and management practices can drive substantial variability in the NDVI, there are still human practices and environmental conditions on the ground that satellite imagery was not able to perceive. For example, NC showed management of fertilizers as a good predictor and could be used along with NDVI to estimate yields. SC predictor variables relied more on environmental conditions than NDVI, such as soil water storage and management practices associated with weather conditions (e.g., fungicide application). Lastly, West Kansas showed the potential of using NDVI predictor variables during grain filling stages and the importance of management region-specific variables such as sowing date. Thus, this study provides important insights in using satellite imagery to predict winter wheat yields at field scale across different subregions, considering important subregional environmental and management practices that can potentially improve a winter wheat yield prediction model in Kansas.

Among the limitations, Landsat imagery is usually constrained by missing data due to its low temporal frequency (one image every 16 days at best in most cases) and frequent cloud cover; thus, we anticipate that future work to use additional observations of the measured yield data to improve the ability of yield estimation at field scale in Kansas. We also consider the application of different vegetation indices and a combination with satellite imagery in the yield prediction model.

References

Abbas, F., Afzaal, H., Farooque, A. A., & Tang, S. (2020). Crop Yield Prediction through Proximal Sensing and Machine Learning Algorithms. *Agronomy*, *10*(7), 1046. https://doi.org/10.3390/agronomy10071046

Adeniyi, O. D., Szabo, A., Tamás, J., & Nagy, A. (2020). *Wheat Yield Forecasting Based on Landsat NDVI and SAVI Time Series* [Preprint]. EARTH SCIENCES. https://doi.org/10.20944/preprints202007.0065.v1

Ali, A. M., Abouelghar, M., Belal, A. A., Saleh, N., Yones, M., Selim, A. I., Amin, M. E. S., Elwesemy, A., Kucher, D. E., Maginan, S., & Savin, I. (2022). Crop Yield Prediction Using Multi Sensors Remote Sensing (Review Article). *The Egyptian Journal of Remote Sensing and Space Science*, *25*(3), 711–716. https://doi.org/10.1016/j.ejrs.2022.04.006

Alvarez, R. (2009). Predicting average regional yield and production of wheat in the Argentine Pampas by an artificial neural network approach. *European Journal of Agronomy*, *30*(2), 70–77. https://doi.org/10.1016/j.eja.2008.07.005

Amidror, I. (2002). Scattered data interpolation methods for electronic imaging systems: A survey. *Journal of Electronic Imaging*, *11*(2), 157. https://doi.org/10.1117/1.1455013

Amirruddin, A. D., & Muharam, F. M. (2019). Evaluation of linear discriminant and support vector machine classifiers for classification of nitrogen status in mature oil palm from SPOT-6 satellite images: Analysis of raw spectral bands and spectral indices. *Geocarto International*, *34*(7), 735–749. https://doi.org/10.1080/10106049.2018.1434687

Andújar, D., Rueda-Ayala, V., Moreno, H., Rosell-Polo, J., Escolá, A., Valero, C., Gerhards, R., Fernández-Quintanilla, C., Dorado, J., & Griepentrog, H.-W. (2013). Discriminating

Crop, Weeds and Soil Surface with a Terrestrial LIDAR Sensor. *Sensors*, *13*(11), 14662–14675. https://doi.org/10.3390/s131114662

Ansarifar, J., Wang, L., & Archontoulis, S. V. (2021). An interaction regression model for crop yield prediction. *Scientific Reports*, *11*(1), 17754. https://doi.org/10.1038/s41598-021-97221-7

Atzberger, C., & Eilers, P. H. C. (2011). Evaluating the effectiveness of smoothing algorithms in the absence of ground reference measurements. *International Journal of Remote Sensing*, *32*(13), 3689–3709. https://doi.org/10.1080/01431161003762405

Azadbakht, M., Ashourloo, D., Aghighi, H., Homayouni, S., Shahrabi, H. S., Matkan, A., & Radiom, S. (2022). Alfalfa yield estimation based on time series of Landsat 8 and PROBA-V images: An investigation of machine learning techniques and spectral-temporal features. *Remote Sensing Applications: Society and Environment*, *25*, 100657. https://doi.org/10.1016/j.rsase.2021.100657

Backer, D., & Billing, T. (2021). Validating Famine Early Warning Systems Network projections of food security in Africa, 2009–2020. *Global Food Security*, *29*, 100510. https://doi.org/10.1016/j.gfs.2021.100510

Bannari, A., Morin, D., Bonn, F., & Huete, A. R. (1995). A review of vegetation indices. *Remote Sensing Reviews*, *13*(1–2), 95–120. https://doi.org/10.1080/02757259509532298

Barkley, A., Tack, J., Nalley, L. L., Bergtold, J., Bowden, R., & Fritz, A. (2014). Weather, Disease, and Wheat Breeding Effects on Kansas Wheat Varietal Yields, 1985 to 2011. *Agronomy Journal*, *106*(1), 227–235. https://doi.org/10.2134/agronj2013.0388

Barrow, C. J. (1992). World atlas of desertification. In *Land degradation and development.*

Baruth, B., Royer, A., Klisch, A., & Genovese, G. (2008). *THE USE OF REMOTE SENSING WITHIN THE MARS CROP YIELD MONITORING SYSTEM OF THE EUROPEAN COMMISSION*.

Basso, B., & Liu, L. (2019a). Seasonal crop yield forecast: Methods, applications, and accuracies. In *Advances in Agronomy* (Vol. 154, pp. 201–255). Elsevier. https://doi.org/10.1016/bs.agron.2018.11.002

Basso, B., & Liu, L. (2019b). Seasonal crop yield forecast: Methods, applications, and accuracies. In *Advances in Agronomy* (Vol. 154, pp. 201–255). Elsevier. https://doi.org/10.1016/bs.agron.2018.11.002

Bauer, M. E. (1975). The Role of Remote Sensing In Determining The Distribution and Yield of Crops. In *Advances in Agronomy* (Vol. 27, pp. 271–304). Elsevier. https://doi.org/10.1016/S0065-2113(08)70012-9

Becker-Reshef, I., Barker, B., Humber, M., Puricelli, E., Sanchez, A., Sahajpal, R., McGaughey, K., Justice, C., Baruth, B., Wu, B., Prakash, A., Abdolreza, A., & Jarvis, I. (2019). The GEOGLAM crop monitor for AMIS: Assessing crop conditions in the context of global markets. *Global Food Security*, *23*, 173–181. https://doi.org/10.1016/j.gfs.2019.04.010

Becker-Reshef, I., Justice, C., Sullivan, M., Vermote, E., Tucker, C., Anyamba, A., Small, J., Pak, E., Masuoka, E., Schmaltz, J., Hansen, M., Pittman, K., Birkett, C., Williams, D., Reynolds, C., & Doorn, B. (2010). Monitoring Global Croplands with Coarse Resolution Earth Observations: The Global Agriculture Monitoring (GLAM) Project. *Remote Sensing*, *2*(6), 1589–1609. https://doi.org/10.3390/rs2061589

Becker-Reshef, I., Vermote, E., Lindeman, M., & Justice, C. (2010). A generalized regression-based model for forecasting winter wheat yields in Kansas and Ukraine using MODIS

data. *Remote Sensing of Environment*, *114*(6), 1312–1323. https://doi.org/10.1016/j.rse.2010.01.010

Bégué, A., Arvor, D., Bellon, B., Betbeder, J., de Abelleyra, D., P. D. Ferraz, R., Lebourgeois, V., Lelong, C., Simões, M., & R. Verón, S. (2018). Remote Sensing and Cropping Practices: A Review. *Remote Sensing*, *10*(2), 99. https://doi.org/10.3390/rs10010099

Belward, A. S., & Skøien, J. O. (2015). Who launched what, when and why; trends in global land-cover observation capacity from civilian earth observation satellites. *ISPRS Journal of Photogrammetry and Remote Sensing*, *103*, 115–128. https://doi.org/10.1016/j.isprsjprs.2014.03.009

Beres, B. L., Hatfield, J. L., Kirkegaard, J. A., Eigenbrode, S. D., Pan, W. L., Lollato, R. P., Hunt, J. R., Strydhorst, S., Porker, K., Lyon, D., Ransom, J., & Wiersma, J. (2020). Toward a Better Understanding of Genotype × Environment × Management Interactions—A Global Wheat Initiative Agronomic Research Strategy. *Frontiers in Plant Science*, *11*, 828. https://doi.org/10.3389/fpls.2020.00828

Bian, C., Shi, H., Wu, S., Zhang, K., Wei, M., Zhao, Y., Sun, Y., Zhuang, H., Zhang, X., & Chen, S. (2022). Prediction of Field-Scale Wheat Yield Using Machine Learning Method and Multi-Spectral UAV Data. *Remote Sensing*, *14*(6), 1474. https://doi.org/10.3390/rs14061474

Bokusheva, R., Kogan, F., Vitkovskaya, I., Conradt, S., & Batyrbayeva, M. (2016). Satellite-based vegetation health indices as a criteria for insuring against drought-related yield losses. *Agricultural and Forest Meteorology*, *220*, 200–206. https://doi.org/10.1016/j.agrformet.2015.12.066

Bönecke, E., Breitsameter, L., Brüggemann, N., Chen, T., Feike, T., Kage, H., Kersebaum, K., Piepho, H., & Stützel, H. (2020). Decoupling of impact factors reveals the response of German winter wheat yields to climatic changes. *Global Change Biology, 26*(6), 3601–3626. https://doi.org/10.1111/gcb.15073

Breiman, L. (2001). Random Forests. *Machine Learning, 45*, 5–32.

Brown, J. C., Kastens, J. H., Coutinho, A. C., Victoria, D. D. C., & Bishop, C. R. (2013). Classifying multiyear agricultural land use data from Mato Grosso using time-series MODIS vegetation index data. *Remote Sensing of Environment, 130*, 39–50. https://doi.org/10.1016/j.rse.2012.11.009

Brown, J., Howard, D., Wylie, B., Frieze, A., Ji, L., & Gacke, C. (2015). Application-Ready Expedited MODIS Data for Operational Land Surface Monitoring of Vegetation Condition. *Remote Sensing, 7*(12), 16226–16240. https://doi.org/10.3390/rs71215825

Brown, M. E. (2008). *Famine early warning systems and remote sensing data*. Springer.

Byamukama, E., Ali, S., Kleinjan, J., Yabwalo, D. N., Graham, C., Caffe-Treml, M., Mueller, N. D., Rickertsen, J., & Berzonsky, W. A. (2019). Winter Wheat Grain Yield Response to Fungicide Application is Influenced by Cultivar and Rainfall. *The Plant Pathology Journal*, *35*(1), 63–70. https://doi.org/10.5423/PPJ.OA.04.2018.0056

Cai, Y., Guan, K., Lobell, D., Potgieter, A. B., Wang, S., Peng, J., Xu, T., Asseng, S., Zhang, Y., You, L., & Peng, B. (2019). Integrating satellite and climate data to predict wheat yield in Australia using machine learning approaches. *Agricultural and Forest Meteorology*, *274*, 144–159. https://doi.org/10.1016/j.agrformet.2019.03.010

Calicioglu, O., Flammini, A., Bracco, S., Bellù, L., & Sims, R. (2019). The Future Challenges of Food and Agriculture: An Integrated Analysis of Trends and Solutions. *Sustainability*, *11*(1), 222. https://doi.org/10.3390/su11010222

Cammalleri, C., McCormick, N., & Toreti, A. (2022). Analysis of the relationship between yield in cereals and remotely sensed fAPAR in the framework of monitoring drought impacts in Europe. *Natural Hazards and Earth System Sciences*, *22*(11), 3737–3750. https://doi.org/10.5194/nhess-22-3737-2022

Cao, R., Chen, Y., Shen, M., Chen, J., Zhou, J., Wang, C., & Yang, W. (2018). A simple method to improve the quality of NDVI time-series data by integrating spatiotemporal information with the Savitzky-Golay filter. *Remote Sensing of Environment*, *217*, 244–257. https://doi.org/10.1016/j.rse.2018.08.022

Chan, S. K., Bindlish, R., O'Neill, P., Jackson, T., Njoku, E., Dunbar, S., Chaubell, J., Piepmeier, J., Yueh, S., Entekhabi, D., Colliander, A., Chen, F., Cosh, M. H., Caldwell, T., Walker, J., Berg, A., McNairn, H., Thibeault, M., Martínez-Fernández, J., … Kerr, Y. (2018). Development and assessment of the SMAP enhanced passive soil moisture product. *Remote Sensing of Environment*, *204*, 931–941. https://doi.org/10.1016/j.rse.2017.08.025

Chen, K., O'Leary, R. A., & Evans, F. H. (2019). A simple and parsimonious generalised additive model for predicting wheat yield in a decision support tool. *Agricultural Systems*, *173*, 140–150. https://doi.org/10.1016/j.agsy.2019.02.009

Chen, Y., Zhang, Z., & Tao, F. (2018). Improving regional winter wheat yield estimation through assimilation of phenology and leaf area index from remote sensing data. *European Journal of Agronomy*, *101*, 163–173. https://doi.org/10.1016/j.eja.2018.09.006

Christensen, P., Gillingham, K., & Nordhaus, W. (2018). Uncertainty in forecasts of long-run economic growth. *Proceedings of the National Academy of Sciences*, *115*(21), 5409–5414. https://doi.org/10.1073/pnas.1713628115

Cook, E. R., Meko, D. M., Stahle, D. W., & Cleaveland, M. K. (1999). Drought Reconstructions for the Continental United States*. *Journal of Climate*, *12*(4), 1145–1162. https://doi.org/10.1175/1520-0442(1999)012<1145:DRFTCU>2.0.CO;2

Correndo, A. A., Tremblay, N., Coulter, J. A., Ruiz-Diaz, D., Franzen, D., Nafziger, E., Prasad, V., Rosso, L. H. M., Steinke, K., Du, J., Messina, C. D., & Ciampitti, I. A. (2021). Unraveling uncertainty drivers of the maize yield response to nitrogen: A Bayesian and machine learning approach. *Agricultural and Forest Meteorology*, *311*, 108668. https://doi.org/10.1016/j.agrformet.2021.108668

Couëdel, A., Edreira, J. I. R., Pisa Lollato, R., Archontoulis, S., Sadras, V., & Grassini, P. (2021). Assessing environment types for maize, soybean, and wheat in the United States as determined by spatio-temporal variation in drought and heat stress. *Agricultural and Forest Meteorology*, *307*, 108513. https://doi.org/10.1016/j.agrformet.2021.108513

Cruppe, G., DeWolf, E., Jaenisch, B. R., Andersen Onofre, K., Valent, B., Fritz, A. K., & Lollato, R. P. (2021). Experimental and producer-reported data quantify the value of foliar fungicide to winter wheat and its dependency on genotype and environment in the U.S. central Great Plains. *Field Crops Research*, *273*, 108300. https://doi.org/10.1016/j.fcr.2021.108300

Cruppe, G., Edwards, J. T., & Lollato, R. P. (2017). In-Season Canopy Reflectance Can Aid Fungicide and Late-Season Nitrogen Decisions on Winter Wheat. *Agronomy Journal*, *109*(5), 2072–2086.

Cruppe, G., Giordano, N., Simão, L. M., Ryan, L., Pradella, L. O., Soler, J. R., & Lollato, R. P. (2022). Winter Wheat Response to Timing of Fungicide Application During the 2020–2021 Growing Season. *Kansas Agricultural Experiment Station Research Reports*, *8*(4). https://doi.org/10.4148/2378-5977.8304

de Jong van Lier, Q., Wendroth, O., & van Dam, J. C. (2015). Prediction of winter wheat yield with the SWAP model using pedotransfer functions: An evaluation of sensitivity, parameterization and prediction accuracy. *Agricultural Water Management*, *154*, 29–42. https://doi.org/10.1016/j.agwat.2015.02.011

de Wit, A., Duveiller, G., & Defourny, P. (2012). Estimating regional winter wheat yield with WOFOST through the assimilation of green area index retrieved from MODIS observations. *Agricultural and Forest Meteorology*, *164*, 39–52. https://doi.org/10.1016/j.agrformet.2012.04.011

Delécolle, R., Maas, S. J., Guérif, M., & Baret, F. (1992). Remote sensing and crop production models: Present trends. *ISPRS Journal of Photogrammetry and Remote Sensing*, *47*(2–3), 145–161. https://doi.org/10.1016/0924-2716(92)90030-D

Dhau, I., Adam, E., Mutanga, O., Ayisi, K., Abdel-Rahman, E. M., Odindi, J., & Masocha, M. (2018). Testing the capability of spectral resolution of the new multispectral sensors on detecting the severity of grey leaf spot disease in maize crop. *Geocarto International*, *33*(11), 1223–1236. https://doi.org/10.1080/10106049.2017.1343391

Di Mauro, G., Cipriotti, P. A., Gallo, S., & Rotundo, J. L. (2018). Environmental and management variables explain soybean yield gap variability in Central Argentina. *European Journal of Agronomy*, *99*, 186–194. https://doi.org/10.1016/j.eja.2018.04.012

Diepen, C. A., Wolf, J., Keulen, H., & Rappoldt, C. (1989). WOFOST: A simulation model of crop production. *Soil Use and Management*, *5*(1), 16–24. https://doi.org/10.1111/j.1475-2743.1989.tb00755.x

Dinh, T. L. A., & Aires, F. (2022). Nested leave-two-out cross-validation for the optimal crop yield model selection. *Geoscientific Model Development*, *15*(9), 3519–3535. https://doi.org/10.5194/gmd-15-3519-2022

Dong, J., Lu, H., Wang, Y., Ye, T., & Yuan, W. (2020). Estimating winter wheat yield based on a light use efficiency model and wheat variety data. *ISPRS Journal of Photogrammetry and Remote Sensing*, *160*, 18–32. https://doi.org/10.1016/j.isprsjprs.2019.12.005

Dong, T., Liu, J., Qian, B., He, L., Liu, J., Wang, R., Jing, Q., Champagne, C., McNairn, H., Powers, J., Shi, Y., Chen, J. M., & Shang, J. (2020). Estimating crop biomass using leaf area index derived from Landsat 8 and Sentinel-2 data. *ISPRS Journal of Photogrammetry and Remote Sensing*, *168*, 236–250. https://doi.org/10.1016/j.isprsjprs.2020.08.003

Doraiswamy, P. C., Moulin, S., Cook, P. W., & Stern, A. (2003). Crop Yield Assessment from Remote Sensing. *Photogrammetric Engineering & Remote Sensing*, *69*(6), 665–674. https://doi.org/10.14358/PERS.69.6.665

Dorigo, W. A., Zurita-Milla, R., de Wit, A. J. W., Brazile, J., Singh, R., & Schaepman, M. E. (2007). A review on reflective remote sensing and data assimilation techniques for enhanced agroecosystem modeling. *International Journal of Applied Earth Observation and Geoinformation*, *9*(2), 165–193. https://doi.org/10.1016/j.jag.2006.05.003

Durgun, Y. Ö., Gobin, A., Duveiller, G., & Tychon, B. (2020). A study on trade-offs between spatial resolution and temporal sampling density for wheat yield estimation using both

thermal and calendar time. *International Journal of Applied Earth Observation and Geoinformation*, *86*, 101988. https://doi.org/10.1016/j.jag.2019.101988

Duro, D. C., Franklin, S. E., & Dubé, M. G. (2012). A comparison of pixel-based and object-based image analysis with selected machine learning algorithms for the classification of agricultural landscapes using SPOT-5 HRG imagery. *Remote Sensing of Environment*, *118*, 259–272. https://doi.org/10.1016/j.rse.2011.11.020

Efron, B., & Tibshirani, R. (1997). Improvements on Cross-Validation: The 632+ Bootstrap Method. *Journal of the American Statistical Association*, *92*(438), 548–560. https://doi.org/10.1080/01621459.1997.10474007

Eitel, J. U. H., Magney, T. S., Vierling, L. A., Brown, T. T., & Huggins, D. R. (2014). LiDAR based biomass and crop nitrogen estimates for rapid, non-destructive assessment of wheat nitrogen status. *Field Crops Research*, *159*, 21–32. https://doi.org/10.1016/j.fcr.2014.01.008

El Hajj, M., Baghdadi, N., Zribi, M., & Bazzi, H. (2017). Synergic Use of Sentinel-1 and Sentinel-2 Images for Operational Soil Moisture Mapping at High Spatial Resolution over Agricultural Areas. *Remote Sensing*, *9*(12), 1292. https://doi.org/10.3390/rs9121292

Engen, M., Sandø, E., Sjølander, B. L. O., Arenberg, S., Gupta, R., & Goodwin, M. (2021). Farm-Scale Crop Yield Prediction from Multi-Temporal Data Using Deep Hybrid Neural Networks. *Agronomy*, *11*(12), 2576. https://doi.org/10.3390/agronomy11122576

Erickson, J. D. (1984). The LACIE Experiment in Satellite Aided Monitoring of Global Crop Production. *The Role of Terrestrial Vegetation in the Global Carbon Cycle: Measurement by Remote Sensing*.

Evans, F. H., & Shen, J. (2021). Long-Term Hindcasts of Wheat Yield in Fields Using Remotely Sensed Phenology, Climate Data and Machine Learning. *Remote Sensing*, *13*(13), 2435. https://doi.org/10.3390/rs13132435

Everingham, Y. L., Muchow, R. C., Stone, R. C., Inman-Bamber, N. G., Singels, A., & Bezuidenhout, C. N. (2002). Enhanced risk management and decision-making capability across the sugarcane industry value chain based on seasonal climate forecasts. *Agricultural Systems*, *74*(3), 459–477. https://doi.org/10.1016/S0308-521X(02)00050-1

Everingham, Y., Sexton, J., Skocaj, D., & Inman-Bamber, G. (2016). Accurate prediction of sugarcane yield using a random forest algorithm. *Agronomy for Sustainable Development*, *36*(2), 27. https://doi.org/10.1007/s13593-016-0364-z

Fan, M.-S., Zhao, F.-J., Fairweather-Tait, S. J., Poulton, P. R., Dunham, S. J., & McGrath, S. P. (2008). Evidence of decreasing mineral density in wheat grain over the last 160 years. *Journal of Trace Elements in Medicine and Biology*, *22*(4), 315–324. https://doi.org/10.1016/j.jtemb.2008.07.002

FAO. (1978). Report on the Agro-ecological Zones Project. *World Soil Resources*, *1*.

Fermont, A., & Benson, T. (n.d.). *Estimating Yield of Food Crops Grown by Smallholder Farmers*.

Fieuzal, R., Bustillo, V., Collado, D., & Dedieu, G. (2020). Combined Use of Multi-Temporal Landsat-8 and Sentinel-2 Images for Wheat Yield Estimates at the Intra-Plot Spatial Scale. *Agronomy*, *10*(3), 327. https://doi.org/10.3390/agronomy10030327

Filippa, G., Cremonese, E., Migliavacca, M., Galvagno, M., Sonnentag, O., Humphreys, E., Hufkens, K., Ryu, Y., Verfaillie, J., Morra di Cella, U., & Richardson, A. D. (2018). NDVI derived from near-infrared-enabled digital cameras: Applicability across different

plant functional types. *Agricultural and Forest Meteorology*, *249*, 275–285. https://doi.org/10.1016/j.agrformet.2017.11.003

Fink, K. P., Grassini, P., Rocateli, A., Bastos, L. M., Kastens, J., Ryan, L. P., Lin, X., Patrignani, A., & Lollato, R. P. (2022). Alfalfa water productivity and yield gaps in the U.S. central Great Plains. *Field Crops Research*, *289*, 108728. https://doi.org/10.1016/j.fcr.2022.108728

Fischer, G., Shah, M., N. Tubiello, F., & van Velhuizen, H. (2005). Socio-economic and climate change impacts on agriculture: An integrated assessment, 1990–2080. *Philosophical Transactions of the Royal Society B: Biological Sciences*, *360*(1463), 2067–2083. https://doi.org/10.1098/rstb.2005.1744

Fischer, T., Byerlee, D., & Edmeades, G. (2014). *Crop yields and global food security: Will yield increase continue to feed the world?* ACIAR.

Flora, S. (1948). Climate of Kansas. *Report of the Kansas State Board of Agriculture.*

Fonti, V., & Belitser, E. (2017). Feature selection using lasso. *VU Amsterdam Research Paper in Business Analytics*, *30*, 1–25.

Food and Agriculture Organization of the United Nations. (2023). *FAOSTAT Statistical Database.* https://www.fao.org/faostat/en/#data/QCL/visualize

Franch, B., Vermote, E. F., Skakun, S., Roger, J. C., Becker-Reshef, I., Murphy, E., & Justice, C. (2019). Remote sensing based yield monitoring: Application to winter wheat in United States and Ukraine. *International Journal of Applied Earth Observation and Geoinformation*, *76*, 112–127. https://doi.org/10.1016/j.jag.2018.11.012

Frich, P., Alexander, L., Della-Marta, P., Gleason, B., Haylock, M., Klein Tank, A., & Peterson, T. (2002). Observed coherent changes in climatic extremes during the second half of the twentieth century. *Climate Research*, *19*, 193–212. https://doi.org/10.3354/cr019193

Gallo, K. P., & Daughtry, C. S. T. (1987). Differences in vegetation indices for simulated Landsat-5 MSS and TM, NOAA-9 AVHRR, and SPOT-1 sensor systems. *Remote Sensing of Environment*, *23*(3), 439–452. https://doi.org/10.1016/0034-4257(87)90100-3

Gao, F., Anderson, M., Daughtry, C., & Johnson, D. (2018). Assessing the Variability of Corn and Soybean Yields in Central Iowa Using High Spatiotemporal Resolution Multi-Satellite Imagery. *Remote Sensing*, *10*(9), 1489. https://doi.org/10.3390/rs10091489

García-Martínez, H., Flores-Magdaleno, H., Ascencio-Hernández, R., Khalil-Gardezi, A., Tijerina-Chávez, L., Mancilla-Villa, O. R., & Vázquez-Peña, M. A. (2020). Corn Grain Yield Estimation from Vegetation Indices, Canopy Cover, Plant Density, and a Neural Network Using Multispectral and RGB Images Acquired with Unmanned Aerial Vehicles. *Agriculture*, *10*(7), 277. https://doi.org/10.3390/agriculture10070277

Gaso, D. V., Berger, A. G., & Ciganda, V. S. (2019). Predicting wheat grain yield and spatial variability at field scale using a simple regression or a crop model in conjunction with Landsat images. *Computers and Electronics in Agriculture*, *159*, 75–83. https://doi.org/10.1016/j.compag.2019.02.026

Geng, X., Wang, F., Ren, W., & Hao, Z. (2019). Climate Change Impacts on Winter Wheat Yield in Northern China. *Advances in Meteorology*, *2019*, 1–12. https://doi.org/10.1155/2019/2767018

Ghaderpour, E., & Vujadinovic, T. (2020). Change Detection within Remotely Sensed Satellite Image Time Series via Spectral Analysis. *Remote Sensing*, *12*(23), 4001. https://doi.org/10.3390/rs12234001

Giordano, N., Sadras, V. O., & Lollato, R. P. (2023). Late-season nitrogen application increases grain protein concentration and is neutral for yield in wheat. A global meta-analysis. *Field Crops Research*, *290*, 108740. https://doi.org/10.1016/j.fcr.2022.108740

Girma, K., Martin, K. L., Anderson, R. H., Arnall, D. B., Brixey, K. D., Casillas, M. A., Chung, B., Dobey, B. C., Kamenidou, S. K., Kariuki, S. K., Katsalirou, E. E., Morris, J. C., Moss, J. Q., Rohla, C. T., Sudbury, B. J., Tubana, B. S., & Raun, W. R. (2006). Mid-Season Prediction of Wheat-Grain Yield Potential Using Plant, Soil, and Sensor Measurements. *Journal of Plant Nutrition*, *29*(5), 873–897. https://doi.org/10.1080/01904160600649187

Godwin, D., Ritchie, J., Singh, U., & Hunt, L. (1989). A User's Guide to CERES Maize—V2.10. *International Fertilizer Development Center, Muscle Shoals, AL*.

Griffiths, W. E., Newton, L. S., & O'Donnell, C. J. (2010). Predictive densities for models with stochastic regressors and inequality constraints: Forecasting local-area wheat yield. *International Journal of Forecasting*, *26*(2), 397–412. https://doi.org/10.1016/j.ijforecast.2009.12.008

Guo, Y., Xiang, H., Li, Z., Ma, F., & Du, C. (2021). Prediction of Rice Yield in East China Based on Climate and Agronomic Traits Data Using Artificial Neural Networks and Partial Least Squares Regression. *Agronomy*, *11*(2), 282. https://doi.org/10.3390/agronomy11020282

Gupta, R., & Mishra, A. (2019). Climate change induced impact and uncertainty of rice yield of agro-ecological zones of India. *Agricultural Systems*, *173*, 1–11. https://doi.org/10.1016/j.agsy.2019.01.009

Hammer, G. L., Nicholls, N., & Mitchell, C. (Eds.). (2000). *Applications of Seasonal Climate Forecasting in Agricultural and Natural Ecosystems* (Vol. 21). Springer Netherlands. https://doi.org/10.1007/978-94-015-9351-9

Hastie, T., Tibshirani, R., & Friedman, J. (2009). Model Assessment and Selection. In T. Hastie, R. Tibshirani, & J. Friedman, *The Elements of Statistical Learning* (pp. 219–259). Springer New York. https://doi.org/10.1007/978-0-387-84858-7_7

Hatfield, J. L., Wright-Morton, L., & Hall, B. (2018). Vulnerability of grain crops and croplands in the Midwest to climatic variability and adaptation strategies. *Climatic Change*, *146*(1–2), 263–275. https://doi.org/10.1007/s10584-017-1997-x

He, M., Kimball, J., Maneta, M., Maxwell, B., Moreno, A., Beguería, S., & Wu, X. (2018). Regional Crop Gross Primary Productivity and Yield Estimation Using Fused Landsat-MODIS Data. *Remote Sensing*, *10*(3), 372. https://doi.org/10.3390/rs10030372

Heinemann, A. B., Ramirez-Villegas, J., Souza, T. L. P. O., Didonet, A. D., di Stefano, J. G., Boote, K. J., & Jarvis, A. (2016). Drought impact on rainfed common bean production areas in Brazil. *Agricultural and Forest Meteorology*, *225*, 57–74. https://doi.org/10.1016/j.agrformet.2016.05.010

Hermance, J. F., Jacob, R. W., Bradley, B. A., & Mustard, J. F. (2007). Extracting Phenological Signals From Multiyear AVHRR NDVI Time Series: Framework for Applying High-Order Annual Splines With Roughness Damping. *IEEE Transactions on Geoscience and Remote Sensing*, *45*(10), 3264–3276. https://doi.org/10.1109/TGRS.2007.903044

Hively, W., Lamb, B., Daughtry, C., Shermeyer, J., McCarty, G., & Quemada, M. (2018). Mapping Crop Residue and Tillage Intensity Using WorldView-3 Satellite Shortwave Infrared Residue Indices. *Remote Sensing*, *10*(10), 1657. https://doi.org/10.3390/rs10101657

Holman, J. D., Lollato, R. P., Zarnstorff, M., Houx, J., & Assefa, Y. (2023). Impact of simulated hail damage at different growth stages and canopy positions on rainfed and irrigated winter wheat. *Agronomy Journal*, *115*(2), 859–872. https://doi.org/10.1002/agj2.21256

Hosseini, M., McNairn, H., Merzouki, A., & Pacheco, A. (2015). Estimation of Leaf Area Index (LAI) in corn and soybeans using multi-polarization C- and L-band radar data. *Remote Sensing of Environment*, *170*, 77–89. https://doi.org/10.1016/j.rse.2015.09.002

Houborg, R., & McCabe, M. (2016). High-Resolution NDVI from Planet's Constellation of Earth Observing Nano-Satellites: A New Data Source for Precision Agriculture. *Remote Sensing*, *8*(9), 768. https://doi.org/10.3390/rs8090768

Hu, Y., Wei, X., Hao, M., Fu, W., Zhao, J., & Wang, Z. (2018). Partial Least Squares Regression for Determining Factors Controlling Winter Wheat Yield. *Agronomy Journal*, *110*(1), 281–292. https://doi.org/10.2134/agronj2017.02.0108

Huang, J., Gómez-Dans, J. L., Huang, H., Ma, H., Wu, Q., Lewis, P. E., Liang, S., Chen, Z., Xue, J.-H., Wu, Y., Zhao, F., Wang, J., & Xie, X. (2019). Assimilation of remote sensing into crop growth models: Current status and perspectives. *Agricultural and Forest Meteorology*, *276–277*, 107609. https://doi.org/10.1016/j.agrformet.2019.06.008

Huang, J., Wang, X., Li, X., Tian, H., & Pan, Z. (2013). Remotely Sensed Rice Yield Prediction Using Multi-Temporal NDVI Data Derived from NOAA's-AVHRR. *PLoS ONE*, *8*(8), e70816. https://doi.org/10.1371/journal.pone.0070816

Hubert-Moy, L. (2001). A Comparison of Parametric Classification Procedures of Remotely Sensed Data Applied on Different Landscape Units. *Remote Sensing of Environment, 75*(2), 174–187. https://doi.org/10.1016/S0034-4257(00)00165-6

Huddleston, H. F. (1978). Sampling techniques for measuring and forecasting crop yields. *Economics, Statistics, and Cooperatives Service, U.S. Dept. of Agriculture*. https://handle.nal.usda.gov/10113/26702

Hunt, M. L., Blackburn, G. A., Carrasco, L., Redhead, J. W., & Rowland, C. S. (2019). High resolution wheat yield mapping using Sentinel-2. *Remote Sensing of Environment, 233*, 111410. https://doi.org/10.1016/j.rse.2019.111410

Jaenisch, B. R., Munaro, L. B., Bastos, L. M., Moraes, M., Lin, X., & Lollato, R. P. (2021). On-farm data-rich analysis explains yield and quantifies yield gaps of winter wheat in the U.S. central Great Plains. *Field Crops Research, 272*, 108287. https://doi.org/10.1016/j.fcr.2021.108287

Jaenisch, B. R., Munaro, L. B., Jagadish, S. V. K., & Lollato, R. P. (2022). Modulation of Wheat Yield Components in Response to Management Intensification to Reduce Yield Gaps. *Frontiers in Plant Science, 13*, 772232. https://doi.org/10.3389/fpls.2022.772232

Jaenisch, B. R., Oliveira Silva, A., DeWolf, E., Ruiz-Diaz, D. A., & Lollato, R. P. (2019). Plant Population and Fungicide Economically Reduced Winter Wheat Yield Gap in Kansas. *Agronomy Journal*, *111*(2), 650–665. https://doi.org/10.2134/agronj2018.03.0223

Ji, L., Gallo, K., Eidenshink, J. C., & Dwyer, J. (2008). Agreement evaluation of AVHRR and MODIS 16-day composite NDVI data sets. *International Journal of Remote Sensing*, *29*(16), 4839–4861. https://doi.org/10.1080/01431160801927194

Ji, Z., Pan, Y., Zhu, X., Wang, J., & Li, Q. (2021). Prediction of Crop Yield Using Phenological Information Extracted from Remote Sensing Vegetation Index. *Sensors*, *21*(4), 1406. https://doi.org/10.3390/s21041406

Jiang, B., Liang, S., Wang, J., & Xiao, Z. (2010). Modeling MODIS LAI time series using three statistical methods. *Remote Sensing of Environment*, *114*(7), 1432–1444. https://doi.org/10.1016/j.rse.2010.01.026

Jiao, C., Yu, G., Ge, J., Chen, X., Zhang, C., He, N., Chen, Z., & Hu, Z. (2017). Analysis of spatial and temporal patterns of aboveground net primary productivity in the Eurasian steppe region from 1982 to 2013. *Ecology and Evolution*, *7*(14), 5149–5162. https://doi.org/10.1002/ece3.3027

Jin, X., Kumar, L., Li, Z., Feng, H., Xu, X., Yang, G., & Wang, J. (2018). A review of data assimilation of remote sensing and crop models. *European Journal of Agronomy*, *92*, 141–152. https://doi.org/10.1016/j.eja.2017.11.002

Johnson, D. M. (2016). A comprehensive assessment of the correlations between field crop yields and commonly used MODIS products. *International Journal of Applied Earth Observation and Geoinformation*, *52*, 65–81. https://doi.org/10.1016/j.jag.2016.05.010

Johnson, D. M., Rosales, A., Mueller, R., Reynolds, C., Frantz, R., Anyamba, A., Pak, E., & Tucker, C. (2021). USA Crop Yield Estimation with MODIS NDVI: Are Remotely Sensed Models Better than Simple Trend Analyses? *Remote Sensing*, *13*(21), 4227. https://doi.org/10.3390/rs13214227

Johnson, M. D., Hsieh, W. W., Cannon, A. J., Davidson, A., & Bédard, F. (2016). Crop yield forecasting on the Canadian Prairies by remotely sensed vegetation indices and machine

learning methods. *Agricultural and Forest Meteorology*, *218–219*, 74–84. https://doi.org/10.1016/j.agrformet.2015.11.003

Jonsson, P., & Eklundh, L. (2002). Seasonality extraction by function fitting to time-series of satellite sensor data. *IEEE Transactions on Geoscience and Remote Sensing*, *40*(8), 1824–1832. https://doi.org/10.1109/TGRS.2002.802519

Joshil Raj, K., & SivaSathya, S. (2014). SVM and Random Forest Classification of Satellite Image with NDVI as an Additional Attribute to the Dataset. In M. Pant, K. Deep, A. Nagar, & J. C. Bansal (Eds.), *Proceedings of the Third International Conference on Soft Computing for Problem Solving* (Vol. 258, pp. 95–107). Springer India. https://doi.org/10.1007/978-81-322-1771-8_9

K. R. Thorp, D. J. Hunsaker, & A. N. French. (2010). Assimilating Leaf Area Index Estimates from Remote Sensing into the Simulations of a Cropping Systems Model. *Transactions of the ASABE*, *53*(1), 251–262. https://doi.org/10.13031/2013.29490

Kadam, N. N., Xiao, G., Melgar, R. J., Bahuguna, R. N., Quinones, C., Tamilselvan, A., Prasad, P. V. V., & Jagadish, K. S. V. (2014). Agronomic and Physiological Responses to High Temperature, Drought, and Elevated CO2 Interactions in Cereals. In *Advances in Agronomy* (Vol. 127, pp. 111–156). Elsevier. https://doi.org/10.1016/B978-0-12-800131-8.00003-0

Kamthonkiat, D., Honda, K., Turral, H., Tripathi, N. K., & Wuwongse, V. (2005a). Discrimination of irrigated and rainfed rice in a tropical agricultural system using SPOT VEGETATION NDVI and rainfall data. *International Journal of Remote Sensing*, *26*(12), 2527–2547. https://doi.org/10.1080/01431160500104335

Kamthonkiat, D., Honda, K., Turral, H., Tripathi, N. K., & Wuwongse, V. (2005b). Discrimination of irrigated and rainfed rice in a tropical agricultural system using SPOT VEGETATION NDVI and rainfall data. *International Journal of Remote Sensing*, *26*(12), 2527–2547. https://doi.org/10.1080/01431160500104335

Kang, Y., Khan, S., & Ma, X. (2009). Climate change impacts on crop yield, crop water productivity and food security – A review. *Progress in Natural Science*, *19*(12), 1665–1674. https://doi.org/10.1016/j.pnsc.2009.08.001

Kansas Department of Agriculture. (2021). Kansas 2021 AG Summit. *Kansas Department of Agriculture*. https://www.agriculture.ks.gov/AgGrowthStrategy/ag-summit-2021

Kasampalis, D., Alexandridis, T., Deva, C., Challinor, A., Moshou, D., & Zalidis, G. (2018). Contribution of Remote Sensing on Crop Models: A Review. *Journal of Imaging*, *4*(4), 52. https://doi.org/10.3390/jimaging4040052

Kern, A., Barcza, Z., Marjanović, H., Árendás, T., Fodor, N., Bónis, P., Bognár, P., & Lichtenberger, J. (2018). Statistical modelling of crop yield in Central Europe using climate data and remote sensing vegetation indices. *Agricultural and Forest Meteorology*, *260–261*, 300–320. https://doi.org/10.1016/j.agrformet.2018.06.009

Khaki, S., & Wang, L. (2019). Crop Yield Prediction Using Deep Neural Networks. *Frontiers in Plant Science*, *10*, 621. https://doi.org/10.3389/fpls.2019.00621

Khanal, S., Kc, K., Fulton, J. P., Shearer, S., & Ozkan, E. (2020). Remote Sensing in Agriculture—Accomplishments, Limitations, and Opportunities. *Remote Sensing*, *12*(22), 3783. https://doi.org/10.3390/rs12223783

Kim, J.-H. (2009). Estimating classification error rate: Repeated cross-validation, repeated hold-out and bootstrap. *Computational Statistics & Data Analysis*, *53*(11), 3735–3745. https://doi.org/10.1016/j.csda.2009.04.009

Knipling, E. B. (1970). Physical and physiological basis for the reflectance of visible and near-infrared radiation from vegetation. *Remote Sensing of Environment*, *1*(3), 155–159. https://doi.org/10.1016/S0034-4257(70)80021-9

Kogan, F., Salazar, L., & Roytman, L. (2012). Forecasting crop production using satellite-based vegetation health indices in Kansas, USA. *International Journal of Remote Sensing*, *33*(9), 2798–2814. https://doi.org/10.1080/01431161.2011.621464

Komp, K. U., & Haub, C. (2012). GLOBAL MONITORING FOR FOOD SECURITY AND SUSTAINABLE LAND MANAGEMENT – RECENT ADVANCES OF REMOTE SENSING APPLICATIONS TO AFRICAN AND SIBERIAN SHOW CASES. *The International Archives of the Photogrammetry, Remote Sensing and Spatial Information Sciences*, *XXXIX-B8*, 265–270. https://doi.org/10.5194/isprsarchives-XXXIX-B8-265-2012

Kong, L., Wang, F., Feng, B., Li, S., Si, J., & Zhang, B. (2010). The structural and photosynthetic characteristics of the exposed peduncle of wheat (Triticum aestivumL.): An important photosynthate source for grain-filling. *BMC Plant Biology*, *10*(1), 141. https://doi.org/10.1186/1471-2229-10-141

Kouadio, L., Newlands, N., Davidson, A., Zhang, Y., & Chipanshi, A. (2014). Assessing the Performance of MODIS NDVI and EVI for Seasonal Crop Yield Forecasting at the Ecodistrict Scale. *Remote Sensing*, *6*(10), 10193–10214. https://doi.org/10.3390/rs61010193

Kuhn, M., & Johnson, K. (2013). *Applied Predictive Modeling*. Springer New York. https://doi.org/10.1007/978-1-4614-6849-3

Lai, Y. R., Pringle, M. J., Kopittke, P. M., Menzies, N. W., Orton, T. G., & Dang, Y. P. (2018). An empirical model for prediction of wheat yield, using time-integrated Landsat NDVI. *International Journal of Applied Earth Observation and Geoinformation*, *72*, 99–108. https://doi.org/10.1016/j.jag.2018.07.013

Landau, S., Mitchell, R. A. C., Barnett, V., Colls, J. J., Craigon, J., & Payne, R. W. (2000). A parsimonious, multiple-regression model of wheat yield response to environment. *Agricultural and Forest Meteorology*, *101*(2–3), 151–166. https://doi.org/10.1016/S0168-1923(99)00166-5

Larina, G. E., Poddymkina, L. M., Ayugin, N. P., Dyakonova, M. A., & Morkovkin, D. E. (2022). Effective hybrids of Zea mays L. under conditions of changes in the boundaries of agro-climatic zones under the influence of global warming. *IOP Conference Series: Earth and Environmental Science*, *1010*(1), 012138. https://doi.org/10.1088/1755-1315/1010/1/012138

Lee, H., Wang, J., & Leblon, B. (2020). Using Linear Regression, Random Forests, and Support Vector Machine with Unmanned Aerial Vehicle Multispectral Images to Predict Canopy Nitrogen Weight in Corn. *Remote Sensing*, *12*(13), 2071. https://doi.org/10.3390/rs12132071

Leprieur, C., Verstraete, M. M., & Pinty, B. (1994). Evaluation of the performance of various vegetation indices to retrieve vegetation cover from AVHRR data. *Remote Sensing Reviews*, *10*(4), 265–284. https://doi.org/10.1080/02757259409532250

Levitan, N., & Gross, B. (2018). Utilizing Collocated Crop Growth Model Simulations to Train Agronomic Satellite Retrieval Algorithms. *Remote Sensing*, *10*(12), 1968. https://doi.org/10.3390/rs10121968

Li, J., Peng, B., Wei, Y., & Ye, H. (2021). Accurate extraction of surface water in complex environment based on Google Earth Engine and Sentinel-2. *PLOS ONE*, *16*(6), e0253209. https://doi.org/10.1371/journal.pone.0253209

Lin, X., Harrington, J., Ciampitti, I., Gowda, P., Brown, D., & Kisekka, I. (2017). Kansas Trends and Changes in Temperature, Precipitation, Drought, and Frost-Free Days from the 1890s to 2015. *Journal of Contemporary Water Research & Education*, *162*, 18–30.

Lingenfelser, J., Davis, H., De Wolf, E., Fritz, A., Knapp, M., Lollato, R. P., Regan, R., & Whitworth, J. (2018). Kansas Performance Tests with Winter Wheat Varieties. *Kansas State University, 19-022-S*.

Lingenfelser, J., DeWolf, E., Fritz, A., Knapp, M., Lollato, R. P., Miller, R., Watson, S., & Whitworth, J. (2017). Kansas Performance Tests with Winter Wheat Varieties. *Kansas State University*, *18-018-S*.

Liu, H., Wang, Z. H., Li, F., Li, K., Yang, N., Yang, Y., Huang, D., Liang, D., Zhao, H., Mao, H., Liu, J., & Qiu, W. (2014). Grain iron and zinc concentrations of wheat and their relationships to yield in major wheat production areas in China. *Field Crops Research*, *156*, 151–160. https://doi.org/10.1016/j.fcr.2013.11.011

Lobell, D. B. (2013). The use of satellite data for crop yield gap analysis. *Field Crops Research*, *143*, 56–64. https://doi.org/10.1016/j.fcr.2012.08.008

Lobell, D. B., Di Tommaso, S., You, C., Yacoubou Djima, I., Burke, M., & Kilic, T. (2019). Sight for Sorghums: Comparisons of Satellite- and Ground-Based Sorghum Yield Estimates in Mali. *Remote Sensing*, *12*(1), 100. https://doi.org/10.3390/rs12010100

Locke, C. R., Carbone, G. J., Filippi, A. M., Sadler, E. J., Gerwig, B. K., & Evans, D. E. (2000). Using remote sensing and modeling to measure crop biophysical variability. *In 5th International Conference on Precision Agriculture.*

Lollato, R. P. (2018). Wheat Growth and Development. *Kansas State University*. https://bookstore.ksre.ksu.edu/pubs/MF3300.pdf

Lollato, R. P., Bavia, G. P., Perin, V., Knapp, M., Santos, E. A., Patrignani, A., & DeWolf, E. D. (2020). Climate-risk assessment for winter wheat using long-term weather data. *Agronomy Journal*, *112*(3), 2132–2151. https://doi.org/10.1002/agj2.20168

Lollato, R. P., & Edwards, J. T. (2015). Maximum Attainable Wheat Yield and Resource-Use Efficiency in the Southern Great Plains. *Crop Science*, *55*(6), 2863–2876. https://doi.org/10.2135/cropsci2015.04.0215

Lollato, R. P., Edwards, J. T., & Ochsner, T. E. (2017). Meteorological limits to winter wheat productivity in the U.S. southern Great Plains. *Field Crops Research*, *203*, 212–226. https://doi.org/10.1016/j.fcr.2016.12.014

Lollato, R. P., Edwards, J. T., & Zhang, H. (2013). Effect of Alternative Soil Acidity Amelioration Strategies on Soil pH Distribution and Wheat Agronomic Response. *Soil Science Society of America Journal*, *77*(5), 1831–1841. https://doi.org/10.2136/sssaj2013.04.0129

Lollato, R. P., Jaenisch, B. R., & Silva, S. R. (2021). Genotype-specific nitrogen uptake dynamics and fertilizer management explain contrasting wheat protein concentration. *Crop Science*, *61*(3), 2048–2066. https://doi.org/10.1002/csc2.20442

Lollato, R. P., Mark, K., & Jaenisch, B. R. (2020). Wheat Variety-Specific Grain Yield Response to Plant Density Under Intensive Management Conditions in Western Kansas. *Kansas Agricultural Experiment Station Research Reports*, *6*(5). https://doi.org/10.4148/2378-5977.7941

Lollato, R. P., Patrignani, A., Ochsner, T. E., & Edwards, J. T. (2016). Prediction of Plant Available Water at Sowing for Winter Wheat in the Southern Great Plains. *Agronomy Journal*, *108*(2), 745–757. https://doi.org/10.2134/agronj2015.0433

Lollato, R. P., Roozeboom, K., Lingenfelser, J. F., Da Silva, C. L., & Sassenrath, G. (2020). Soft winter wheat outyields hard winter wheat in a subhumid environment: Weather drivers, yield plasticity, and rates of yield gain. *Crop Science*, *60*(3), 1617–1633. https://doi.org/10.1002/csc2.20139

Lollato, R. P., Ruiz Diaz, D. A., DeWolf, E., Knapp, M., Peterson, D. E., & Fritz, A. K. (2019). Agronomic Practices for Reducing Wheat Yield Gaps: A Quantitative Appraisal of Progressive Producers. *Crop Science*, *59*(1), 333–350. https://doi.org/10.2135/cropsci2018.04.0249

Lopresti, M. F., Di Bella, C. M., & Degioanni, A. J. (2015). Relationship between MODIS-NDVI data and wheat yield: A case study in Northern Buenos Aires province, Argentina. *Information Processing in Agriculture*, *2*(2), 73–84. https://doi.org/10.1016/j.inpa.2015.06.001

Luciano, A. C. dos S., Picoli, M. C. A., Duft, D. G., Rocha, J. V., Leal, M. R. L. V., & le Maire, G. (2021). Empirical model for forecasting sugarcane yield on a local scale in Brazil using Landsat imagery and random forest algorithm. *Computers and Electronics in Agriculture*, *184*, 106063. https://doi.org/10.1016/j.compag.2021.106063

Lungu, O. N., Chabala, L. M., & Shepande, C. (2020). Satellite-Based Crop Monitoring and Yield Estimation—A Review. *Journal of Agricultural Science*, *13*(1), 180. https://doi.org/10.5539/jas.v13n1p180

Maeoka, R. E., Sadras, V. O., Ciampitti, I. A., Diaz, D. R., Fritz, A. K., & Lollato, R. P. (2020). Changes in the Phenotype of Winter Wheat Varieties Released Between 1920 and 2016 in Response to In-Furrow Fertilizer: Biomass Allocation, Yield, and Grain Protein Concentration. *Frontiers in Plant Science*, *10*, 1786. https://doi.org/10.3389/fpls.2019.01786

Magney, T. S., Eitel, J. U. H., Huggins, D. R., & Vierling, L. A. (2016). Proximal NDVI derived phenology improves in-season predictions of wheat quantity and quality. *Agricultural and Forest Meteorology*, *217*, 46–60. https://doi.org/10.1016/j.agrformet.2015.11.009

Magney, T. S., Eitel, J. U. H., & Vierling, L. A. (2017). Mapping wheat nitrogen uptake from RapidEye vegetation indices. *Precision Agriculture*, *18*(4), 429–451. https://doi.org/10.1007/s11119-016-9463-8

Mallick, J., AlMesfer, M. K., Singh, V. P., Falqi, I. I., Singh, C. K., Alsubih, M., & Kahla, N. B. (2021). Evaluating the NDVI–Rainfall Relationship in Bisha Watershed, Saudi Arabia Using Non-Stationary Modeling Technique. *Atmosphere*, *12*(5), 593. https://doi.org/10.3390/atmos12050593

Martins, G. D., Galo, M. L. B. T., Vieira, B. S., Jorge, R. F., & Almeida, C. X. (2019). Mapping Nutrients Content in a Nematode-Infected Coffee Plantation by Empirical Models Derived from RapidEye Image. *Anuário Do Instituto de Geociências - UFRJ*, *42*(3), 164–177. https://doi.org/10.11137/2019_3_164_177

Mashonganyika, F., Mugiyo, H., Svotwa, E., & Kutywayo, D. (2021). Mapping of Winter Wheat Using Sentinel-2 NDVI Data. A Case of Mashonaland Central Province in Zimbabwe. *Frontiers in Climate, 3*, 715837. https://doi.org/10.3389/fclim.2021.715837

Masialeti, I., Egbert, S., & Wardlow, B. D. (2010). A Comparative Analysis of Phenological Curves for Major Crops in Kansas. *GIScience & Remote Sensing*, *47*(2), 241–259. https://doi.org/10.2747/1548-1603.47.2.241

Mathieu, J. A., & Aires, F. (2018). Assessment of the agro-climatic indices to improve crop yield forecasting. *Agricultural and Forest Meteorology*, *253–254*, 15–30. https://doi.org/10.1016/j.agrformet.2018.01.031

McCown, R. L., Hammer, G. L., Hargreaves, J. N. G., Holzworth, D. P., & Freebairn, D. M. (1996). APSIM: A novel software system for model development, model testing and simulation in agricultural systems research. *Agricultural Systems*, *50*(3), 255–271. https://doi.org/10.1016/0308-521X(94)00055-V

McNairn, H., Ellis, J., Van Der Sanden, J. J., Hirose, T., & Brown, R. J. (2002). Providing crop information using RADARSAT-1 and satellite optical imagery. *International Journal of Remote Sensing*, *23*(5), 851–870. https://doi.org/10.1080/01431160110070753

Meng, L., Liu, H., Ustin, S. L., & Zhang, X. (2021). Assessment of FSDAF Accuracy on Cotton Yield Estimation Using Different MODIS Products and Landsat Based on the Mixed

Degree Index with Different Surroundings. *Sensors*, *21*(15), 5184. https://doi.org/10.3390/s21155184

Mkhabela, M. S., Bullock, P., Raj, S., Wang, S., & Yang, Y. (2011). Crop yield forecasting on the Canadian Prairies using MODIS NDVI data. *Agricultural and Forest Meteorology*, *151*(3), 385–393. https://doi.org/10.1016/j.agrformet.2010.11.012

Morell, F. J., Yang, H. S., Cassman, K. G., Wart, J. V., Elmore, R. W., Licht, M., Coulter, J. A., Ciampitti, I. A., Pittelkow, C. M., Brouder, S. M., Thomison, P., Lauer, J., Graham, C., Massey, R., & Grassini, P. (2016). Can crop simulation models be used to predict local to regional maize yields and total production in the U.S. Corn Belt? *Field Crops Research*, *192*, 1–12. https://doi.org/10.1016/j.fcr.2016.04.004

Morgounov, A., Gómez-Becerra, H. F., Abugalieva, A., Dzhunusova, M., Yessimbekova, M., Muminjanov, H., Zelenskiy, Y., Ozturk, L., & Cakmak, I. (2007). Iron and zinc grain density in common wheat grown in Central Asia. *Euphytica*, *155*(1–2), 193–203. https://doi.org/10.1007/s10681-006-9321-2

Moriondo, M., Maselli, F., & Bindi, M. (2007). A simple model of regional wheat yield based on NDVI data. *European Journal of Agronomy*, *26*(3), 266–274. https://doi.org/10.1016/j.eja.2006.10.007

Moulin, S., Bondeau, A., & Delecolle, R. (1998). Combining agricultural crop models and satellite observations: From field to regional scales. *International Journal of Remote Sensing*, *19*(6), 1021–1036. https://doi.org/10.1080/014311698215586

Mulla, D. J. (2013). Twenty five years of remote sensing in precision agriculture: Key advances and remaining knowledge gaps. *Biosystems Engineering*, *114*(4), 358–371. https://doi.org/10.1016/j.biosystemseng.2012.08.009

Munaro, L. B., Hefley, T. J., DeWolf, E., Haley, S., Fritz, A. K., Zhang, G., Haag, L. A., Schlegel, A. J., Edwards, J. T., Marburger, D., Alderman, P., Jones-Diamond, S. M., Johnson, J., Lingenfelser, J. E., Unêda-Trevisoli, S. H., & Lollato, R. P. (2020). Exploring long-term variety performance trials to improve environment-specific genotype × management recommendations: A case-study for winter wheat. *Field Crops Research*, *255*, 107848. https://doi.org/10.1016/j.fcr.2020.107848

Murakami, T., Ogawa, S., Ishitsuka, N., Kumagai, K., & Saito, G. (2001). Crop discrimination with multitemporal SPOT/HRV data in the Saga Plains, Japan. *International Journal of Remote Sensing*, *22*(7), 1335–1348. https://doi.org/10.1080/01431160151144378

Nabati, J., Nezami, A., Neamatollahi, E., & Akbari, M. (2020). GIS-based agro-ecological zoning for crop suitability using fuzzy inference system in semi-arid regions. *Ecological Indicators*, *117*, 106646. https://doi.org/10.1016/j.ecolind.2020.106646

Nelson, K. S., Patalee, B., & Yao, B. (2022). Higher landscape diversity associated with improved crop production resilience in Kansas-USA. *Environmental Research Letters*, *17*(8), 084011. https://doi.org/10.1088/1748-9326/ac7e5f

Nguyen, H. T. T., Nguyen, L. V., de Bie, C. A. J. M. (Kees), Ciampitti, I. A., Nguyen, D. A., Nguyen, M. V., Nieto, L., Schwalbert, R., & Nguyen, L. V. (2020). Mapping Maize Cropping Patterns in Dak Lak, Vietnam Through MODIS EVI Time Series. *Agronomy*, *10*(4), 478. https://doi.org/10.3390/agronomy10040478

Nguyen, M., Baez-Villanueva, O., Bui, D., Nguyen, P., & Ribbe, L. (2020). Harmonization of Landsat and Sentinel 2 for Crop Monitoring in Drought Prone Areas: Case Studies of Ninh Thuan (Vietnam) and Bekaa (Lebanon). *Remote Sensing*, *12*(2), 281. https://doi.org/10.3390/rs12020281

Nolasco, M., Ovando, G., Sayago, S., Magario, I., & Bocco, M. (2021). Estimating soybean yield using time series of anomalies in vegetation indices from MODIS. *International Journal of Remote Sensing*, *42*(2), 405–421. https://doi.org/10.1080/01431161.2020.1809736

Obembe, O. S., Hendricks, N. P., & Tack, J. (2021a). Decreased wheat production in the USA from climate change driven by yield losses rather than crop abandonment. *PLOS ONE*, *16*(6), e0252067. https://doi.org/10.1371/journal.pone.0252067

Obembe, O. S., Hendricks, N. P., & Tack, J. (2021b). Decreased wheat production in the USA from climate change driven by yield losses rather than crop abandonment. *PLOS ONE*, *16*(6), e0252067. https://doi.org/10.1371/journal.pone.0252067

Odenweller, J. B., & Johnson, K. I. (n.d.). *Crop Identification Using I_ ndsat TemporM-Spectral Profiles*.

Olesen, J. E., & Bindi, M. (2002). Consequences of climate change for European agricultural productivity, land use and policy. *European Journal of Agronomy*, *16*(4), 239–262. https://doi.org/10.1016/S1161-0301(02)00004-7

Palosuo, T., Kersebaum, K. C., Angulo, C., Hlavinka, P., Moriondo, M., Olesen, J. E., Patil, R. H., Ruget, F., Rumbaur, C., Takáč, J., Trnka, M., Bindi, M., Çaldağ, B., Ewert, F., Ferrise, R., Mirschel, W., Şaylan, L., Šiška, B., & Rötter, R. (2011). Simulation of winter wheat yield and its variability in different climates of Europe: A comparison of eight crop growth models. *European Journal of Agronomy*, *35*(3), 103–114. https://doi.org/10.1016/j.eja.2011.05.001

Panek, E., & Gozdowski, D. (2021). Relationship between MODIS Derived NDVI and Yield of Cereals for Selected European Countries. *Agronomy*, *11*(2), 340. https://doi.org/10.3390/agronomy11020340

Pang, A., Chang, M. W. L., & Chen, Y. (2022). Evaluation of Random Forests (RF) for Regional and Local-Scale Wheat Yield Prediction in Southeast Australia. *Sensors*, *22*(3), 717. https://doi.org/10.3390/s22030717

Parece, T. E., & Campbell, J. B. (2017). Assessing Urban Community Gardens' Impact on Net Primary Production using NDVI. *Urban Agriculture & Regional Food Systems*, *2*(1), 1–17. https://doi.org/10.2134/urbanag2016.07.0004

Passioura, J. B. (1996). Simulation Models: Science, Snake Oil, Education, or Engineering? *Agronomy Journal*, *88*(5), 690–694. https://doi.org/10.2134/agronj1996.00021962008800050002x

Patrignani, A., Lollato, R. P., Ochsner, T. E., Godsey, C. B., & Edwards, Jeff. T. (2014). Yield Gap and Production Gap of Rainfed Winter Wheat in the Southern Great Plains. *Agronomy Journal*, *106*(4), 1329–1339. https://doi.org/10.2134/agronj14.0011

Paulsen, G. M. (1997). Growth and development In: Wheat production handbook. *Kansas State University*.

Paulsen, G. M., & Heyne, E. G. (1983). Grain Production of Winter Wheat after Spring Freeze Injury. *Agronomy Journal*, *74*(4), 705–707.

Peralta, N., Assefa, Y., Du, J., Barden, C., & Ciampitti, I. (2016). Mid-Season High-Resolution Satellite Imagery for Forecasting Site-Specific Corn Yield. *Remote Sensing*, *8*(10), 848. https://doi.org/10.3390/rs8100848

Ratliff, L. F., Ritchie, J. T., & Cassel, D. K. (1983). Field-Measured Limits of Soil Water Availability as Related to Laboratory-Measured Properties. *Soil Science Society of America Journal*, *47*(4), 770–775. https://doi.org/10.2136/sssaj1983.03615995004700040032x

Rattalino Edreira, J. I., Cassman, K. G., Hochman, Z., Van Ittersum, M. K., Van Bussel, L., Claessens, L., & Grassini, P. (2018). Beyond the plot: Technology extrapolation domains for scaling out agronomic science. *Environmental Research Letters*, *13*(5), 054027. https://doi.org/10.1088/1748-9326/aac092

Rattalino Edreira, J. I., Mourtzinis, S., Azzari, G., Andrade, J. F., Conley, S. P., Lobell, D., Specht, J. E., & Grassini, P. (2020). From sunlight to seed: Assessing limits to solar radiation capture and conversion in agro-ecosystems. *Agricultural and Forest Meteorology*, *280*, 107775. https://doi.org/10.1016/j.agrformet.2019.107775

Rattalino Edreira, J. I., Mourtzinis, S., Conley, S. P., Roth, A. C., Ciampitti, I. A., Licht, M. A., Kandel, H., Kyveryga, P. M., Lindsey, L. E., Mueller, D. S., Naeve, S. L., Nafziger, E., Specht, J. E., Stanley, J., Staton, M. J., & Grassini, P. (2017). Assessing causes of yield gaps in agricultural areas with diversity in climate and soils. *Agricultural and Forest Meteorology*, *247*, 170–180. https://doi.org/10.1016/j.agrformet.2017.07.010

Raun, W. R., Solie, J. B., Johnson, G. V., Stone, M. L., Lukina, E. V., Thomason, W. E., & Schepers, J. S. (2001). In-Season Prediction of Potential Grain Yield in Winter Wheat Using Canopy Reflectance. *Agronomy Journal*, *93*(1), 131–138. https://doi.org/10.2134/agronj2001.931131x

Reeves, M. C., Zhao, M., & Running, S. W. (2005). Usefulness and limits of MODIS GPP for estimating wheat yield. *International Journal of Remote Sensing*, *26*(7), 1403–1421. https://doi.org/10.1080/01431160512331326567

Rembold, F., Atzberger, C., Savin, I., & Rojas, O. (2013). Using Low Resolution Satellite Imagery for Yield Prediction and Yield Anomaly Detection. *Remote Sensing*, *5*(4), 1704–1733. https://doi.org/10.3390/rs5041704

Ren, J., Chen, Z., Zhou, Q., & Tang, H. (2008). Regional yield estimation for winter wheat with MODIS-NDVI data in Shandong, China. *International Journal of Applied Earth Observation and Geoinformation*, *10*(4), 403–413. https://doi.org/10.1016/j.jag.2007.11.003

Řezník, T., Pavelka, T., Herman, L., Lukas, V., Širůček, P., Leitgeb, Š., & Leitner, F. (2020). Prediction of Yield Productivity Zones from Landsat 8 and Sentinel-2A/B and Their Evaluation Using Farm Machinery Measurements. *Remote Sensing*, *12*(12), 1917. https://doi.org/10.3390/rs12121917

Rife, T. W., Graybosch, R. A., & Poland, J. A. (2019). A Field-Based Analysis of Genetic Improvement for Grain Yield in Winter Wheat Cultivars Developed in the US Central Plains from 1992 to 2014. *Crop Science*, *59*, 905–910.

Rouse, W., & Haas, R. H. (n.d.). *MONITORING VEGETATION SYSTEMS IN THE GREAT PLAINS WITH ERTS*.

Roy, D. P., & Yan, L. (2020). Robust Landsat-based crop time series modelling. *Remote Sensing of Environment*, *238*, 110810. https://doi.org/10.1016/j.rse.2018.06.038

Saad El Imanni, H., El Harti, A., & El Iysaouy, L. (2022). Wheat Yield Estimation Using Remote Sensing Indices Derived from Sentinel-2 Time Series and Google Earth Engine

in a Highly Fragmented and Heterogeneous Agricultural Region. *Agronomy*, *12*(11), 2853. https://doi.org/10.3390/agronomy12112853

Sadras, V. O., Giordano, N., Correndo, A., Cossani, C. M., Ferreyra, J. M., Caviglia, O. P., Coulter, J. A., Ciampitti, I. A., & Lollato, R. P. (2022). Temperature-Driven Developmental Modulation of Yield Response to Nitrogen in Wheat and Maize. *Frontiers in Agronomy*, *4*, 903340. https://doi.org/10.3389/fagro.2022.903340

Schillerberg, T. A., Tian, D., & Miao, R. (2019). Spatiotemporal patterns of maize and winter wheat yields in the United States: Predictability and impact from climate oscillations. *Agricultural and Forest Meteorology*, *275*, 208–222. https://doi.org/10.1016/j.agrformet.2019.05.019

Schwalbert, R. A., Amado, T., Corassa, G., Pott, L. P., Prasad, P. V. V., & Ciampitti, I. A. (2020). Satellite-based soybean yield forecast: Integrating machine learning and weather data for improving crop yield prediction in southern Brazil. *Agricultural and Forest Meteorology*, *284*, 107886. https://doi.org/10.1016/j.agrformet.2019.107886

Schwalbert, R. A., Amado, T. J. C., Nieto, L., Varela, S., Corassa, G. M., Horbe, T. A. N., Rice, C. W., Peralta, N. R., & Ciampitti, I. A. (2018). Forecasting maize yield at field scale based on high-resolution satellite imagery. *Biosystems Engineering*, *171*, 179–192. https://doi.org/10.1016/j.biosystemseng.2018.04.020

Shafiee, S., Lied, L. M., Burud, I., Dieseth, J. A., Alsheikh, M., & Lillemo, M. (2021). Sequential forward selection and support vector regression in comparison to LASSO regression for spring wheat yield prediction based on UAV imagery. *Computers and Electronics in Agriculture*, *183*, 106036. https://doi.org/10.1016/j.compag.2021.106036

Shahhosseini, M., Hu, G., & Archontoulis, S. V. (2020). Forecasting Corn Yield With Machine Learning Ensembles. *Frontiers in Plant Science*, *11*, 1120. https://doi.org/10.3389/fpls.2020.01120

Shammi, S. A., & Meng, Q. (2021). Use time series NDVI and EVI to develop dynamic crop growth metrics for yield modeling. *Ecological Indicators*, *121*, 107124. https://doi.org/10.1016/j.ecolind.2020.107124

Shen, J., & Evans, F. H. (2021). The Potential of Landsat NDVI Sequences to Explain Wheat Yield Variation in Fields in Western Australia. *Remote Sensing*, *13*(11), 2202. https://doi.org/10.3390/rs13112202

Shiferaw, B., Smale, M., Braun, H.-J., Duveiller, E., Reynolds, M., & Muricho, G. (2013). Crops that feed the world 10. Past successes and future challenges to the role played by wheat in global food security. *Food Security*, *5*(3), 291–317. https://doi.org/10.1007/s12571-013-0263-y

Shirley, R., Pope, E., Bartlett, M., Oliver, S., Quadrianto, N., Hurley, P., Duivenvoorden, S., Rooney, P., Barrett, A. B., Kent, C., & Bacon, J. (2020). An empirical, Bayesian approach to modelling crop yield: Maize in USA. *Environmental Research Communications*, *2*(2), 025002. https://doi.org/10.1088/2515-7620/ab67f0

Shroyer, J. P. (1996). Kansas Crop Planting Guide. *Kansas State University*.

Shroyer, J. P., Mikesell, M. E., & Paulsen, G. M. (1995). Spring freeze injury to Kansas wheat. *Kansas State University*.

Siachalou, S., Mallinis, G., & Tsakiri-Strati, M. (2015). A Hidden Markov Models Approach for Crop Classification: Linking Crop Phenology to Time Series of Multi-Sensor Remote Sensing Data. *Remote Sensing*, *7*(4), 3633–3650. https://doi.org/10.3390/rs70403633

Silvestro, P., Pignatti, S., Pascucci, S., Yang, H., Li, Z., Yang, G., Huang, W., & Casa, R. (2017). Estimating Wheat Yield in China at the Field and District Scale from the Assimilation of Satellite Data into the Aquacrop and Simple Algorithm for Yield (SAFY) Models. *Remote Sensing*, *9*(5), 509. https://doi.org/10.3390/rs9050509

Sishodia, R. P., Ray, R. L., & Singh, S. K. (2020). Applications of Remote Sensing in Precision Agriculture: A Review. *Remote Sensing*, *12*(19), 3136. https://doi.org/10.3390/rs12193136

Skakun, S., Kalecinski, N. I., Brown, M. G. L., Johnson, D. M., Vermote, E. F., Roger, J.-C., & Franch, B. (2021). Assessing within-Field Corn and Soybean Yield Variability from WorldView-3, Planet, Sentinel-2, and Landsat 8 Satellite Imagery. *Remote Sensing*, *13*(5), 872. https://doi.org/10.3390/rs13050872

Skakun, S., Kussul, N., Shelestov, A., & Kussul, O. (2016). The use of satellite data for agriculture drought risk quantification in Ukraine. *Geomatics, Natural Hazards and Risk*, *7*(3), 901–917. https://doi.org/10.1080/19475705.2015.1016555

Skakun, S., Vermote, E., Franch, B., Roger, J.-C., Kussul, N., Ju, J., & Masek, J. (2019). Winter Wheat Yield Assessment from Landsat 8 and Sentinel-2 Data: Incorporating Surface Reflectance, Through Phenological Fitting, into Regression Yield Models. *Remote Sensing*, *11*(15), 1768. https://doi.org/10.3390/rs11151768

Skakun, S., Vermote, E., Roger, J.-C., Franch, B., 1 Department of Geographical Sciences, University of Maryland, College Park, MD 20742, USA, & 2 NASA Goddard Space Flight Center Code 619, 8800 Greenbelt Road, Greenbelt, MD 20771, USA. (2017). Combined Use of Landsat-8 and Sentinel-2A Images for Winter Crop Mapping and

Winter Wheat Yield Assessment at Regional Scale. *AIMS Geosciences*, *3*(2), 163–186. https://doi.org/10.3934/geosci.2017.2.163

Slafer, G. A., Savin, R., Pinochet, D., & Calderini, D. F. (2021). Wheat. In *Crop Physiology Case Histories for Major Crops* (pp. 98–163). Elsevier. https://doi.org/10.1016/B978-0-12-819194-1.00003-7

Soltani, A., & Sinclair, T. R. (2012). Modeling physiology of crop development, growth and yield. *Model. Physiol. Crop Dev. Growth Yield.* https://doi.org/10.1079/9781845939700.0000.

Stewart, B. A., Thapa, S., Xue, Q., & Shrestha, R. (2018). Climate change effect on winter wheat (*Triticum aestivum* L.) yields in the US Great Plains. *Journal of Soil and Water Conservation*, *73*(6), 601–609. https://doi.org/10.2489/jswc.73.6.601

Stöckle, C. O., Donatelli, M., & Nelson, R. (2003). CropSyst, a cropping systems simulation model. *European Journal of Agronomy*, *18*(3–4), 289–307. https://doi.org/10.1016/S1161-0301(02)00109-0

Stone, M. L., Solie, J. B., Raun, W. R., Whitney, R. W., Taylor, S. L., & Ringer, J. D. (1996). Use of spectral radiance for correcting in-season fertilizer nitrogen deficiencies in winter wheat. *Transactions of the ASAE, 39*(5), 1623–1631.

Sudmanns, M., Tiede, D., Augustin, H., & Lang, S. (2020). Assessing global Sentinel-2 coverage dynamics and data availability for operational Earth observation (EO) applications using the EO-Compass. *International Journal of Digital Earth*, *13*(7), 768–784. https://doi.org/10.1080/17538947.2019.1572799

Sun, Y., Zhang, S., Tao, F., Aboelenein, R., & Amer, A. (2022). Improving Winter Wheat Yield Forecasting Based on Multi-Source Data and Machine Learning. *Agriculture*, *12*(5), 571. https://doi.org/10.3390/agriculture12050571

Tack, J., Barkley, A., & Nalley, L. L. (2014). Heterogeneous effects of warming and drought on selected wheat variety yields. *Climatic Change*, *125*(3–4), 489–500. https://doi.org/10.1007/s10584-014-1185-1

Tack, J., Barkley, A., & Nalley, L. L. (2015). Effect of warming temperatures on US wheat yields. *Proceedings of the National Academy of Sciences*, *112*(22), 6931–6936. https://doi.org/10.1073/pnas.1415181112

Taghizadeh-Mehrjardi, R., Nabiollahi, K., Rasoli, L., Kerry, R., & Scholten, T. (2020). Land Suitability Assessment and Agricultural Production Sustainability Using Machine Learning Models. *Agronomy*, *10*(4), 573. https://doi.org/10.3390/agronomy10040573

Tatem, A., Goetz, S., & Hay, S. (2008). Fifty Years of Earth-observation Satellites. *American Scientist*, *96*(5), 390. https://doi.org/10.1511/2008.74.390

Teimouri, N., Dyrmann, M., & Jørgensen, R. N. (2019). A Novel Spatio-Temporal FCN-LSTM Network for Recognizing Various Crop Types Using Multi-Temporal Radar Images. *Remote Sensing*, *11*(8), 990. https://doi.org/10.3390/rs11080990

Thenkabail, P. S., Mariotto, I., Gumma, M. K., Middleton, E. M., Landis, D. R., & Huemmrich, K. F. (2013). Selection of Hyperspectral Narrowbands (HNBs) and Composition of Hyperspectral Twoband Vegetation Indices (HVIs) for Biophysical Characterization and Discrimination of Crop Types Using Field Reflectance and Hyperion/EO-1 Data. *IEEE Journal of Selected Topics in Applied Earth Observations and Remote Sensing*, *6*(2), 427–439. https://doi.org/10.1109/JSTARS.2013.2252601

Thenkabail, P. S., Ward, A. D., & Lyon, J. G. (1994). Landsat-5 Thematic Mapper models of soybean and corn crop characteristics. *International Journal of Remote Sensing*, *15*(1), 49–61. https://doi.org/10.1080/01431169408954050

Tibshirani, R. (1996). Regression Shrinkage and Selection Via the Lasso. *Journal of the Royal Statistical Society: Series B (Methodological)*, *58*(1), 267–288. https://doi.org/10.1111/j.2517-6161.1996.tb02080.x

Tiede, D., Sudmanns, M., Augustin, H., & Baraldi, A. (2021). Investigating ESA Sentinel-2 products' systematic cloud cover overestimation in very high altitude areas. *Remote Sensing of Environment*, *252*, 112163. https://doi.org/10.1016/j.rse.2020.112163

Travlos, I., Tsekoura, A., Antonopoulos, N., Kanatas, P., & Gazoulis, I. (2021). Novel sensor-based method (quick test) for the in-season rapid evaluation of herbicide efficacy under real field conditions in durum wheat. *Weed Science*, *69*(2), 147–160. https://doi.org/10.1017/wsc.2021.8

Tripathy, R., Chaudhari, K. N., Mukherjee, J., Ray, S. S., Patel, N. K., Panigrahy, S., & Parihar, J. S. (2013). Forecasting wheat yield in Punjab state of India by combining crop simulation model WOFOST and remotely sensed inputs. *Remote Sensing Letters*, *4*(1), 19–28. https://doi.org/10.1080/2150704X.2012.683117

Tucker, C. J. (1979). Red and Photographic Infrared l,lnear Combinations for Monitoring Vegetation. *Remote Sensing of Environment*, *8*, 24. http://dx.doi.org/10.1016/0034-4257(79)90013-0

U.S. Department of Agriculture. (2022). Wheat Data. *Economic Research Service*.

USDA National Agricultural Statistics Service Cropland Data Layer. (2023). *Published crop-specific data layer*. USDA-NASS. https://nassgeodata.gmu.edu/CropScape

USDA NRCS. (1993). Soil Survey Manual. *U.S. Department of Agriculture Handbook 18*.

USDA-NASS. (2019). *Natl. Agric. Stat. Serv.* https://quickstats.nass.usda.gov/results/542A42F1-A26B-3E0A-B3AC-4792D11A167E#386D082B-8800-3BC0-BB75-29F7314DC1E3

USDA-NASS. (2023a). *Natl. Agric. Stat. Serv.* [Data set]. https://quickstats.nass.usda.gov/

USDA-NASS. (2023b). Surveys. *United States Department of Agriculture - National Agricultural Statistics Service*. https://www.nass.usda.gov/Surveys/

USDA-NRCS. (2015). *Web Soil Survey. Soil Survey Staff*. https://websoilsurvey.sc.egov.usda.gov/App/HomePage.htm

USDA-NRCS. (2017). Harney series. *USDA Natl. Resour. Conserv. Serv.* https://soilseries.sc.egov.usda.gov/OSD_Docs/H/HARNEY.html

USGS. (2022). *Landsat Collections*. https://www.usgs.gov/landsat-missions/landsat-collections

USGS. (2023). *Landsat Collection 1 Level-1 Quality Assessment Band.* https://www.usgs.gov/landsat-missions/landsat-collection-1-level-1-quality-assessment-band

Vallentin, C., Harfenmeister, K., Itzerott, S., Kleinschmit, B., Conrad, C., & Spengler, D. (2022). Suitability of satellite remote sensing data for yield estimation in northeast Germany. *Precision Agriculture*, *23*(1), 52–82. https://doi.org/10.1007/s11119-021-09827-6

van Ittersum, M. K. (2016). Crop Yields and Global Food Security. Will Yield Increase Continue to Feed the World? *European Review of Agricultural Economics*, *43*(1), 191–192. https://doi.org/10.1093/erae/jbv034

van Klompenburg, T., Kassahun, A., & Catal, C. (2020). Crop yield prediction using machine learning: A systematic literature review. *Computers and Electronics in Agriculture*, *177*, 105709. https://doi.org/10.1016/j.compag.2020.105709

van Wart, J., van Bussel, L. G. J., Wolf, J., Licker, R., Grassini, P., Nelson, A., Boogaard, H., Gerber, J., Mueller, N. D., Claessens, L., van Ittersum, M. K., & Cassman, K. G. (2013). Use of agro-climatic zones to upscale simulated crop yield potential. *Field Crops Research*, *143*, 44–55. https://doi.org/10.1016/j.fcr.2012.11.023

Vandendriessche, H. J., & van Ittersum, M. K. (1995). Crop Models and Decision Support Systems for Yield Forecasting and Management of the Sugar Beet Crop. *European Journal of Agronomy*, *4*(3), 269–279. https://doi.org/10.1016/S1161-0301(14)80027-0

Vannoppen, A., & Gobin, A. (2021). Estimating Farm Wheat Yields from NDVI and Meteorological Data. *Agronomy*, *11*(5), 946. https://doi.org/10.3390/agronomy11050946

Vannoppen, A., Gobin, A., Kotova, L., Top, S., De Cruz, L., Vīksna, A., Aniskevich, S., Bobylev, L., Buntemeyer, L., Caluwaerts, S., De Troch, R., Gnatiuk, N., Hamdi, R., Reca Remedio, A., Sakalli, A., Van De Vyver, H., Van Schaeybroeck, B., & Termonia, P. (2020). Wheat Yield Estimation from NDVI and Regional Climate Models in Latvia. *Remote Sensing*, *12*(14), 2206. https://doi.org/10.3390/rs12142206

Verger, A., Vigneau, N., Chéron, C., Gilliot, J.-M., Comar, A., & Baret, F. (2014). Green area index from an unmanned aerial system over wheat and rapeseed crops. *Remote Sensing of Environment*, *152*, 654–664. https://doi.org/10.1016/j.rse.2014.06.006

Viña, A., Peters, A. J., & Ji, L. (2003). Use of Multispectral Ikonos Imagery for Discriminating between Conventional and Conservation Agricultural Tillage Practices. *Photogrammetric Engineering & Remote Sensing*, *69*(5), 537–544. https://doi.org/10.14358/PERS.69.5.537

Wang, J., Xiao, X., Liu, L., Wu, X., Qin, Y., Steiner, J. L., & Dong, J. (2020). Mapping sugarcane plantation dynamics in Guangxi, China, by time series Sentinel-1, Sentinel-2

and Landsat images. *Remote Sensing of Environment*, *247*, 111951. https://doi.org/10.1016/j.rse.2020.111951

Wang, Y., Zhang, Z., Feng, L., Du, Q., & Runge, T. (2020). Combining Multi-Source Data and Machine Learning Approaches to Predict Winter Wheat Yield in the Conterminous United States. *Remote Sensing*, *12*(8), 1232. https://doi.org/10.3390/rs12081232

Wardlow, B. D., Egbert, S. L., & Kastens, J. H. (2007). Analysis of time-series MODIS 250 m vegetation index data for crop classification in the U.S. Central Great Plains. *Remote Sensing of Environment*, *108*(3), 290–310. https://doi.org/10.1016/j.rse.2006.11.021

Watson-Hernández, F., Gómez-Calderón, N., & da Silva, R. P. (2022). Oil Palm Yield Estimation Based on Vegetation and Humidity Indices Generated from Satellite Images and Machine Learning Techniques. *AgriEngineering*, *4*(1), 279–291. https://doi.org/10.3390/agriengineering4010019

Wiegand, C. L., Everitt, J. H., & Richardson, A. J. (1992). Comparison of multispectral video and SPOT-1 HRV observations for cotton affected by soil salinity. *International Journal of Remote Sensing*, *13*(8), 1511–1525. https://doi.org/10.1080/01431169208904205

Wilson, W. W., & Sebaugh, J. L. (n.d.). *1981: ESTABLISHED CRITERIA AND SELECTED METHODS FOR EVALUATING CROP YIELD MODELS IN THE AgRISTARS PROGRAM*.

Wójtowicz, M., Wójtowicz, A., & Piekarczyk, J. (2010). *Application of remote sensing methods in agriculture*. 20.

Wright, M. N., & Ziegler, A. (2017). **ranger**: A Fast Implementation of Random Forests for High Dimensional Data in *C++* and *R*. *Journal of Statistical Software*, *77*(1). https://doi.org/10.18637/jss.v077.i01

Wu, B., Gommes, R., Zhang, M., Zeng, H., Yan, N., Zou, W., Zheng, Y., Zhang, N., Chang, S., Xing, Q., & van Heijden, A. (2015). Global Crop Monitoring: A Satellite-Based Hierarchical Approach. *Remote Sensing*, *7*(4), 3907–3933. https://doi.org/10.3390/rs70403907

Wulder, M. A., Loveland, T. R., Roy, D. P., Crawford, C. J., Masek, J. G., Woodcock, C. E., Allen, R. G., Anderson, M. C., Belward, A. S., Cohen, W. B., Dwyer, J., Erb, A., Gao, F., Griffiths, P., Helder, D., Hermosilla, T., Hipple, J. D., Hostert, P., Hughes, M. J., … Zhu, Z. (2019). Current status of Landsat program, science, and applications. *Remote Sensing of Environment*, *225*, 127–147. https://doi.org/10.1016/j.rse.2019.02.015

Yadegari, M., Shamshiri, R. R., Mohamed Shariff, A. R., Balasundram, S. K., & Mahns, B. (2020). Using SPOT-7 for Nitrogen Fertilizer Management in Oil Palm. *Agriculture*, *10*(4), 133. https://doi.org/10.3390/agriculture10040133

Yang, C., Everitt, J. H., & Bradford, J. M. (2009). Evaluating high resolution SPOT 5 satellite imagery to estimate crop yield. *Precision Agriculture*, *10*(4), 292–303. https://doi.org/10.1007/s11119-009-9120-6

Yang, X., Chen, J., Guan, Q., Gao, H., & Xia, W. (2022). Enhanced Spatial–Temporal Savitzky–Golay Method for Reconstructing High-Quality NDVI Time Series: Reduced Sensitivity to Quality Flags and Improved Computational Efficiency. *IEEE Transactions on Geoscience and Remote Sensing*, *60*, 1–17. https://doi.org/10.1109/TGRS.2022.3190475

Yao, F., Tang, Y., Wang, P., & Zhang, J. (2015). Estimation of maize yield by using a process-based model and remote sensing data in the Northeast China Plain. *Physics and Chemistry of the Earth, Parts A/B/C*, *87–88*, 142–152. https://doi.org/10.1016/j.pce.2015.08.010

Yin, H., Udelhoven, T., Fensholt, R., Pflugmacher, D., & Hostert, P. (2012). How Normalized Difference Vegetation Index (NDVI) Trendsfrom Advanced Very High Resolution Radiometer (AVHRR) and Système Probatoire d'Observation de la Terre VEGETATION (SPOT VGT) Time Series Differ in Agricultural Areas: An Inner Mongolian Case Study. *Remote Sensing*, *4*(11), 3364–3389. https://doi.org/10.3390/rs4113364

Yli-Heikkila, M., Wittke, S., Luotamo, M., Puttonen, E., Sulkava, M., Pellikka, P., Heiskanen, J., & Klami, A. (2022). Scalable Crop Yield Prediction with Sentinel-2 Time Series and Temporal Convolutional Network. *Remote Sensing*, *14*(17), 4193. https://doi.org/10.3390/rs14174193

Zhang, D., Fang, S., She, B., Zhang, H., Jin, N., Xia, H., Yang, Y., & Ding, Y. (2019). Winter Wheat Mapping Based on Sentinel-2 Data in Heterogeneous Planting Conditions. *Remote Sensing*, *11*(22), 2647. https://doi.org/10.3390/rs11222647

Zhang, J., Guan, K., Peng, B., Jiang, C., Zhou, W., Yang, Y., Pan, M., Franz, T. E., Heeren, D. M., Rudnick, D. R., Abimbola, O., Kimm, H., Caylor, K., Good, S., Khanna, M., Gates, J., & Cai, Y. (2021). Challenges and opportunities in precision irrigation decision-support systems for center pivots. *Environmental Research Letters*, *16*(5), 053003. https://doi.org/10.1088/1748-9326/abe436

Zhang, N., Zhao, C., Quiring, S. M., & Li, J. (2017). Winter Wheat Yield Prediction Using Normalized Difference Vegetative Index and Agro-Climatic Parameters in Oklahoma. *Agronomy Journal*, *109*(6), 2700–2713. https://doi.org/10.2134/agronj2017.03.0133

Zhang, Y., Liu, L., Chen, X., & Li, J. (2022). Effects of Low-Temperature Stress during the Anther Differentiation Period on Winter Wheat Photosynthetic Performance and Spike-Setting Characteristics. *Plants*, *11*(3), 389. https://doi.org/10.3390/plants11030389

Zhao, H., Zhang, L., Kirkham, M. B., Welch, S. M., Nielsen-Gammon, J. W., Bai, G., Luo, J., Andresen, D. A., Rice, C. W., Wan, N., Lollato, R. P., Zheng, D., Gowda, P. H., & Lin, X. (2022). U.S. winter wheat yield loss attributed to compound hot-dry-windy events. *Nature Communications*, *13*(1), 7233. https://doi.org/10.1038/s41467-022-34947-6

Zhao, Y., Potgieter, A. B., Zhang, M., Wu, B., & Hammer, G. L. (2020). Predicting Wheat Yield at the Field Scale by Combining High-Resolution Sentinel-2 Satellite Imagery and Crop Modelling. *Remote Sensing*, *12*(6), 1024. https://doi.org/10.3390/rs12061024

Zhong, L., Hu, L., Zhou, H., & Tao, X. (2019). Deep learning based winter wheat mapping using statistical data as ground references in Kansas and northern Texas, US. *Remote Sensing of Environment*, *233*, 111411. https://doi.org/10.1016/j.rse.2019.111411

Zhou, F., Zhong, D., & Peiman, R. (2020). Reconstruction of Cloud-free Sentinel-2 Image Time-series Using an Extended Spatiotemporal Image Fusion Approach. *Remote Sensing*, *12*(16), 2595. https://doi.org/10.3390/rs12162595

Zhu, X., Guo, R., Liu, T., & Xu, K. (2021). Crop Yield Prediction Based on Agrometeorological Indexes and Remote Sensing Data. *Remote Sensing*, *13*(10), 2016. https://doi.org/10.3390/rs13102016